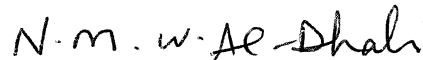


ANALYSIS OF SOURCE-CHANNEL CODING AND EQUALIZATION FOR  
WIRELESS COMMUNICATIONS

APPROVED BY SUPERVISORY COMMITTEE:



Dr. Aria Nosratinia, Chair



Dr. Naofal Al-Dhahir



Dr. John Fonseca



Dr. Mohammed Saquib

Copyright 2004

Ahmadreza Hedayat

All Rights Reserved

To My Parents

ANALYSIS OF SOURCE-CHANNEL CODING AND EQUALIZATION FOR  
WIRELESS COMMUNICATIONS

by

AHMADREZA HEDAYAT, B.S.E.E., M.S.E.E.

DISSERTATION

Presented to the Faculty of  
The University of Texas at Dallas

in Partial Fulfillment

of the Requirements

for the Degree of

DOCTOR OF PHILOSOPHY IN ELECTRICAL ENGINEERING

THE UNIVERSITY OF TEXAS AT DALLAS

December 2004

UMI Number: 3151744



---

UMI Microform 3151744

Copyright 2005 by ProQuest Information and Learning Company.  
All rights reserved. This microform edition is protected against  
unauthorized copying under Title 17, United States Code.

---

ProQuest Information and Learning Company  
300 North Zeeb Road  
P.O. Box 1346  
Ann Arbor, MI 48106-1346

## ACKNOWLEDGEMENTS

My gratitude and respect first go to my advisor Professor Aria Nosratinia. Aria supported me technically and financially during my Ph.D. studies. His constant input has gone towards improving my technical writing style. He has helped his students in many ways and provided them a friendly environment to carry out research and collaborate. I would also like to thank Professor Naofal Al-Dhahir, Professor John Fonseka, and Professor Mohammed Saquib for serving in my supervisory committee and for their feedback on my dissertation.

During my studies in Dallas I enjoyed friendship and collaboration of many incredible individuals. I would like to thank them all for the enjoyable and memorable moments we shared. Particularly, I am very grateful to my current and former colleagues Harsh, Hong Bo, Mohammad, Name, Nikhil, Ramakrishna, Shahab, Todd, Vijay, and Vimal as well as to wonderful friends Afsaneh, Amir, Dorita, Ehsan, Isabella, Mahmoud, Mahnaz, Maryam, Nikki, Rahim, Shahram, and Shayan.

Last, but far from least, my heartfelt thanks go to my family for their support, encouragement, and care. Most importantly, I would like to thank my parents, to whom this dissertation is dedicated, for their never-ending love and affection, for the unconditional support they have given me throughout my life, and for the constant encouragement during my studies.

ANALYSIS OF SOURCE-CHANNEL CODING AND EQUALIZATION FOR  
WIRELESS COMMUNICATIONS

Ahmadreza Hedayat, Ph.D.

The University of Texas at Dallas, 2004

Supervisor: Dr. Aria Nosratinia

Future communication applications will include image and video transmission in addition to mostly-voice services of today. The high rate of these applications, their high quality of service, and combating the hostile wireless channel require advanced algorithms and techniques in various layers and blocks of the system. This dissertation looks at the problem of digital data transmission from two perspectives.

In the first part of the dissertation we investigate is the interaction between channel coding in physical layer and source coding in higher layers. Efficient compression of finite-alphabet sources requires variable-length codes, however, in the presence of noisy channels, error propagation in the decoding of these codes severely degrades performance. To address this problem, we consider redundant entropy codes and iterative source channel decoding and obtain performance bounds and design criteria for the composite system. We also improve upon the performance of residual redundancy source channel decoding via an iterative list decoder.

In the second part of the dissertation, we investigate the performance of channel equalizers in wireless fading channels. Due to the existence of temporal and spatial interference in wireless channels equalizers must be employed. We analyze various equalizers in single- and multi-antenna frequency-selective channels.

## TABLE OF CONTENTS

Acknowledgements	v
Abstract	vi
List of Figures	x
List of Tables	xiii
Chapter 1. Introduction	1
1.1 Outline of the Dissertation . . . . .	2
Chapter 2. Concatenated Error-correcting Entropy Codes and Channels Codes	4
2.1 Introduction . . . . .	5
2.2 Variable-length Codes with Error-Correcting Capability . . . . .	8
2.3 Trellis Representation of Variable Length Codes . . . . .	10
2.4 Serial Concatenation of VLC and Channel Codes . . . . .	11
2.5 Iterative VLC and Channel Decoding . . . . .	17
2.5.1 SISO Channel Decoder . . . . .	17
2.5.2 Bit-Level SISO VLC Decoder . . . . .	18
2.5.3 Iterative Decoding and Density Evolution . . . . .	20
2.6 List-Decoding Serially Concatenated VLC and Channel Codes . . . . .	22
2.6.1 List-Decoding of Variable-Length Codes . . . . .	23
2.6.2 Proposed Iterative List-Decoder . . . . .	24
2.6.3 Non-Binary CRC . . . . .	25
2.7 Experimental Results . . . . .	26
2.7.1 Iterative List Decoding . . . . .	34
2.8 Chapter Summary . . . . .	35



Chapter 3. Performance of Equalizers in Frequency-Selective Single-Antenna Fading Channels	38
3.1 Introduction	38
3.2 MLSE Equalizer	39
3.3 Linear Equalizers	43
3.3.1 Outage Probability of Linear Equalizers	49
3.3.2 Simulation Results	59
3.4 Decision-Feedback Equalizers	60
3.5 Chapter Summary	61
Chapter 4. Performance of Equalizers in Flat Fading Multiple-Antenna Channels	62
4.1 Introduction	62
4.2 Maximum Likelihood Equalizer	64
4.3 Linear Equalizers	66
4.3.1 Outage Probability in Separate Spatial Encoding	69
4.3.2 Outage Probability in Joint Spatial Encoding	72
4.3.3 Simulation Results	78
4.4 Decision-Feedback Equalizers	82
4.4.1 Outage Probability in Separate Spatial Encoding	83
4.4.2 Outage Probability in Joint Spatial Encoding	85
4.5 Simulation Results	85
4.6 Chapter Summary	86
Chapter 5. Performance of Equalizers in Frequency-Selective Multiple-Antenna Fading Channels	88
5.1 Introduction	88
5.2 Maximum Likelihood Equalizer	89
5.3 Linear Equalizers	91
5.3.1 ZF-LE	92
5.3.2 MMSE-LE	95
5.3.3 Simulation Results	97
5.4 Chapter Summary	99

Chapter 6. Conclusions and future work	100
6.1 Contributions . . . . .	100
6.2 Future Work . . . . .	102
Bibliography	105
VITA	

## LIST OF FIGURES

2.1	System block diagram . . . . .	6
2.2	The tree and bit-level trellis of [1], $C_1=\{00, 11, 10, 010, 011\}$ . . . . .	11
2.3	Concatenation of $n$ error events with no gap in between, used in calculating the inner code multiplicity. . . . .	14
2.4	Pair of codewords showing concatenation of $m$ error events with no trivial error event in between, used for calculating the VLC multiplicity. . . . .	15
2.5	Illustration of SISO calculation in a bit-level trellis . . . . .	18
2.6	Iterative VLC and convolutional decoding . . . . .	20
2.7	Empirically measured histograms of the output of a channel code and an RVLC SISO modules. From left to right 1,5,10,20 iterations. $E_b/N_0 = 1.5\text{dB}$ . . . . .	21
2.8	Asymptotic analysis of list Viterbi algorithm. . . . .	24
2.9	Iterative- and list-decoding of VLC and channel code . . . . .	25
2.10	Symbol error rate of $C_2+CC_1$ , $K = 20$ and $200$ symbols. . . . .	28
2.11	Performance of $C_2+CC_1$ , $C_4+CC_1$ (punctured to rate $8/9$ ), and $C_3+CC_3$ . $K = 2000$ symbols. . . . .	29
2.12	Approximate Gaussian density evolution of $C_2+CC_1$ and $C_4+CC_1$ (punctured to rate $8/9$ ), $K = 2000$ symbols. An instance of the convergence of the decoders at $E_b/N_0 = 1.5\text{dB}$ (dashed line staircase) is shown. . . . .	30
2.13	FER comparison between $C_2+CC_1$ , $C_4+CC_1$ (punctured to rate $8/9$ ), and $C_3+CC_3$ . $K = 2000$ symbols. . . . .	31
2.14	Approximate Gaussian density evolution of $C_3+CC_3$ . . . . .	32
2.15	Comparison of concatenated redundant VLC and convolutional codes versus concatenated Huffman code and SCCC's, $K = 2000$ symbols. . . . .	33
2.16	List-decoding of $C_2$ in AWGN channel, $K=200$ . . . . .	34
2.17	Iterative list-decoding of $C_2+CC_1$ (dashed) and $C_3+CC_3$ (solid line) in AWGN channel, $K=500$ . . . . .	36
2.18	Iterative list-decoding of $C_2+CC_1$ (dashed) and $C_3+CC_3$ (solid line) in fully-interleaved Rayleigh channel, $K=200$ . . . . .	36
3.1	Single-carrier frequency-domain equalizer . . . . .	44
3.2	Moment generating function of $\Gamma$ (a) $L = \nu + 1 = 2, 4, 8$ (b) $\nu = 1$ and $L = 2, 10, 20, 40$ . . . . .	48

3.3	Outage regions of linear equalizers in a two-tap channel, $\rho = 10$ dB . . . . .	52
3.4	Outage probability of ML and linear equalizers, $\nu = 1, L = 10$ . ML (solid line), MMSE-LE (solid line marked with $\circ$ ) and ZF-LE (dashed line). The curves correspond, from top left clockwise, to rates $R=1,2,4,3$ bits. . . . .	54
3.5	CDF of capacity of the frequency-selective channel (solid line), MMSE-LE (dashed line), and ZF-LE (dashed-dot line) in a two-tap channel, $\nu = 1$ , and $L = 8$ . In each plot, the SNR for the left set of curves is 13 dB, and 23 dB for the other set. . . . .	54
3.6	Outage probability of ML and linear equalizers in a two-tap channel with 0.5 correlation between the fading coefficients, $\nu = 1, L = 10$ . ML (solid line), MMSE-LE (solid line marked with $\circ$ ) and ZF-LE (dashed line). The curves correspond, from top left clockwise, to rates $R=1,2,4,3$ bits. . . . .	55
3.7	Outage probability of ML and linear equalizers, $\nu = 2, L = 10$ . ML (solid line), MMSE-LE (solid line with $\circ$ ) and ZF-LE (dashed line). The curves correspond, from top left clockwise, to rates $R=1,2,5,3$ bits/sec/Hz. . . . .	58
3.8	Numerical evaluation of CDF of $\Gamma$ in (3.29) . . . . .	59
3.9	Symbol error rate of BPSK signaling and linear equalizers (left) ZF-LE $\nu = 1$ , and $L = 4, 10, 20$ , and (right) ZF-LE versus MMSE-LE $\nu = 1$ , and $L = 10$ . . . . .	60
4.1	Outage probability of linear equalizers. Left: $M = N = 2$ , the pairs solid and dashed lines, from left, correspond to MMSE-LE and ZF-LE for rates $R=1,2,4,10$ bits/sec/Hz. Right: $M = N = 4$ , $R=4,8,12,16$ bits/sec/Hz. . . . .	78
4.2	Outage probability of unconstrained receiver and linear equalizers, Left: $M = N = 2$ , unconstrained receiver (solid line), MMSE-LE (solid line with $\circ$ ) and ZF-LE (dashed line), $R=1,2,4,10$ bits/sec/Hz. Right: $M = N = 4$ , $R=4,8,12,16$ bits/sec/Hz. . . . .	79
4.3	Outage probability of MMSE-LE and the upper bound (4.39). $M = N = 2$ , the curves correspond, from left to right, to rates $R=1,2,4,10$ bits/sec/Hz. . . . .	80
4.4	Outage probability of unconstrained receiver and linear equalizers, $M = N = 2$ and correlated transmit antennas, $\rho_t = 0.5$ . Left: unconstrained receiver (solid line), MMSE-LE (solid line with $\circ$ ) and ZF-LE (dashed line). Right: MMSE outage probability and the upper bound. $R=1,2,4,10$ bits/sec/Hz. . . . .	81
4.5	CDF of capacity of the unconstrained receiver (solid line), MMSE-LE (dashed line), and ZF-LE (dashed-dot line) in a MIMO channel with $M = N = 2$ . The SNR is, from left to right, 5,10,15,20,25 dB. . . . .	81
4.6	CDF of capacity of the unconstrained receiver (solid line), MMSE-LE (dashed line), and ZF-LE (dashed-dot line) in a MIMO channel with (left) $M = 2, N = 4$ , and (right) $M = N = 4$ . The SNR is, from left to right, 5,10,15,20,25 dB. . . . .	82

4.7	Outage probability of DFE equalizers in separate spatial encoding, $M = N = 2$ . The pairs of solid and dashed lines, from left, correspond to MMSE-DFE and ZF-DFE for rates $R = 1, 2, 4, 10$ bits/sec/Hz. . .	86
4.8	Outage probability of DFE equalizers in joint spatial encoding, $M = N = 2$ . The pairs of solid and dashed lines, from left, correspond to MMSE-DFE and ZF-DFE for rates $R = 1, 2, 4, 10$ bits/sec/Hz. Unconstrained equalizer has the same outage probability as MMSE-DFE.	87
5.1	Outage probability of unconstrained and linear equalizers, $M = N = 2, \nu = 1, L = 10$ . Unconstrained (solid line), MMSE-LE (solid line with $\circ$ ) and ZF-LE (dashed line). The curves correspond, from top left clockwise, to rates $R=2,4,8,6$ bits/sec/Hz. . . . .	98
5.2	Outage probability of MMSE-LE and the upper bound (5.23). $M = N = 2, \nu = 1, L = 10$ , the curves correspond, from left to right, to rates $R=2,4,6,8$ bits/sec/Hz. . . . .	99

## LIST OF TABLES

2.1	Family variable-length codes used in Section 2.7 . . . . .	27
2.2	Generator polynomials of convolutional codes used in Section 2.7 (from [2])	27

## CHAPTER 1

### INTRODUCTION

Future communication applications will include image and video transmission in addition to mostly-voice systems of today. The high rate of these applications, their high quality of service, and combating the hostile wireless channel require advanced algorithms and techniques in various layers and blocks of the system.

In this dissertation, we look at the problem of multimedia digital transmission from two perspectives. First, we look at a cross-layer issue: interaction between channel coding in physical layer and source coding in higher layers, which issue is important in both wireline and wireless systems. Second, we investigate the performance of channel equalizers in wireless fading channels.

Source compression schemes are designed independently of communication channel. This is mainly motivated by the celebrated Shannon source channel separation theorem, which states that optimal source and channel coders can be designed separately. The separation theorem requires based on asymptotically long sequences and unconstrained complexity which, needless to say, are not met in practice. In reality, a joint approach is necessary for optimality, subject to finite delay and complexity. Joint source channel (JSC) coding approaches benefit systems operating over both benign Gaussian channel as well as hostile fading channels.

In the second part of this dissertation, we investigate the performance of various equalizers in fading channels. Wireless channels suffer from multi-path fading, which causes non-flat frequency response. The detrimental effect of frequency-

selective channels is removed by equalization. We analyze the performance of several practical equalizers.

## 1.1 Outline of the Dissertation

A fundamental block of every compression system is entropy coding. Since source samples usually do not possess uniform distribution, constant-length entropy codes cannot remove the redundancy efficiently. Variable-length codes (VLC) are more efficient and are widely used. Whenever variable-length entropy codes are used in the presence of a noisy channel, each channel error propagates and causes significant harm. Despite using channel codes, some residual errors always remain, whose effect is magnified by error propagation. Mitigating this undesirable effect is of great practical interest.

One approach is to use the residual redundancy of variable length codes for joint source channel decoding. In Chapter 2, we consider the JSC coding problem by focusing on entropy codes and channel codes. Motivated by the principle of turbo decoding, we investigate the role of intentionally left redundancy in VLC and the optimum way of source and channel decoding. Since the performance of concatenated codes depend on the constituent codes, we calculate performance bounds for the source channel system and investigate the role of redundancy in the VLC and the channel code. Our analysis leads to a generalized form of VLC which provides better performance than the VLC currently used in some compression standards.

Chapters 3, 4, and 5 concentrate on the performance of various equalizers in fading channels where the interference may occur in time, space or both.

In frequency-selective single-antenna channels interference occurs in time. In Chapter 3, we consider such channels and evaluate the performance of maximum like-



likelihood, linear, and decision-feedback equalizers and determine their diversity order.

Chapter 4 considers frequency-nonselctive multiple-antenna channels where spatial interference exists. We evaluate the performance of linear and decision-feedback equalizers for two spatial encoding architectures.

In Chapter 5, we bring the two previous chapters together and consider multiple-antenna frequency-selective channels where the interference occurs in time and space. We evaluate the performance of maximum likelihood and linear equalizers and determine their diversity order.

Finally, Chapter 6 reviews the contribution of the dissertation and discusses future work.

## CHAPTER 2

### CONCATENATED ERROR-CORRECTING ENTROPY CODES AND CHANNELS CODES

Efficient compression of finite-alphabet sources requires variable-length codes (VLC). However, in the presence of noisy channels, error propagation in the decoding of VLC severely degrades performance. To address this problem, redundant entropy codes and iterative source/channel decoding have been suggested, but to date neither performance bounds nor design criteria for the composite system have been available. We calculate performance bounds for the source/channel system by generalizing techniques originally developed for serial concatenated convolutional codes (SCCC). Using this analysis we demonstrate the role of a recursive structure for the inner code and the distance properties of the outer code. We use density evolution to study the convergence of our decoders. Finally, we pose the question: under a fixed rate and complexity constraint, when should we use source-channel decoding (as opposed to separable decoding). We offer answers in several specific cases.

We also improve the performance of residual redundancy source/channel decoding via an iterative list decoder made possible by a non-binary outer CRC code. We show that the list decoding of VLC's is beneficial for the redundant codes used in state-of-art video coding standards. The proposed list-decoder improves the overall performance significantly in AWGN and fully-interleaved Rayleigh fading channels even with a short list.

## 2.1 Introduction

In this chapter we consider the problem of the transmission of discrete, finite-alphabet sources over a noisy channel. Since efficient entropy codes are often variable length codes (VLC), a conventional channel decoding followed by a typical symbol-by-symbol entropy decoding will result in error propagation, thus a single uncorrected channel error may result in a long sequence of data errors. This difficulty has led to a search for error resilient entropy codes. A prominent example is the reversible variable length code (RVLC) [3] utilized in the video coding standard H.263+ and its descendants. RVLC consist of a class of codes that have not only a prefix property, but also a suffix property, thus they can be decoded from both directions.

A more comprehensive attempt at introducing error resilience into variable-length entropy codes was made by Buttigieg [4, 5], who studied the general class of entropy codes with error-correction ability, and introduced various sequence decoding algorithms. Subbalakshmi and Vaisey also provided a trellis for describing VLC's and introduced an optimal maximum *a posteriori* probability decoder for variable-length encoded sources over a binary-symmetric channel [6, 7].

Error resilient codes mentioned above are not strong enough to handle the error rates generated by most communication channels, thus a separate layer of channel coding is usually necessary (see Figure 2.1). In such a concatenated system, iterative decoding methods, originally introduced for channel codes [8, 2], provide another opportunity for improved source/channel coding. To the best of our knowledge, the first attempt at iterative decoding of source and channel codes is due to Bauer and Hagenauer [1, 9], who proposed an iterative (turbo) decoding scheme between a channel code and the residual redundancy of a reversible variable-length code (RVLC).<sup>1</sup>

---

<sup>1</sup>For an example of iterative source-channel decoding of *fixed-length* codes see [10].

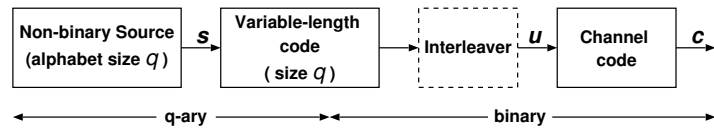


Figure 2.1. System block diagram

They reported a significant coding gain compared to a system with equivalent transmission rate. Guyader *et. al* [11] proposed various algorithms in the framework of Bayesian networks for the iterative decoding of the chain in Figure 2.1 with a Markov non-binary source. Lakovic and Villasenor [12] studied the performance of VLC's followed by turbo codes and suggested combining the trellises of the VLC and the upper convolutional code of the turbo code for more coding gain.

Despite many interesting and useful results including those mentioned above, to date neither a comprehensive analysis nor design criteria has been available for iteratively decoded source-channel coding systems. In this chapter, we analyze this concatenated system, study design criteria for the constituent codes, and present comparisons of various tradeoffs in the design of such codes, supported by extensive simulations.

To start, we generalize the source-channel structure by assigning the error-correcting entropy codes of Buttigieg as the outer code of the source-channel concatenated system. We study, via simulations, the performance of this generalized system compared to other existing scenarios.

The central contribution of this chapter, however, is an analysis of the performance of the concatenated source-channel codes. We employ the techniques originally developed for serial concatenated convolutional codes (SCCC's) [2], with the critical difference that our outer codes (and hence our overall codes) are nonlinear, thus the techniques of [2] need to be appropriately extended. Our analysis is general with

respect to the choice of outer VLC's and inner channel codes: the outer code can be an RVLC similar to [1, 9, 12], it can be a VLC with higher redundancy, similar to the codes introduced in [4], or a VLC with minimum redundancy such as Huffman codes. The analysis clarifies the roles of the inner and outer codes in the overall performance, allowing us to make statements about the free distance of the outer code and the desirability of a recursive structure for the inner code. To the best of our knowledge, these or similar results have not been previously reported in the literature on source-channel coding.

The analysis and simulations presented in this chapter enable us to make several observations with practical implications. For example, the method of Bauer and Hagenauer [9] achieved significant gain compared to systems with similar rate. We found, however, that it is possible to improve on the scheme of [9], while maintaining the same overall rate and complexity, by using separable source decoding and an iteratively decoded SCCC. Thus in this case, investing computational resources into the channel decoder alone gives better returns in terms of system performance. This suggests that whenever the entropy code has small free distance (such as the RVLC used in [9]) one may be better off spending the computational budget mostly on the inner code and not on iterative decoding between source and channel codes. We also found that in several cases, even with outer codes having larger free distance, iterative source channel decoding may yield only a slight advantage compared with a separable baseline system of equivalent rate and complexity. These findings are expressed in more detail in the sequel<sup>2</sup>.

---

<sup>2</sup>The contribution of this chapter has been published in [13, 14, 15] and will appear in [16, 17].

## 2.2 Variable-length Codes with Error-Correcting Capability

Buttigieg [4] introduced a class of entropy codes with error-correction ability under the name of *variable-length error-correcting codes* (VLECC's). These codes have entropy coding property, in the sense that low probability symbols have longer codewords compared to high-probability symbols. On the other hand, these codes also have error correction capability, arising from a careful assignment of codewords to symbols such that a minimum Hamming distance is maintained between all codeword pairs. Obviously, maintaining a minimum distance introduces redundancy into the code, such that its average length will be bounded away from the entropy of the source.

Consider a  $q$ -ary source with elements denoted by  $u$ , and a variable length code whose codewords are denoted by  $b(u)$ . The minimum and maximum length of  $b(u_i)$ 's are denoted by  $\ell_{min}$  and  $\ell_{max}$  respectively, and the average length by  $\ell_{ave}$ . To perform maximum likelihood decoding, we need to consider a sequence of  $K$  codewords. We now define such composite codewords. Assume the source sequence  $\mathbf{u} = (u_i : i = 1, \dots, K)$  is entropy-encoded to the bit sequence

$$\mathbf{c} = (b(u_1), b(u_2), \dots, b(u_K)) = (c_1, c_2, \dots, c_N) .$$

Because the codewords  $b(u)$  are variable length, the length of the output sequence  $\mathbf{c}$ , denoted by  $N$ , is variable. This leads to difficulty in analysis, therefore we partition the overall code  $\mathcal{C}$  into subcodes  $\mathcal{C}_i$  such that each partition consists only of codewords of length  $i$ . The *free distance* of  $\mathcal{C}$ , denoted  $d_f$ , is defined as the minimum value of the minimum Hamming distances of the individual binary codes  $\mathcal{C}_i$ . Note that  $\mathcal{C}_i$  are in general nonlinear codes.

Buttigieg [4] calculates the upper bounds for the error event probability of a VLC in the same manner as convolutional codes, by introducing the average number

of converging paths on an appropriate trellis at a given Hamming distance. Unfortunately, this approach is not appropriate for our purposes since, unlike Buttigieg, we intend to use the variable length codes in concatenation with another code. Instead, we use the codeword enumeration technique [2]. Considering that  $N$ , the length of the bit-sequence  $\mathbf{c}$ , is a random variable that takes value in  $[N_{\min}, N_{\max}] = [\ell_{\min}K, \ell_{\max}K]$ , the upper bounds for the codeword error probability (frame error rate),  $P_E$ , and symbol error probability,  $P_S$  are :

$$\begin{aligned} P_E &\leq \sum_{N=N_{\min}}^{N_{\max}} \Pr(N) \sum_{h \geq d_f} A_h(N) P_h \\ &= \sum_{h \geq d_f} \left( \sum_{N=N_{\min}}^{N_{\max}} \Pr(N) A_h(N) \right) P_h \end{aligned} \quad (2.1)$$

$$\begin{aligned} P_S &\leq \frac{1}{K} \sum_{N=N_{\min}}^{N_{\max}} \Pr(N) \sum_{h \geq d_f} B_h(N) P_h \\ &= \frac{1}{K} \sum_{h \geq d_f} \left( \sum_{N=N_{\min}}^{N_{\max}} \Pr(N) B_h(N) \right) P_h, \end{aligned} \quad (2.2)$$

where  $P_h$  is the pairwise error probability, which has value  $P_h = 0.5 \operatorname{erfc}(\sqrt{hE_s/N_0})$  in AWGN channel, and  $A_h(N), B_h(N)$  are multiplicities. Specifically,  $A_h(N)$  is the number of codeword pairs in  $\mathcal{C}_N$  with Hamming distance  $h$ . Eventually, we are interested in the distance between symbol strings corresponding to codeword pairs with Hamming distance  $h$ . The average contribution of two codewords of Hamming distance  $h$  to the Levenshtein distance is denoted  $B_h(N)$ . Note that  $A_h(N)$  and  $B_h(N)$  are normalized by the size of the respective codebooks  $\mathcal{C}_N$ . The exchange of summations in Equations (2.1) and (2.2) allow us to think of the terms inside parentheses as equivalent  $A_h$  and  $B_h$  for the entire code, without the need to consider individual code partitions separately. It is in fact more convenient to calculate  $A_h, B_h$  instead of  $A_h(N), B_h(N)$ ; see for example [4, 1].

Computation of  $B_h$  is based on the Levenshtein distance between the two symbol sequences;  $d_L(\mathbf{u}_i, \mathbf{u}_j)$ . The Levenshtein distance is defined as the minimum number of insertions, deletions or substitutions to transform one symbol sequence into another [18, 4]. The Levenshtein distance is widely used as an error measure for VLC's, justified partly in light of the self-synchronization property of VLC's [4], and partly because of the lack of other more meaningful and useful distance measures for VLC's.

### 2.3 Trellis Representation of Variable Length Codes

Various trellis representation for VLC's have been proposed [6, 9, 1]. Subbalakshmi and Vaisey [6] proposed a trellis based on the notion of complete and incomplete states. The decoder is in a complete state if the most recently received bit completes a codeword, otherwise it is in an incomplete state. The number of states sums up to  $S + \ell_{\max} - 1$ , where  $S$  is the number of codewords. Bauer and Hagenauer proposed a novel two-dimensional trellis which provides bit-level and symbol-level trellises in its axis [9]. The maximum number of states depends on the length of the sequence in bits and symbols and is  $N - \ell_{\min}K + 1$ .

In this chapter we employ the bit-level trellis that was proposed by Balakirsky [19], and later used by Murad and Fuja [20] as well as Bauer and Hagenauer [1]. This trellis is obtained simply by assigning the states of the trellis to the nodes of the VLC tree. The root node and all terminal nodes are assumed to represent the same state, since they all show the start of a new sequence of bits. Other nodes, the so called internal nodes, are assigned one-by-one to the other states of the trellis. The number of states of the trellis is equal to the number of internal nodes of the tree plus one. As an example, Figure 2.2 shows the trellis corresponding to a



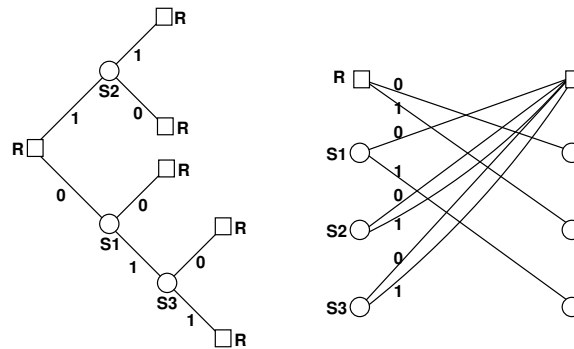


Figure 2.2. The tree and bit-level trellis of [1],  $C_1=\{00, 11, 10, 010, 011\}$

Huffman code  $C_1=\{00, 11, 10, 010, 011\}$ .

## 2.4 Serial Concatenation of VLC and Channel Codes

In this section, we present an analysis of the performance of the overall system shown in Figure 2.1. The outer VLC can be a Huffman code, an RVLC, or a VLECC and the inner code may be a convolutional or block code. Similar to [4, 1], we treat redundant variable length codes as channel codes. We then build arguments similar to those presented for the case of serial concatenated convolutional codes (SCCC) [2]. The key difference with SCCC is the nonlinearity of our outer code. Through the developments in this section, we will see that it is possible to carry over several of the design criteria of the SCCC to the concatenated source-channel codes, despite the differences.

The interleaver maps the output of the outer codeword into another codeword with similar weight. Unfortunately it is often not tractable to calculate weight enumerators in such codes due to the complicated dependencies introduced by a specific interleaver. Instead, we use the concept of a *uniform interleaver* developed originally by Benedetto and Montorsi, and subsequently used to analyze serial concatenated codes [2]. A uniform interleaver avoids the problem of weight assignment by random-

izing over the space of all possible interleavers: it maps a codeword of weight  $\ell$  into all distinct  $\binom{N}{\ell}$  permutations with equal probability  $1/\binom{N}{\ell}$ .

In the following, functions and variables related to the inner code will be distinguished by the superscript  $i$ , and those related to the outer code with superscript  $o$ . Assume the inner code,  $C^i$ , is a convolutional code with rate  $R^i = \frac{k}{n}$ . The input-output weight enumerating function (IOWEF) of the equivalent block code of the inner convolutional code, with the input length  $N$ , is [2]:

$$A^i(L, H) = \sum_{\ell=0}^N \sum_{h=d_f^i}^{N/R^i} A_{\ell,h}^i(N) L^\ell H^h \quad (2.3)$$

where  $A_{\ell,h}^i(N)$  represents the number of codewords with weight  $h$  generated by information words of weight  $\ell$ , and  $L$  and  $H$  are dummy variables.

We use a uniform interleaver, which maps a codeword of weight  $\ell$  into all distinct  $\binom{N}{\ell}$  permutations with equal probability. The outer VLC has free distance  $d_f^o$ , therefore:

$$\begin{aligned} A_h(N) &= \sum_{\ell=d_f^o}^N \frac{A_\ell^o(N) A_{\ell,h}^i(N)}{\binom{N}{\ell}}, \\ B_h(N) &= \sum_{\ell=d_f^o}^N \frac{B_\ell^o(N) A_{\ell,h}^i(N)}{\binom{N}{\ell}}, \end{aligned} \quad (2.4)$$

where  $A_\ell^o(N)$  and  $B_\ell^o(N)$  are the associated multiplicities for  $\mathcal{C}_N$ , the length- $N$  sub-code of the outer code,  $A_{\ell,h}^i(N)$  are the multiplicities of the inner code. Summing the contributions over all the possible  $\ell$ 's gives the associated coefficients  $A_h(N)$  and  $B_h(N)$ .

This derivation was facilitated by two facts. First, for two codewords  $\mathbf{a}$  and  $\mathbf{b}$  we have  $d_H(\mathbf{a}, \mathbf{b}) = d_H(\pi(\mathbf{a}), \pi(\mathbf{b}))$ , where  $\pi$  is the interleaving function. Second, since the inner code is a linear code, we may speak equivalently of codeword weights

or codeword pair distances. In particular, for the inner code, two sequences with distance  $\ell = d_H(\pi(\mathbf{a}), \pi(\mathbf{b}))$ , will result in two codewords with *coded distance*  $h$ . It is due to this “invariance” of the interleaver and the linearity of the inner code that our analysis remains tractable.

We can now calculate the frame error rate,  $P_E$ , and symbol error rate,  $P_S$ , of the concatenated scheme:

$$\begin{aligned} P_E &\leq \sum_{N=N_{\min}}^{N_{\max}} \Pr(N) \sum_{h=d_f}^{N/R^i} A_h(N) P_h \\ &= \frac{1}{2} \sum_{N=N_{\min}}^{N_{\max}} \sum_{h=d_f}^{N/R^i} \sum_{\ell \geq d_f^o} \Pr(N) \frac{A_\ell^o(N) A_{\ell,h}^i(N)}{\binom{N}{\ell}} \operatorname{erfc} \left( \sqrt{hE_s/N_0} \right), \end{aligned} \quad (2.5)$$

$$\begin{aligned} P_S &\leq \frac{1}{K} \sum_{N=N_{\min}}^{N_{\max}} \Pr(N) \sum_{h=d_f}^{N/R^i} B_h(N) P_h \\ &= \frac{1}{2K} \sum_{N=N_{\min}}^{N_{\max}} \sum_{h=d_f}^{N/R^i} \sum_{\ell \geq d_f^o} \Pr(N) \frac{B_\ell^o(N) A_{\ell,h}^i(N)}{\binom{N}{\ell}} \operatorname{erfc} \left( \sqrt{hE_s/N_0} \right), \end{aligned} \quad (2.6)$$

where  $d_f$  is the free distance of the concatenated code. Similar to (2.1) and (2.2), the above results may be presented in terms of equivalent  $A_\ell$  and  $B_\ell$ . This alternative form is omitted here for sake of brevity. One may also obtain bounds similar to (2.5) and (2.6) for the average interleaver size  $N_{ave}$ . We note that the above union bounds can be used with different choices of inner code, for example a convolutional code as in [1], or a turbo code as in [12].

The asymptotic performance of the bounds above can be studied by looking at the behavior of coefficients  $A_h$  and  $B_h$ . We mainly present the analysis for  $A_h$ ; similar developments are possible for  $B_h$ .

Following [21], the multiplicities  $A_h$  can be modeled as a polynomial function of interleaver size, i.e.,  $A_h \approx \beta_0 N^\alpha + \beta_1 N^{(\alpha-1)} + \dots$ . We are in particular interested

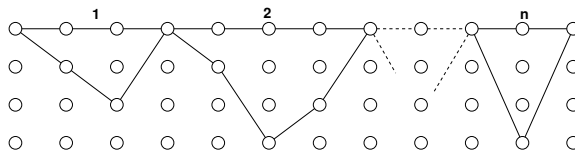


Figure 2.3. Concatenation of  $n$  error events with no gap in between, used in calculating the inner code multiplicity.

in the exponent  $\alpha$  of the highest order term in this polynomial, which is indicative of the asymptotic improvement of the multiplicity (and hence code performance) with increasing interleaver length. To eliminate the dependency on  $h$  define

$$\hat{\alpha} = \max_h \lim_{N \rightarrow \infty} \log_N A_h. \quad (2.7)$$

Thus  $\hat{\alpha}$  is the dominant coefficient of  $\alpha(h)$ , where we here emphasize the dependence on  $h$ , the Hamming distance. The dominant multiplicity exponent  $\hat{\alpha}$  is referred to as *interleaver gain* in the literature [2]. The performance of the code, except in very high-SNR regime, is dependent on the multiplicities of the code and therefore depends on  $\hat{\alpha}$ . Whenever  $\hat{\alpha} < 0$ , the dominant multiplicity gets smaller with increasing interleaver size, therefore we will be motivated to design codes with  $\hat{\alpha} < 0$ .

We define  $\hat{h}$  as the Hamming distance of codeword pairs having the dominant multiplicity (the maximizer in the expression above). We now wish to calculate  $\hat{\alpha}$  and  $\hat{h}$ . The inner code multiplicity,  $A_{\ell,h}^i$ , can be expressed as

$$A_{\ell,h}^i \leq \sum_{n \geq 1} \binom{N/k}{n} A_{\ell,h,n}^i, \quad (2.8)$$

where  $A_{\ell,h,n}^i$  are the multiplicities for codewords with input/output weights  $(\ell, h)$  having exactly  $n$  consecutive error events with no gap in between, as shown in Figure 2.3. Equation (2.8) derives the overall multiplicities by inserting zero-runs before some of the error events such that the overall number of trellis sections is  $N/k$  [21].

For the outer variable-length code, a similar expression can be derived with certain modifications. Because of the nonlinearity of VLC's weight enumeration has

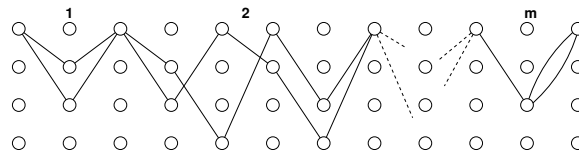


Figure 2.4. Pair of codewords showing concatenation of  $m$  error events with no trivial error event in between, used for calculating the VLC multiplicity.

to be carried out through *all pairs of codewords*, as is shown in Figure 2.4. All error events for the VLC must initiate and terminate in a “root state,” which is the state where the bit sequence for a source symbol begins or terminates (see Figure 2.2). In Figure 2.4 we show the root state as the top node. A pair of codewords of a VLC are illustrated in Figure 2.4, using the trellis of Figure 2.2. Following a similar argument as in [21], we obtain

$$A_\ell^o \leq \sum_{m \geq 1} \binom{N}{m} A_{\ell,m}^o, \quad (2.9)$$

where  $A_{\ell,m}^o$  is the multiplicity of the pair of codewords at distance  $\ell$  consisting of a concatenation of exactly  $m$  simple error events, with no trivial error event in between. Trivial error event is a section of the bit-trellis of the two codewords that are identical, and furthermore it starts and ends in the root state. Equation (2.9) illustrates the expansion of simple codepaths with  $m$  error events, to compound codepaths that include trivial error events.

One may obtain the coefficients  $A_h$  of the concatenated code by substituting (2.8) and (2.9) in (2.4)

$$\begin{aligned} A_h &\leq \sum_{\ell=d_f^o}^N \sum_{m \geq 1} \sum_{n \geq 1} \frac{\binom{N}{m} \binom{N/k}{n}}{\binom{N}{\ell}} A_{\ell,m}^o A_{\ell,h,n}^i \\ &\leq \sum_{\ell=d_f^o}^N \sum_{m \geq 1} \sum_{n \geq 1} \frac{\ell!}{m!n!k^n} N^{m+n-\ell} A_{\ell,m}^o A_{\ell,h,n}^i, \end{aligned} \quad (2.10)$$

where the approximation of  $\binom{N}{x} \approx N^x/x!$  is used. Substituting (2.10) in (2.7) we

obtain

$$\hat{\alpha} = \max_h(m+n) - \ell \leq \lfloor \frac{\ell}{d_f^o} \rfloor + \lfloor \frac{\ell}{w_{min}} \rfloor - \ell, \quad (2.11)$$

where the bound for the outer code,  $\lfloor \frac{\ell}{d_f^o} \rfloor$ , reflects the possibility of the concatenation of error events all with minimum distance  $d_f^o$ , while the bound for the inner code,  $\lfloor \frac{\ell}{w_{min}} \rfloor$ , shows the maximum number of concatenated error events with minimum uncoded weight  $w_{min}$ . For block codes and non-recursive convolutional codes  $w_{min} = 1$  which results in a positive value for  $\hat{\alpha}$ , thus the concatenated code will not have any interleaving gain. For recursive convolutional codes  $w_{min} = 2$  since no finite error event with  $w = 1$  exists.<sup>3</sup> Evaluating the maximum of the right hand side of (2.11) for the recursive convolutional code results in

$$\hat{\alpha} \leq -\lfloor \frac{d_f^o + 1}{2} \rfloor + 1 \quad (2.12)$$

offering interleaving gain for frame error rate  $P_E$  whenever  $d_f^o$  is greater than two.<sup>4</sup> Depending on whether  $d_f^o$  is odd or even  $\hat{h}$  is calculated differently. The design of recursive convolutional codes is [2, 21].

To summarize, there are two important factors in the performance of source-channel concatenated codes: the free distance of the outer code and the recursive structure for the inner code. This was demonstrated by an extension of the techniques of [2] in order to accommodate the nonlinear codes of interest in source-channel coding. The design issues of the inner code are similar to the case of ordinary SCCC's, which have been well developed in the literature [2, 21].

Our analysis is based on the concept of union bound, which diverges at low  $E_b/N_0$  values (in particular at SNR values below those corresponding to the channel

---

<sup>3</sup>In other words, in block codes and non-recursive convolutional codes, a single "1" leads to a finite error event, while in recursive convolutional codes at least two "1"s are needed in the data sequence for a finite error event.

<sup>4</sup>Similarly, calculations for  $B_h$  indicate that the interleaving gain for symbol error rate  $P_S$  is  $\hat{\alpha}_B = \hat{\alpha} - 1$ .

cutoff rate [2]). There is no solid theoretical ground for using union bound analysis below cutoff rate. However, as has been noted in the literature [2], design criteria based on these bounds perform surprisingly well even at SNR values where the bounds do not converge. Our simulations also support that conclusion.

## 2.5 Iterative VLC and Channel Decoding

Iterative detection (decoding) is possible when a sequence has two or more sets of concurrent likelihood expressions for a data sequence. These sets of expressions represent different constraints over the sequence. Obviously, all constraints have to be satisfied for the detection process. Iterative decoding suggests satisfying each constraint separately and repeating the process.

In iterative decoding, each decoder in turn processes the available information about the desired signal, typically log likelihood ratios, thus modifying and hopefully improving in each iteration the pool of available information on the received signal. The additional information is called *extrinsic information* [8, 22]. Extrinsic information represents the new information obtained in each half-iteration by applying the constraint of a constituent decoder. An efficient way to calculate extrinsic information is via the soft-input soft-output (SISO) algorithm [23]. In the following we discuss the structure of the SISO module for a channel code as well as a VLC.

### 2.5.1 SISO Channel Decoder

A soft-output algorithm for channel decoding was introduced in [24]. A slightly different version of this algorithm, called the SISO module, was introduced in [23]. We give a system-level description of this block below.

The SISO module for the convolutional code, shown in Figure 2.6, works on

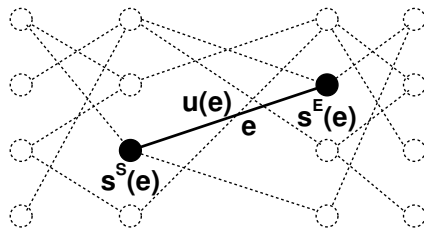


Figure 2.5. Illustration of SISO calculation in a bit-level trellis

the channel code trellis. It accepts two probability streams  $\mathbf{P}(c; I)$  and  $\mathbf{P}(u; I)$  as inputs: the former is about the coded sequence  $\mathbf{c}$  and the latter is about the information sequence,  $\mathbf{u}$ . Applying the constraints provided by the channel code, additional information (extrinsic information) is obtained for both sequences,  $\mathbf{P}(c; O)$  and  $\mathbf{P}(u; O)$ , which in turn is passed to the other decoder. Each decoder repeats this process by using the extrinsic information that was fed back as its new input.

### 2.5.2 Bit-Level SISO VLC Decoder

Many efficient channel decoding algorithms are trellis-based. In particular, the Viterbi algorithm (VA), and SISO algorithms [24], [23] are all trellis-based. By building a trellis for a VLC, one may employ these algorithms in the decoding of VLC's.

The trellis-based algorithms for the VLC are simpler than those for the inner code for two reasons: First, for the VLC trellis only one node (root node) has multiple incoming branches, thus the compare-select operation of the Viterbi algorithm and selection of surviving path is done only for the root node. At other nodes only the metric is calculated. Second, for VLC we do bit-level detection and there is no reference to the input symbols except connections of the trellis, which simplifies the SISO module.

Based on the trellis representation of a VLC introduced in Section 2.3, we



derive an SISO algorithm for VLC's. Following the notation of [23], the extrinsic information is calculated as follows. At time  $k$  the output probability distribution is evaluated as

$$\tilde{P}_k(u; O) = \tilde{h} \sum_{e:u(e)=u} A_{k-1}(s^S(e))B_k(s^E(e))P_k(u; I) \quad (2.13)$$

where  $e$  represents a branch of the trellis;  $u(e)$ ,  $s^S(e)$ , and  $s^E(e)$  are, respectively, the branch value, the starting state, and the ending state of the branch  $e$ , as shown in Figure 2.5. The constant  $\tilde{h}$  is a normalizing factor to ensure  $\tilde{P}_k(0; O) + \tilde{P}_k(1; O) = 1$ . The quantities  $A_k(\cdot)$  and  $B_k(\cdot)$  are calculated through forward and backward recursions, respectively, as follows.

$$\begin{aligned} A_k(s) &= \sum_{e:s^E(e)=s} A_{k-1}(s^S(e))P_k(u; I) \\ B_k(s) &= \sum_{e:s^S(e)=s} B_{k+1}(s^E(e))P_{k+1}(u; I) \end{aligned}$$

with initial values  $A_0(s) = B_N(s) = 1$  for the root state (since the trellis always starts and ends at the root state) and  $A_0(s) = B_N(s) = 0$  for all other states. In order to exclude the input information,  $P_k(u; I)$ , from the output probability, and obtain the so called extrinsic information, both sides of (2.13) are divided by  $P_k(u; I)$ :

$$P_k(u; O) = \frac{\tilde{P}_k(u; O)}{P_k(u; I)} = h \sum_{e:u(e)=u} A_{k-1}(s^S(e))B_k(s^E(e))$$

where,  $h$  is again a normalization factor.

Therefore  $P_k(u; I)$  (input probability), and  $P_k(u; O)$  (extrinsic information) together form the *a posteriori* probability (APP) of the input sequence. In practice, the additive (logarithmic) version of an SISO algorithm is employed to avoid multiplications and prevent numerical problems.

### 2.5.3 Iterative Decoding and Density Evolution

An iterative decoder is shown in Figure 2.6, using the SISO blocks already introduced. Blocks denoted  $\pi$  and  $\pi^{-1}$  are the interleaver and deinterleaver, respectively.

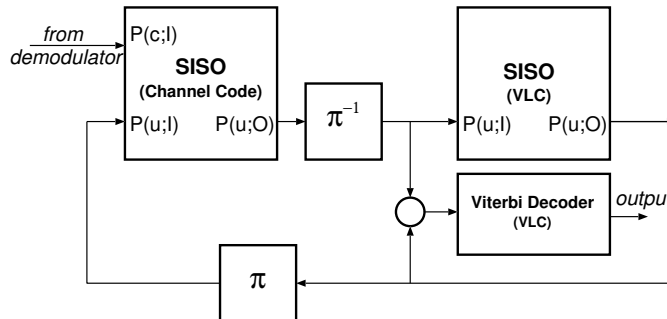


Figure 2.6. Iterative VLC and convolutional decoding

In each iteration, only the extrinsic information generated by each SISO block,  $P_{CC}(u; O)$  and  $P_{VLC}(u; O)$ , are exchanged between the soft-output decoders. After the final iteration, the soft-sequence,  $P_{VLC}(u; I) + P_{VLC}(u; O)$ , is decoded at symbol-level by the Viterbi decoder over the same bit-level trellis.

The convergence of the iterative decoder can be illustrated by the density evolution method [25], or alternatively by EXIT charts [26]. We use the density evolution method for our analysis. We have verified the corresponding Gaussian approximation assumption in our setting. Density evolution treats the decoder as a nonlinear dynamical feedback system where the nonlinear input-output functions are calculated empirically. For further information on density evolution, we refer the reader to [25].

Density evolution considers the iterative decoder as a nonlinear dynamical feedback system, where the corresponding nonlinear functions are calculated empirically.

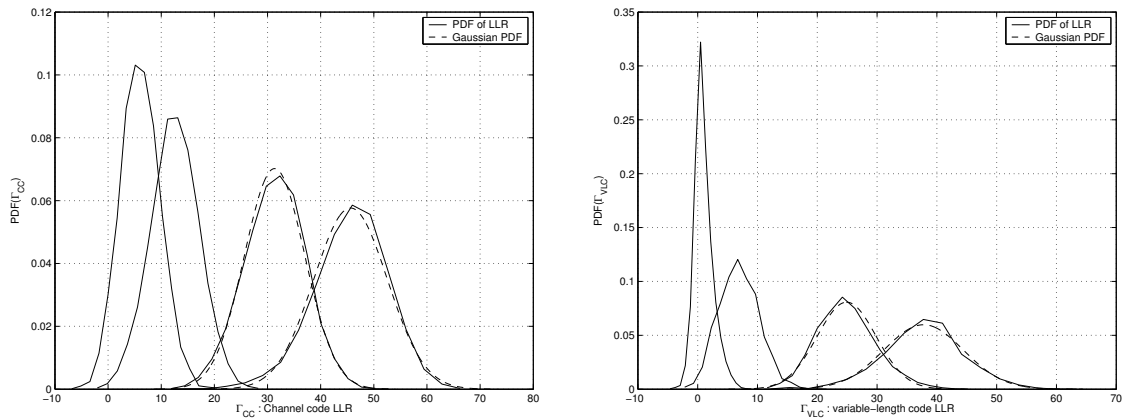


Figure 2.7. Empirically measured histograms of the output of a channel code and an RVLC SISO modules. From left to right 1,5,10,20 iterations.  $E_b/N_0 = 1.5\text{dB}$

ically. The functions describe the improvement in output extrinsic information by a given input extrinsic information. To quantify the input and output extrinsic sequences and their evolution, the sequence is approximated by a Gaussian distribution, which is mathematically justified for very large and random interleavers [25]. We have experimentally verified this assumption for the iterative VLC and channel decoders. A sample result of a RVLC is shown in Figure 2.7.

Each decoder is characterized with a single parameter, the ratio of the squared mean by the variance of the empirical distribution of the extrinsic information, also called the signal to noise ratio (SNR).<sup>5</sup>

Assume, referring to Figure 2.6, that the input and output SNR of the channel SISO decoder are related with the function  $\text{SNR}_{\text{out}}^{\text{CC}} = G^{\text{CC}}(\text{SNR}_{\text{in}}^{\text{CC}}, E_b/N_0)$ , where  $E_b/N_0$  is the signal to channel noise ratio normalized per information bit. A similar relationship exists for the variable-length SISO decoder, except it depends only on its sole input:  $\text{SNR}_{\text{out}}^{\text{VLC}} = G^{\text{VLC}}(\text{SNR}_{\text{in}}^{\text{VLC}})$ , where  $\text{SNR}_{\text{in}}^{\text{VLC}} = \text{SNR}_{\text{out}}^{\text{CC}}$ . The functions

<sup>5</sup>To avoid confusion we should emphasize the distinction between the channel-induced  $E_b/N_0$  and what we call “SNR.” The latter is a quantity that describes the reliability of the extrinsic information during the decoding process.

$G^{\text{CC}}$  and  $G^{\text{VLC}}$  are evaluated empirically by simulation [25]. One may inspect the convergence of the iterative decoder by the evolution of the extrinsic information from one half-iteration to another. This is simply done by plotting  $\text{SNR}_{\text{out}}^{\text{CC}}$  versus  $\text{SNR}_{\text{in}}^{\text{CC}}$ ,  $G^{\text{CC}}$  curve, and in the same plot,  $\text{SNR}_{\text{in}}^{\text{VLC}}$  versus  $\text{SNR}_{\text{out}}^{\text{VLC}}$ , the curve associated with the inverse of  $G^{\text{VLC}}$ . When the curves are far apart the decoder converges rapidly. The convergence may take many iterations if the curves are close, or may not converge if they intersect. We verify the convergence behavior of some the schemes in the following section.

## 2.6 List-Decoding Serially Concatenated VLC and Channel Codes

A list-decoder provides an ordered list of the  $L$  most probable sequences in maximum likelihood sense. Then, an outer error detecting code, usually a cyclic redundancy check (CRC) code, verifies the validity of the candidates and selects the error-free sequence, if exists, among the candidates. Two variations of the list Viterbi-algorithm (LVA) are reported in [27].

The advantage of the list decoder can be explained as follows. In a regular ML decoder, for an error to occur, the closest codeword to the received sequence must be an erroneous one. For the list-decoder to make an error, the correct sequence must lie outside of the  $L$  nearest neighbors of the received sequence. This error is less probable than the corresponding error in the ML decoder.

In a list-decoder, the distance between the received sequence and all the candidates determines the performance. Therefore, determining the exact performance is mathematically intractable. But it is possible to calculate the asymptotic coding gain, e.g. see [27]. In the case of AWGN channel, a geometrical argument reveals that the asymptotic coding gain is  $G = 10 \log(\frac{2L}{L+1})$  dB for a list of length  $L$ . However,

the actual gain is often less due to the multiplicity of the set of  $L$  nearest neighbors, which is neglected in the analysis [27].

### 2.6.1 List-Decoding of Variable-Length Codes

List-decoders can also be applied for variable-length encoded sequences, given an appropriate trellis (e.g. the bit-level trellises mentioned earlier). Our list decoding is constructed with the help of a non-binary CRC code, which verifies the validity of the  $L$  most probable paths in the VLC trellis. The alphabet set of the CRC code must cover all codewords of the VLC (size  $q$ ). If  $q$  is a power of a prime, it is possible to construct a  $q$ -ary CRC code, otherwise the size of VLC should be extended to the nearest power of a prime. One can use the a-priori knowledge that these additional symbols are never present in the data sequence, but only (possibly) present in the parity sequence.

The asymptotic error rate for a list of size  $L = 2$  is based on a simple geometric construction due to Seshadri and Sundberg [27] (see Figure 2.8). When the three codewords are pairwise equi-distant, it produces a worst-case error probability. In this case, the minimum-magnitude noise resulting in an error is shown by the vector terminating at the center of the triangle. This is an effective minimum distance, denoted  $d_{\text{eff}}$ , which is larger than  $d_{\text{free}}/2$ , explaining the list decoding gain, which is equal to  $10 \log(\frac{2L}{L+1})$  dB, as calculated in [27].

This value of asymptotic gain, however, ignores the multiplicities of the minimum distance, and in our case minimum distance error event has high multiplicities<sup>6</sup>. Therefore, we augment the asymptotic analysis of [27, 28] for  $L = 2, 3$  list-decoder of VLC's so that multiplicities are taken into account. We denote by  $N_{\text{free}}$  the multiplic-

---

<sup>6</sup>More information on the distance spectrum of VLC's is available in [4], and two examples are given in [1].

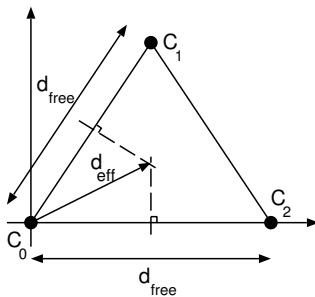


Figure 2.8. Asymptotic analysis of list Viterbi algorithm.

ity of the minimum distance errors.<sup>7</sup> The number of codeword triplets at minimum distance that include the transmitted codeword is  $N_{\text{eff}} = N_{\text{free}}(N_{\text{free}} - 1)/2$ . Thus, for  $L = 2$  and assuming an AWGN channel, coding gain is the difference  $\Delta\gamma = \gamma_1 - \gamma_2$ , where  $\gamma_1$  and  $\gamma_2$  are the two values of  $\frac{E_b}{N_0}$  such that

$$N_{\text{eff}} Q\left(\sqrt{2d_{\text{eff}}\gamma_2}\right) = N_{\text{free}} Q\left(\sqrt{2d_{\text{free}}\gamma_1}\right) .$$

Closed form solutions are not available for this equation, however, the resulting coding gain is closer to simulation results than the results of [27, 28].

Similar worst case analysis can be repeated for  $L = 3$  list-decoder to calculate  $d_{\text{eff}}$ . To obtain a more realistic approximation of the coding gain, we consider the multiplicity of the worst case of the set of three codewords, which is  $N_{\text{eff}} = N_{\text{free}}(N_{\text{free}} - 1)(N_{\text{free}} - 2)/6$ , given  $N_{\text{free}} \geq 3$ . The coding gain is calculated in a similar way as  $L = 2$ .

### 2.6.2 Proposed Iterative List-Decoder

We now introduce an approximated list-decoder for the concatenation of VLC's and channel codes. Our proposed iterative and list decoder is demonstrated in Figure 2.9. After the last iteration, the final soft-output sequence, which is the sum of

<sup>7</sup>The multiplicities of VLC's in general are not integer-valued since we must average the multiplicities of the subcodes. In our analysis we round the multiplicities up to simplify the calculation.

the input and output of SISO-VLC is decoded at symbol-level by employing the LVA over the same bit-level trellis used by SISO-VLC.

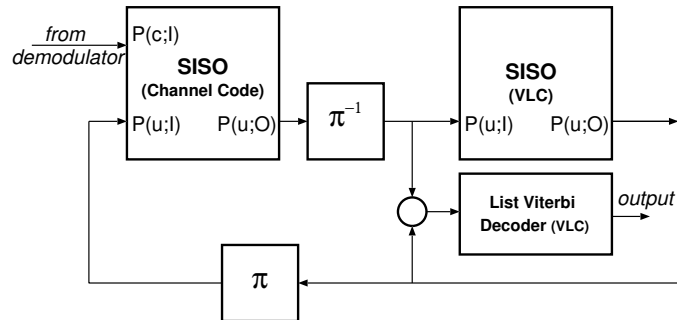


Figure 2.9. Iterative- and list-decoding of VLC and channel code

The asymptotic analysis of the list-decoder of turbo codes in [28] shows that the coding gain of list turbo decoder is higher than the coding gain of list-convolutional decoder. Specifically, due to the low probability of multiple free-distance error events in a turbo-encoded sequence, the asymptotic coding gain is determined by the second minimum distance, yielding higher gain [28]. For the case of serially concatenated VLC's and convolutional codes, we show experimentally in Section 2.7 that significant improvements in coding performance can be achieved.

### 2.6.3 Non-Binary CRC

Wicker [29] provides a comprehensive background on Galois fields, rings of polynomials on Galois fields, and the construction of cyclic codes. We give here a quick summary of the key results and as well as the procedure for designing non-binary CRC's.

Cyclic codes are built using a generator polynomial on the underlying Galois field  $\text{GF}(q)$ . If the number of symbols in our application is not a power of a prime, the next higher appropriate  $q$  must be chosen, since for a field  $\text{GF}(q)$ ,  $q$  must be either

a prime or a power of a prime.. Cyclic codes are built from a generator polynomial  $g(X)$  on  $\text{GF}(q)$ . The codewords are all the multiples of  $g(X)$  modulo  $X^n - 1$ , where  $g(X)$  is a degree- $r$  polynomial that divides  $X^n - 1$ .

CRC codes are shortened cyclic codes that can encode up to  $n - r$  information symbols. CRC codes have excellent error detection capability. The CRC code with a generator of degree  $r$  detects all burst errors of length  $r$  or less, and the probability that the CRC will not detect a random error is  $q^{-r}$ . Due to the lack of a convenient way to calculate the error spectrum of a CRC code, ad-hoc methods have been used for code design in the binary case.

Unfortunately the existing ad-hoc techniques for binary CRC design are not particularly helpful for the  $q$ -ary case, but nevertheless, the general structural properties, error coverage, and burst error detection properties remain the same across different underlying Galois fields. Therefore, even though we cannot design CRC with specified minimum distance, still it is possible to arrive at codes that have very respectable error detection performance. For example, for the 5-ary code used in the next section, a reasonable choice for generator polynomial is the primitive polynomial  $X^8 + 4X^6 + X^4 + X^3 + X^2 + 3X + 3$  which requires 8 parity symbols for data sequences of up to 390617 symbols. The undetected codeword error probability for this code is only  $2.56 \times 10^{-6}$ .

## 2.7 Experimental Results

Table 2.1 shows the 5-ary source used in our experiments and various codes designed for this source.  $C_1$  is a Huffman code,  $C_2$  is a RVLC for this source reported in [1], and the codes  $C_3$ ,  $C_4$ , and  $C_5$  were designed by us with successively higher redundancies. The redundancy of the VLC's can be quantified by comparing their



Table 2.1. Family variable-length codes used in Section 2.7

$s$	$P_S(s)$	$C_1$	$C_2$ [1]	$C_3$	$C_4$	$C_5$
0	0.33	00	00	11	011	0100
1	0.30	11	11	001	1100	10011
2	0.18	10	010	0100	10111	101001
3	0.10	010	101	0101100	00000	011110
4	0.09	011	0110	0001010	000101	0000111
E[L]	H=2.14	2.19	2.46	3.61	4.13	5.13
$d_{free}$		1	2	3	4	5

Table 2.2. Generator polynomials of convolutional codes used in Section 2.7 (from [2])

Recursive		Non-Recursive	
CC <sub>1</sub> : rate $\frac{1}{2}$	$\left(1, \frac{1+D^2}{1+D+D^2}\right)$	CC <sub>2</sub> : rate $\frac{1}{2}$	$(1+D^2, 1+D+D^2)$
CC <sub>3</sub> : rate $\frac{2}{3}$	$\begin{pmatrix} 1 & 0 & \frac{1+D^2}{1+D+D^2} \\ 0 & 1 & \frac{1+D}{1+D+D^2} \end{pmatrix}$	CC <sub>4</sub> : rate $\frac{2}{3}$	$\begin{pmatrix} 1+D & D & 1 \\ 1+D & 1 & 1+D \end{pmatrix}$

average length to that of the Huffman code. The Levenshtein distance [18, 4] is used in reporting symbol error rates (SER).

It is noteworthy that despite the differences, the trellises of the different codes have roughly the same order of complexity. This arises due to the sparseness of the VLC trellises, which becomes more pronounced when the code has redundancy. For a more meaningful comparison of complexity, one may construct more compact trellises with minimal number of states. For example,  $C_3$  has a sparse trellis with 13 states and only 17 single-bit branches, which is equivalent to a 4-state compact trellis with 8 branches, the same as the equivalent trellis of code  $C_2$ . Thus the complexities are comparable.

Our inner convolutional codes are four-state codes with rates  $1/2$  or  $2/3$ , as shown in Table 2.2. In our experiments, a packet of  $K$  symbols is entropy-encoded, interleaved, channel encoded, and transmitted using Binary phase-shift keying (BPSK)

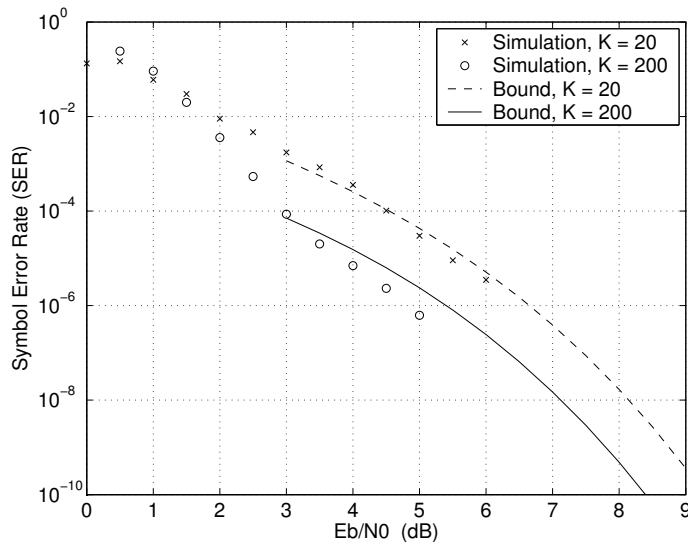


Figure 2.10. Symbol error rate of  $C_2+CC_1$ ,  $K = 20$  and 200 symbols.

modulation over an AWGN channel.

Our first experiment is designed to test the accuracy of our analysis. Figure 2.10 shows union bounds and simulation results for the concatenated code  $C_2+CC_1$ . There are several factors to consider when reading this plot. First, union bounds work in the high  $E_b/N_0$  regions, and the cutoff rate for this code is associated with  $E_b/N_0 = 2.45$  dB. Second, union bounds are calculated for the optimal (ML) decoder, while the simulations, by necessity, use iterative decoding. Finally, calculation of the multiplicities for a nonlinear, variable-length code is a lengthy and time-consuming process, thus we present “truncated bounds” calculated with the first 10 terms of the multiplicities of the outer code that were available in [1]. The decoding experiment was performed with 10 iterations, with packet lengths of 20 and 200. The bounds are in agreement with simulations.

As mentioned in Section 2.4, higher redundancy in the outer VLC leads to higher interleaver gain. To demonstrate this effect, we simulated the variable length codes  $C_4$  and  $C_2$ , each concatenated with the inner code  $CC_1$ . To maintain (approximate)

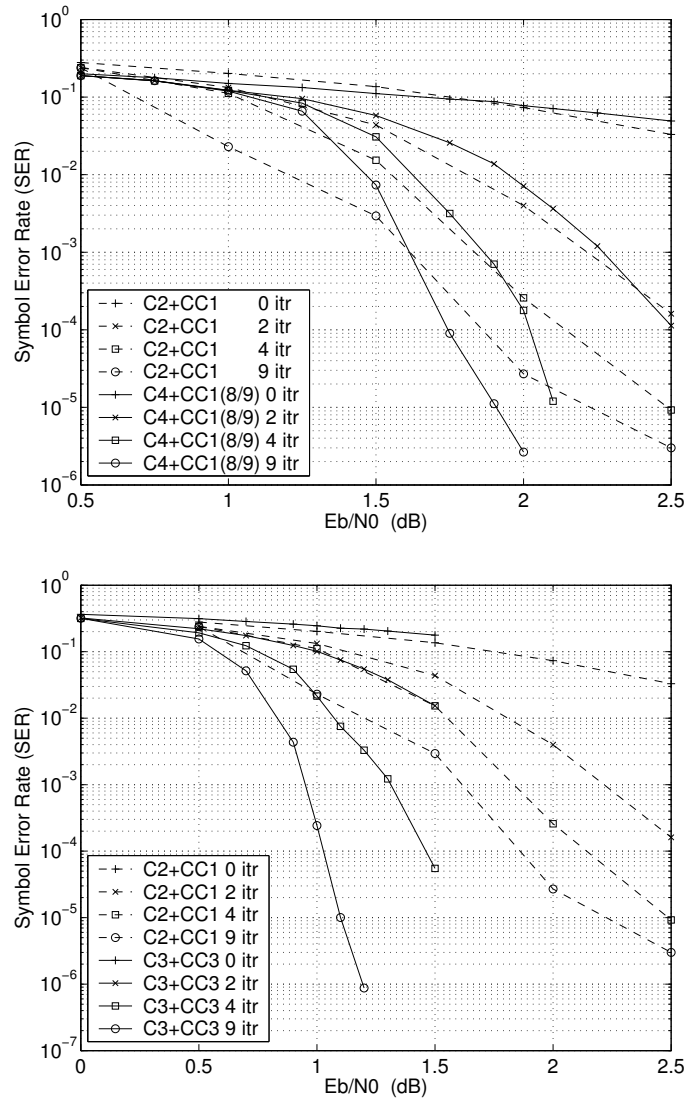


Figure 2.11. Performance of  $C_2+CC_1$ ,  $C_4+CC_1$ (punctured to rate 8/9), and  $C_3+CC_3$ .  $K = 2000$  symbols.

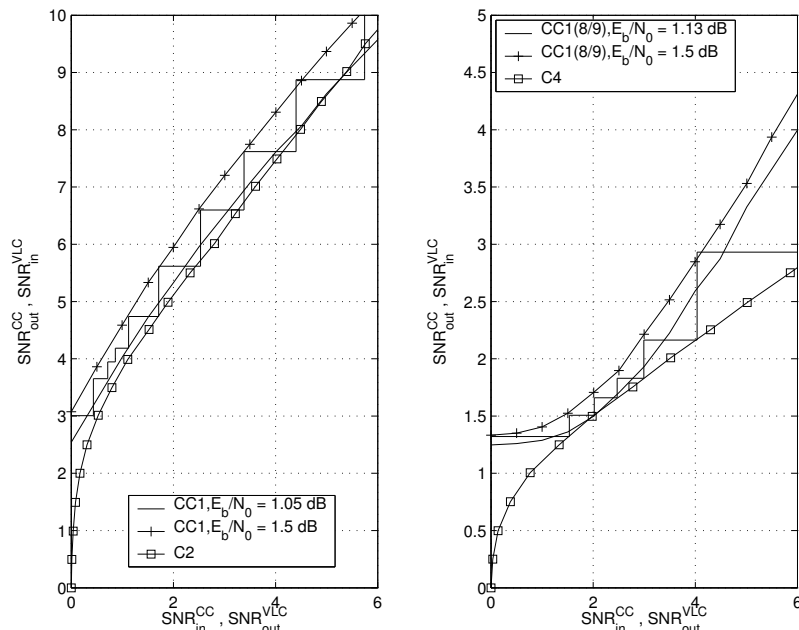


Figure 2.12. Approximate Gaussian density evolution of  $C_2+CC_1$  and  $C_4+CC_1$ (punctured to rate 8/9),  $K = 2000$  symbols. An instance of the convergence of the decoders at  $E_b/N_0 = 1.5$ dB (dashed line staircase) is shown.

mately) the same overall rate, in the experiment with  $C_4$  the inner code is punctured to rate 8/9, hence the notation  $C_4+CC_1(8/9)$ . The overall rates of the two experiments are 0.445 for  $C_2+CC_1$  and 0.471 for  $C_4+CC_1(8/9)$ , where the equivalent “code rate” of a VLC is calculated by dividing the average length of the code by the average length of the Huffman code. The symbol and frame error rates are shown in Figure 2.11 for  $K = 2000$  symbols. For small values of  $E_b/N_0$ , the code  $C_2+CC_1$  outperforms  $C_4+CC_1(8/9)$  due to the more powerful inner code. However, the latter starts outperforming the former for  $E_b/N_0 > 1.5$ dB. The sharper drop in error rate of the latter code is noteworthy.

The corresponding density evolutions of the iterative decoders are shown in Figure 2.12. We use the approximate Gaussian density evolution of [25]. We show density evolutions at  $E_b/N_0 = 1.5$ dB (the dashed-line staircase curve). When  $E_b/N_0 =$

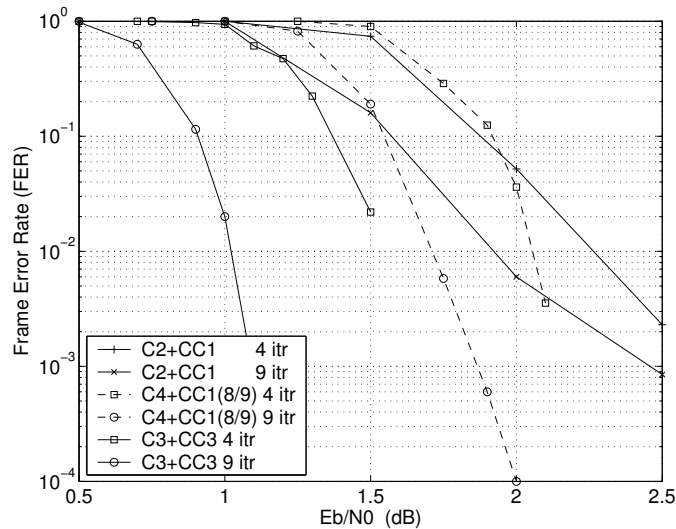


Figure 2.13. FER comparison between  $C_2+CC_1$ ,  $C_4+CC_1$ (punctured to rate 8/9), and  $C_3+CC_3$ .  $K = 2000$  symbols.

1dB, the method predicts that neither of the codes converge. When  $E_b/N_0 = 1.5$ , both codes converge but  $C_4+CC_1(8/9)$  converges faster.

For further comparisons, we used the code  $C_3$  with free distance  $d_f^o = 3$ , concatenated with the inner code  $CC_3$ , a rate 2/3 recursive convolutional code. The concatenated code has overall rate 0.404. The SER and FER of the this code are shown in Figure 2.11. The code  $C_3+CC_3$  outperforms  $C_2+CC_1$  in the entire range of  $E_b/N_0$  after the second iteration of the decoder. The density evolutions of the iterative decoder of  $C_3+CC_3$  is shown in Figure 2.14.

As mentioned previously, Bauer and Hagenauer [1] demonstrated coding gain via iterative source/channel decoding. But in their case the baseline system did not have the advantage of iterative decoding. We pose a slightly different question: assuming we have a fixed computational and rate budget, we would like to compare the source/channel iterative decoder with a separable decoder whose channel decoder is iterative. For experimental verification of this and similar questions, we

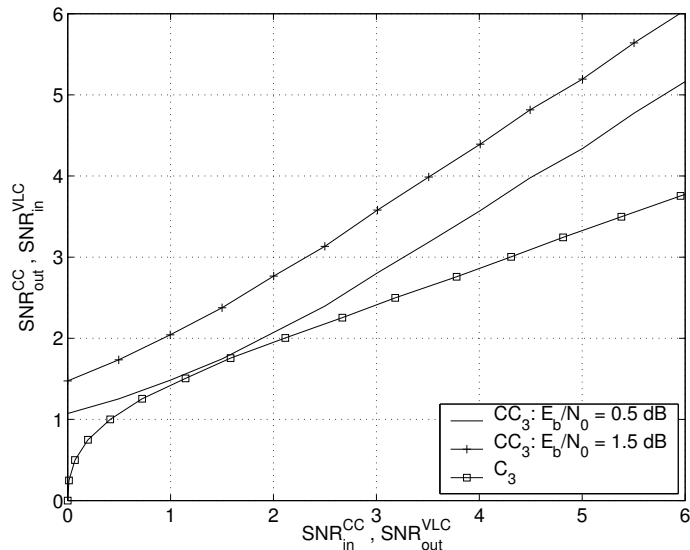


Figure 2.14. Approximate Gaussian density evolution of  $C_3+CC_3$ .

introduce three serial concatenated convolutional codes:  $SCCC_1$ :  $CC_2+CC_1(8/9)$  and  $SCCC_2$ :  $CC_4+CC_3$ , both with overall rate  $4/9$ , and  $SCCC_3$ :  $CC_2+CC_3$  with overall rate  $1/3$ .

We compare the iterative source/channel decoding of  $C_2+CC_1$  with a system consisting of the Huffman code  $C_1$  concatenated with  $SCCC_2$ . The two systems have the same overall rate and decoder complexity. The simulation results are not shown in a separate figure, but one can compare the results of  $C_2+CC_1$  in Figure 2.11 with the results of  $C_1+SCCC_2$  in Figure 2.15 (both for 9 iterations). The comparison indicates that the case of separable source/channel decoding is superior to joint source/channel decoding. We believe this is largely due to the small  $d_{free}$  of  $C_2$ , which is the RVLC used by Bauer and Hagenauer [1]. Therefore, it seems that separable decoding (with an iterative channel decoder) can be superior to iterative source/channel decoding when the outer code has small free distance.

Then one may ask: how does a joint source/channel decoder compare with a separable decoder if we increase the free distance of the outer source code? We

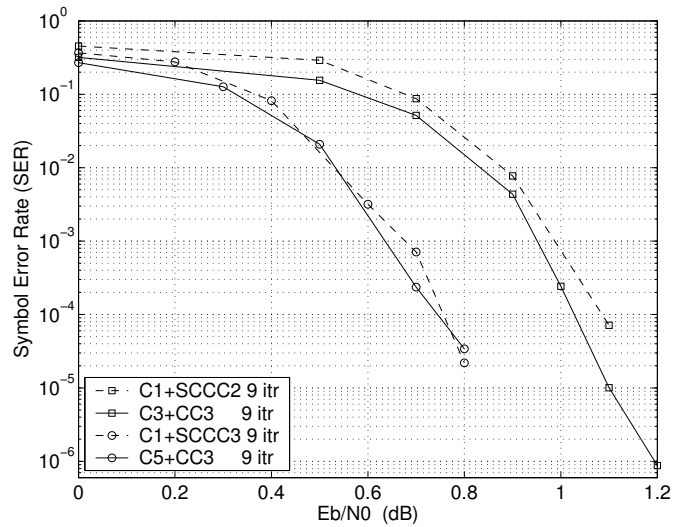


Figure 2.15. Comparison of concatenated redundant VLC and convolutional codes versus concatenated Huffman code and SCCC's,  $K = 2000$  symbols.

designed several experiments to address this question. In a comparison of the separable code  $C_1 + \text{SCCC}_1$  with the joint source/channel decoding of  $C_4 + \text{CC}_1(8/9)$ , we found that especially at higher  $E_b/N_0$ , the joint source/channel decoding works much better, while at intermediate  $E_b/N_0$  the two methods perform the same.

We conducted two more experiments, whose results are shown in Figure 2.15. The separable code  $C_1 + \text{SCCC}_2$ , is compared against  $C_3 + \text{CC}_3$  (both with rates  $\sim 4/9$ ), where  $C_3 + \text{CC}_3$  outperforms  $C_1 + \text{SCCC}_2$  slightly. In the same Figure 2.15,  $C_1 + \text{SCCC}_3$  is compared against  $C_5 + \text{CC}_3$  (both with rate  $\sim 1/3$ ), and they perform roughly similarly.

Thus, the simulations did not point to a clear and universal advantage for either the joint or separable approach. In some cases, where the outer entropy code has low redundancy, the separable case is clearly better, while in other cases either the joint or the separable solution might be superior. The design choices must be made on a case-by-case basis.

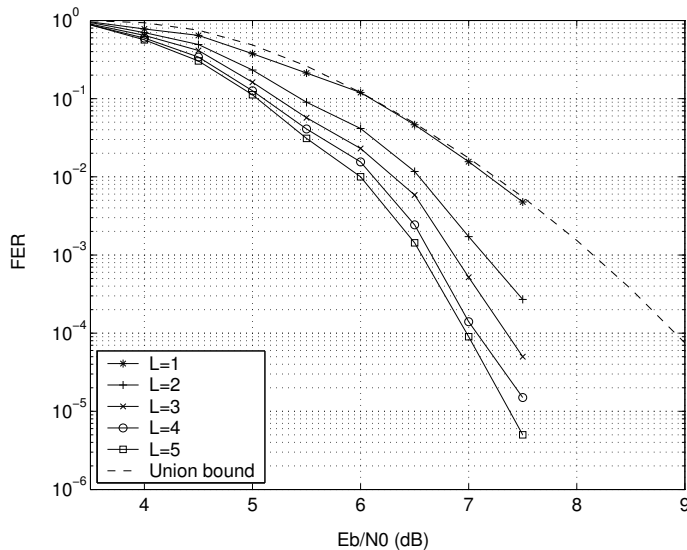


Figure 2.16. List-decoding of  $C_2$  in AWGN channel,  $K=200$ .

### 2.7.1 Iterative List Decoding

We first present the performance of list-decoding of a VLC with no channel coding. The FER of  $C_2$ , with  $K = 200$  symbols in the AWGN channel is shown in Figure 2.16. The coding gain of the list-decoder is almost 1.1dB for  $L = 2$ , 1.5dB for  $L = 3$ , and 1.8dB for the  $L = 4$ . The upper bound of the  $L = 1$  case is calculated based on the truncated union bound and the distance spectrum given in [1].

The coding gain predicted by [27] for  $L = 2$  and  $L = 3$  list-decoders are 1.25dB and 1.75dB, respectively. From Figure 2.16, we observe that the predicted gains are more than the actual gain. Using the multiplicity of the free distance of  $C_2$  provided in [1], one can calculate the more realistic coding gain as described in Section 2.6.1. Minor modifications may be necessary because we seek coding gain in FER and with  $K = 200$ . The coding gain at FER= $10^{-4}$  is 1dB for  $L = 2$  and 1.4dB for  $L = 3$ . We see that these gains better match the results of Figure 2.16.

To demonstrate the performance of the proposed iterative list-decoder, we consider the two concatenated codes presented previously:  $C_2+CC_1$  and  $C_3+CC_3$ .



Figure 2.17 presents the FER of the list-iterative decoder at the first, second, and third iterations with  $L = 1, 3$  in AWGN channel with  $K = 500$ . We observe that the coding gain of list-decoding varies for each code at each iteration. The coding gain for the two codes for a given FER and at a given iteration are about the same. For example, at the third iteration the list-decoder  $L = 3$  provides a coding gain of 0.25dB at FER=  $10^{-3}$ . We also notice that  $C_3+CC_3$  outperforms  $C_2+CC_1$ . Figure 2.18 reports the FER of the concatenated codes in a fully-interleaved Rayleigh channel with  $K = 200$ . At this frame size, which is a tenth of the frame size of the experiment in Figure 2.11(b), the difference of the two concatenated codes is less pronounced, but still  $C_3+CC_3$  has lower error rate except in the first iteration. The coding gain of list-decoding is higher in fully-interleaved Rayleigh channel. In fact, list-decoding provides improved diversity in this channel due to an increase in the equivalent free distance of the code [27]. Thus, regardless of the channel type, the coding gain of list decoding increases in higher  $E_b/N_0$ .

Iterative list-decoder of the concatenated code  $C_2+CC_2$  has a slightly different coding gain. For example, the coding gain at the fifth iteration for  $L = 2$  is about 1.5dB in Rayleigh fading channel and 0.75dB with  $L = 5$  in AWGN channel.

## 2.8 Chapter Summary

We obtain union bounds for the symbol and frame error rates of concatenated source/channel codes for finite-alphabet sources. We generalize the previous notions of outer entropy code by inserting an unrestricted redundant variable length code; thus our analysis is general with respect to the choice of the outer code, including non-redundant (Huffman) codes, RVLC codes, and the so-called variable-length error correcting codes. We use techniques originally developed for the serial concatenated

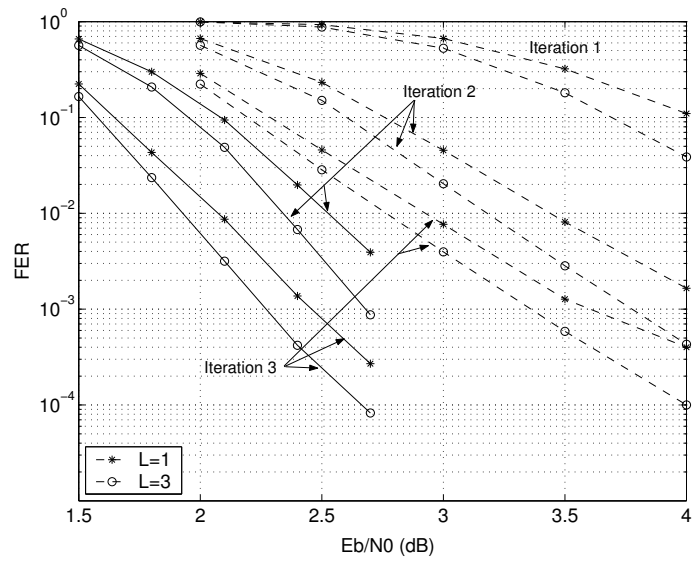


Figure 2.17. Iterative list-decoding of  $C_2+CC_1$  (dashed) and  $C_3+CC_3$  (solid line) in AWGN channel,  $K=500$ .

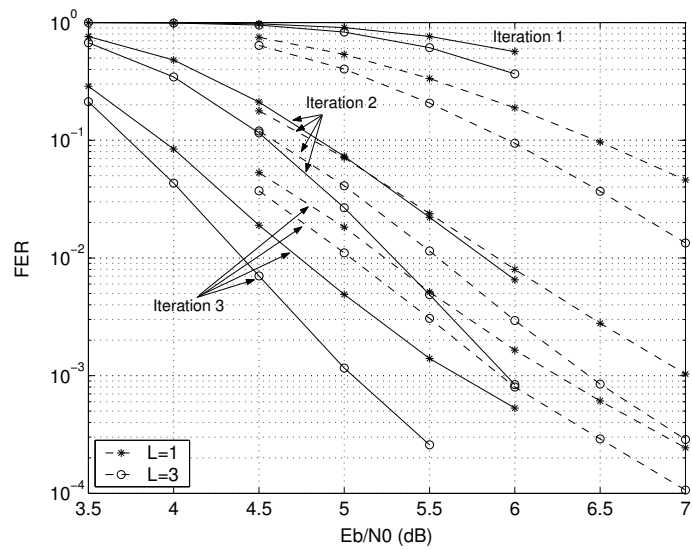


Figure 2.18. Iterative list-decoding of  $C_2+CC_1$  (dashed) and  $C_3+CC_3$  (solid line) in fully-interleaved Rayleigh channel,  $K=200$ .

convolutional codes and adapt them so that they can be used with the nonlinear outer codes that are of interest in source/channel coding. By evaluating the union bounds of the concatenated scheme, we further studied the role of the constituent codes, and illustrated through simulations the relevance of the suggested design rules.

We also propose an iterative list-decoder for VLC-based source-channel codes. The list decoder is made possible by a non-binary CRC code which also provides a stopping criterion for the iterative decoder. At a given iteration of the iterative decoder, the proposed list decoder improves the overall performance of the system. Extensive experimental results are provided in AWGN and fully-interleaved Rayleigh channels.

## CHAPTER 3

### PERFORMANCE OF EQUALIZERS IN FREQUENCY-SELECTIVE SINGLE-ANTENNA FADING CHANNELS

The performance of equalizers in fading channels is mainly characterized by diversity. First, we evaluate the performance and diversity order of maximum-likelihood equalizers, and extend the results to cases with and without correlation between the channel taps. Next, we derive the performance linear equalizers. We focus on outage probability as a theoretical lower bound on the performance. We consider decision-feedback equalizers as well and evaluate their performance.

#### 3.1 Introduction

In frequency-selective fading channels, each symbol is affected by multiple fading coefficients, providing a natural diversity to encounter the unreliable channel. However, the inter-symbol interference makes it difficult for the receiver to exploit this diversity.

It is known that the maximum likelihood sequence estimator (MLSE) equalizer is able to extract the full diversity. Through pair-wise error probability and moment generating function (MGF), we show in Section 3.2 that the maximum likelihood (ML) detector does not prevent the receiver from achieving full diversity. We extend the results to the case where the channel taps are correlated.

Maximum-likelihood equalizers are complex and have limited application in practice. Linear equalizers, zero-forcing (ZF) and minimum mean square error (MMSE)

equalizers, are attractive because of their low-complexity. However, compared to ML equalizers, linear equalizers have inferior performance and lower diversity. In Section 3.3, we show analytically and experimentally that zero-forcing linear equalizers are unable to harvest the available diversity in the frequency-selective channel. In high spectral efficiency, minimum mean square linear equalizers behave the same, however, in low spectral efficiency they are capable of achieving some of the available diversity<sup>1</sup>.

### 3.2 MLSE Equalizer

In the following, we derive the error rate of MLSE equalizers in frequency-selective SISO channels. Assume the frequency-selective channel  $h(D)$  whose taps are symmetric complex Gaussian random variables :

$$h(D) = h_0 + h_1D + h_2D^2 \cdots + h_\nu D^\nu$$

where  $\nu$  represents the memory of the channel. Assuming additive white Gaussian noise (AWGN), the transmission of  $L$  symbols over such channel results in the following matrix system model:

$$\mathbf{r} = \mathbf{H}\mathbf{c} + \mathbf{n}$$

$$\begin{pmatrix} r_L \\ r_{L-1} \\ \vdots \\ r_1 \end{pmatrix} = \begin{pmatrix} h_0 & h_1 & \cdots & h_\nu & 0 & \cdots & 0 \\ 0 & h_0 & h_1 & \cdots & h_\nu & \cdots & 0 \\ \vdots & \ddots & \ddots & \ddots & \ddots & \ddots & \vdots \\ 0 & \cdots & 0 & h_0 & h_1 & \cdots & h_\nu \end{pmatrix} \begin{pmatrix} c_L \\ c_{L-1} \\ \vdots \\ c_1 \end{pmatrix} + \begin{pmatrix} n_L \\ n_{L-1} \\ \vdots \\ n_1 \end{pmatrix} . \quad (3.1)$$

Assuming perfect knowledge about the channel taps  $h_i$ 's at the receiver, the maximum likelihood (ML) metric is given by :

$$m(\mathbf{r}, \mathbf{c}) = \|\mathbf{r} - \mathbf{H}\mathbf{c}\|^2 .$$

---

<sup>1</sup>The contribution of this chapter appears in part in [30].

An error occurs when the MLSE equalizer decides in favor of the sequence  $\hat{\mathbf{c}}$  when the sequence  $\mathbf{c}$  is actually transmitted. The pairwise error probability of  $\mathbf{c}$  and  $\hat{\mathbf{c}}$ :

$$\Pr(\mathbf{c}, \hat{\mathbf{c}}|\mathbf{H}) = Q\left(\sqrt{\frac{\gamma}{2}}\|\mathbf{H}\Delta\|\right), \quad (3.2)$$

where  $\Delta = \mathbf{c} - \hat{\mathbf{c}}$ . The unconditional pairwise error probability is

$$\Pr(\mathbf{c}, \hat{\mathbf{c}}) = \mathbb{E}_{\mathbf{H}}(\Pr(\mathbf{c}, \hat{\mathbf{c}}|\mathbf{H})),$$

and the overall error probability is the average of  $\Pr(\mathbf{c}, \hat{\mathbf{c}})$  over all possible pairs of  $\mathbf{c}$  and  $\hat{\mathbf{c}}$ . Using the alternative definition of Q-function by a finite integral [31]

$$Q(x) = \int_0^{\pi/2} \exp\left(-\frac{x^2}{2\sin^2\theta}\right) d\theta, \quad (3.3)$$

and by integrating over all channel realizations we obtain the unconditional PEP as follows:

$$P(\mathbf{c}, \hat{\mathbf{c}}) = \mathbb{E}_{\mathbf{H}}(Pr(\mathbf{c}, \hat{\mathbf{c}}|\mathbf{H})) = \int_0^{\pi/2} \Phi_{\Gamma}\left(-\frac{\rho}{4\sin^2\theta}\right) d\theta \quad (3.4)$$

where  $\Phi_{\Gamma}(\cdot)$  is the MGF of the random variable  $\Gamma \triangleq \|\mathbf{H}\Delta\|^2$ , and  $\rho = \frac{\mathcal{E}_x}{N_0}$  is the SNR. For later reference we define  $s \triangleq -\frac{\rho}{4\sin^2\theta}$ . We notice that the PEP is fully expressed by the MGF of  $\Gamma$ . We seek this MGF for performance evaluation. Also, the asymptotic behavior of  $P(\mathbf{c}, \hat{\mathbf{c}})$  is the same as asymptotic behavior of  $\Phi_{\Gamma}(\cdot)$ , which determines the MLSE diversity.

The ML metric  $\Gamma = \|\mathbf{H}\Delta\|^2$  for the system model in (3.1) can be derived as

$$\|\mathbf{H}\Delta\|^2 = \text{tr}(\mathbf{H}\Delta\Delta^H\mathbf{H}^H) = \text{tr}(\Delta^H\mathbf{H}^H\mathbf{H}\Delta) = \Delta^H\mathbf{H}^H\mathbf{H}\Delta. \quad (3.5)$$

Note that because of the structure of the matrix channel  $\mathbf{H}$  in (3.1),  $\mathbf{H}\Delta$  can be written as follows

$$\mathbf{H}\Delta = \begin{pmatrix} h_0 & h_1 & \cdots & h_{\nu} & 0 & \cdots & 0 \\ 0 & h_0 & h_1 & \cdots & h_{\nu} & \cdots & 0 \\ \vdots & \ddots & \ddots & \ddots & \ddots & \ddots & \vdots \\ 0 & \cdots & 0 & h_0 & h_1 & \cdots & h_{\nu} \end{pmatrix} \begin{pmatrix} \delta_L \\ \delta_{L-1} \\ \vdots \\ \delta_1 \end{pmatrix} = \begin{pmatrix} \mathbf{h}\Delta_{L-\nu} \\ \mathbf{h}\Delta_{L-\nu+1} \\ \vdots \\ \mathbf{h}\Delta_L \end{pmatrix}, \quad (3.6)$$

where  $\mathbf{h} = (h_0, h_1, \dots, h_\nu)$ , and  $\mathbf{\Delta}_i \triangleq (\delta_{i+\nu}, \dots, \delta_i)$ , a sub-vector of  $\mathbf{\Delta}$  with length  $\nu + 1$ . Therefore, the ML metric (3.5) can be written as:

$$\|\mathbf{H}\mathbf{\Delta}\|^2 = \sum_{i=0}^{L-\nu} \mathbf{\Delta}_i^H \mathbf{h}^H \mathbf{h} \mathbf{\Delta}_i \quad (3.7)$$

$$= \sum_{i=0}^{L-\nu} \mathbf{h} \mathbf{\Delta}_i \mathbf{\Delta}_i^H \mathbf{h}^H = \mathbf{h} \mathbf{\Omega} \mathbf{h}^H, \quad (3.8)$$

where

$$\mathbf{\Omega} \triangleq \sum_{i=0}^{L-\nu} \mathbf{\Delta}_i \mathbf{\Delta}_i^H \quad (3.9)$$

is a square matrix with size  $\nu + 1$ . The random variable  $\Gamma = \mathbf{h} \mathbf{\Omega} \mathbf{h}^H$  is quadratic in the Gaussian random vector  $\mathbf{h}$ . The following Lemma gives us the MGF of such quadratic forms.

**Lemma** [32]: Let  $\mathbf{A}$  be a Hermitian matrix and  $\mathbf{u}$  a circularly symmetric complex Gaussian vector with mean  $\bar{\mathbf{u}}$  and covariance matrix  $\mathbf{R}_{\mathbf{u}}$ . The MGF of the quadratic form  $y = \mathbf{u} \mathbf{A} \mathbf{u}^H$  is given as

$$\Phi_y(s) = \int_0^\infty e^{sy} p_Y(y) dy = \frac{\exp(-\bar{\mathbf{u}} \mathbf{A} (\mathbf{I} - s \mathbf{R}_{\mathbf{u}} \mathbf{A})^{-1} \bar{\mathbf{u}}^H)}{\det(\mathbf{I} - s \mathbf{R}_{\mathbf{u}} \mathbf{A})}, \quad (3.10)$$

where  $\mathbf{I}$  is the identity matrix with appropriate size.  $\square$

Using above Lemma, we can obtain the MGF of  $\Gamma = \mathbf{h} \mathbf{\Omega} \mathbf{h}^H$ . First consider the case where  $\mathbf{h}$  has independent components, which leads to

$$\Phi_\Gamma(s) = \frac{1}{\det(\mathbf{I} - s \mathbf{\Omega})} = \prod_{i=0}^{\nu} (1 - s \lambda_i(\mathbf{\Omega}))^{-1}, \quad (3.11)$$

where  $\lambda_i(\mathbf{\Omega})$  is an eigenvalue of matrix  $\mathbf{\Omega}$ . In high SNR,  $\Phi_\Gamma(s)$  behaves as

$$\Phi_\Gamma(-s) \doteq \prod_{\lambda_i(\mathbf{\Omega}) \neq 0} (s \lambda_i(\mathbf{\Omega}))^{-1} = \frac{s^{-(\nu+1)}}{\det(\mathbf{\Omega})}, \quad (3.12)$$

where  $\doteq$  expresses the asymptotic equivalence<sup>2</sup>, and for the second equality all the eigenvalues  $\lambda_i(\mathbf{\Omega})$  are assumed nonzero. Equation (3.12) shows that if  $\mathbf{\Omega}$  is full-rank, the MGF, and subsequently the PEP, decays as  $\rho^{-(\nu+1)}$ . Hence, the diversity order is  $\nu + 1$ .

One might ask if the maximum diversity  $\nu + 1$  is obtainable without coding. If the vector  $\mathbf{c}$  does not have any redundancy then  $\mathbf{c}$  and  $\hat{\mathbf{c}}$  are different in at most one position, hence  $\mathbf{\Delta}$  has only one nonzero element. Let's assume that the position of the nonzero element of  $\mathbf{\Delta}$  is somewhere that makes exactly  $\nu + 1$  of  $\mathbf{\Delta}_i$  vectors nonzero. Equation (3.9) shows that  $\mathbf{\Omega}$  becomes a multiple of the identity matrix, hence has rank  $\nu + 1$ . Therefore, to obtain the full frequency diversity the data need not be redundant.

Now consider the case where  $\mathbf{h}$  is a Gaussian vector with covariance  $\mathbf{R}$ . One can write  $\mathbf{h}$  based on the white Gaussian vector  $\tilde{\mathbf{h}}$  as :  $\mathbf{h} = \tilde{\mathbf{h}}\mathbf{R}^{\frac{1}{2}}$ . Hence, the ML metric is  $\Gamma = \tilde{\mathbf{h}}\mathbf{R}^{\frac{1}{2}}\mathbf{\Omega}\mathbf{R}^{\frac{H}{2}}\tilde{\mathbf{h}}^H$ ; still a quadratic form but with a different kernel than the previous case. The MGF is

$$\Phi_{\Gamma}(s) = \frac{1}{\det\left(\mathbf{I} - s\mathbf{R}^{\frac{1}{2}}\mathbf{\Omega}\mathbf{R}^{\frac{H}{2}}\right)} = \frac{1}{\det(\mathbf{I} - s\mathbf{R}\mathbf{\Omega})} = \prod_{i=0}^{\nu} (1 - s\lambda_i(\mathbf{R}\mathbf{\Omega}))^{-1} . \quad (3.13)$$

We notice that in this case, the matrix  $\mathbf{R}\mathbf{\Omega}$  has the same role as  $\mathbf{\Omega}$  had in (3.11). Therefore, as long as the covariance matrix  $\mathbf{R}$  is full-rank, full diversity order can be obtained. However, the correlated vector  $\mathbf{h}$  indeed causes performance loss, but no diversity loss. The incurred loss in performance is  $\det(\mathbf{R})$ . This can be observed in the asymptotic behavior of  $\Phi_{\Gamma}(-s)$  :

$$\Phi_{\Gamma}(-s) \doteq \det(\mathbf{R}) \det(\mathbf{\Omega}) s^{-(\nu+1)} . \quad (3.14)$$

---

<sup>2</sup> $a \doteq b$  is equivalent to  $a = O(b)$ .



### 3.3 Linear Equalizers

To evaluate the performance of linear equalizers in frequency-selective fading channels, we consider block transmission and apply the equalization in matrix-form. Assume the system model (3.1). The block ZF-LE has the matrix form:

$$\mathbf{F}_{\text{ZF}} = (\mathbf{H}^H \mathbf{H})^{-1} \mathbf{H}^H, \quad (3.15)$$

which transforms the received signal to

$$\hat{\mathbf{r}} = \mathbf{F}_{\text{ZF}} \mathbf{r} = \mathbf{c} + (\mathbf{H}^H \mathbf{H})^{-1} \mathbf{H}^H \mathbf{n}. \quad (3.16)$$

The MMSE-LE has the matrix form:

$$\mathbf{F}_{\text{MMSE}} = (\mathbf{H}^H \mathbf{H} + \gamma^{-1} \mathbf{I})^{-1} \mathbf{H}^H, \quad (3.17)$$

which transforms the received signal to

$$\hat{\mathbf{r}} = \mathbf{F}_{\text{MMSE}} \mathbf{r} = (\mathbf{H}^H \mathbf{H} + \gamma^{-1} \mathbf{I})^{-1} \mathbf{H}^H \mathbf{H} \mathbf{c} + (\mathbf{H}^H \mathbf{H} + \gamma^{-1} \mathbf{I})^{-1} \mathbf{H}^H \mathbf{n}. \quad (3.18)$$

In the case of ZF-LE, the equivalent noise is  $\tilde{\mathbf{n}} \triangleq (\mathbf{H}^H \mathbf{H})^{-1} \mathbf{H}^H \mathbf{n}$ , which is a complex Gaussian vector with zero-mean and covariance matrix

$$\mathbf{R}_{\tilde{\mathbf{n}}} = \mathbb{E}((\mathbf{H}^H \mathbf{H})^{-1} \mathbf{H}^H \mathbf{n}) = \sigma_n^2 (\mathbf{H}^H \mathbf{H})^{-1}. \quad (3.19)$$

In linear equalizers, symbols are detected individually, ignoring the correlation between noise components. Therefore, only the diagonal elements of  $\mathbf{R}_{\tilde{\mathbf{n}}}$  are involved in the calculation of SNR.

For mathematical tractability, we assume that the data is appended by cyclic prefix (CP). Adding CP to the data, makes the equivalent channel a circulant matrix, thus facilitating the analysis of  $\mathbf{R}_{\tilde{\mathbf{n}}}$ . We benefit from the following well-known property of circulant matrices.

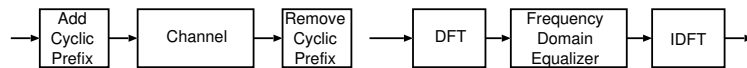


Figure 3.1. Single-carrier frequency-domain equalizer

**Fact:** Let  $\mathbf{H}$  be a circulant matrix of size  $L$ . The eigen decomposition of  $\mathbf{H}$  is  $\mathbf{H} = \mathbf{Q}\mathbf{\Lambda}\mathbf{Q}^H$ , where  $\mathbf{Q}$  is the Discrete Fourier Transform (DFT) matrix:

$$\mathbf{Q}(p, q) = \frac{1}{\sqrt{L}} \exp\left(-j\frac{2\pi}{L}(p-1)(q-1)\right),$$

and the diagonal elements of  $\mathbf{\Lambda}$  are the  $L$ -point Discrete Fourier transform of the first row of  $\mathbf{H}$ .  $\square$

The block-based linear equalizer with CP is equivalent to single-carrier frequency domain equalizer (SC-FDE) [33, 34], as depicted in Figure 3.1, because the noise covariance matrix (3.19), assuming cyclic prefix, is identical to the noise covariance matrix of SC-FDE.

Under the circulant channel model,  $\mathbf{H} = \mathbf{Q}\mathbf{\Lambda}\mathbf{Q}^H$ , the noise covariance in (3.19) is

$$\mathbf{R}_{\tilde{\mathbf{n}}} = \sigma_n^2 (\mathbf{H}^H \mathbf{H})^{-1} = \sigma_n^2 \mathbf{Q} \mathbf{\Lambda}^{-1} \mathbf{\Lambda}^{-H} \mathbf{Q}^H \quad (3.20)$$

where  $\mathbf{\Lambda} = \text{diag}(\boldsymbol{\lambda})$  and  $\boldsymbol{\lambda} = \mathbf{Q}^H \mathbf{h}$ , where  $\mathbf{h}$  is the first row of  $\mathbf{H}$  in (3.1).

We assume the channel taps  $h_i$  to be i.i.d. complex Gaussian variables with zero-mean and variance  $\sigma_i^2$ . Therefore,  $\boldsymbol{\lambda}$ , the  $L$ -point DFT of the channel vector  $\mathbf{h}$ , is a complex Gaussian vector with zero-mean and covariance matrix

$$\mathbf{R}_{\boldsymbol{\lambda}}(m, n) = \frac{1}{L} \sum_{p=0}^{\nu} \sigma_p^2 \exp\left(-j\frac{2\pi}{L}(m-n)p\right). \quad (3.21)$$

Note that, in general,  $\lambda_i$  are dependent Gaussian RV's, but if  $L = \nu + 1$  they become independent.

Evaluation of statistical expressions involving components of  $\boldsymbol{\lambda}$  is difficult. Multivariate Rayleigh and exponential do not in general possess a closed-form probability density function (PDF) or moment generating function (MGF) [35]. Even for the multivariate exponential  $\boldsymbol{\lambda}$  which is based upon a circularly symmetric Gaussian vector, the joint PDF involves multiple integrations. In the following, to simplify the problem, we sometimes assume that the random vector  $\boldsymbol{\lambda}$  is an i.i.d. vector. If  $\nu + 1 = L$  the noise covariance (3.21) is indeed diagonal, therefore  $\boldsymbol{\lambda}$  is i.i.d. If  $\nu$  is large enough, the off-diagonal elements are negligible.

Our objective is to calculate the asymptotic behavior and diversity order of the linear equalizers. The system model (3.1) shows that the diversity order is the same for  $\nu + 1 = L$  and  $\nu + 1 \neq L$ . This observation comes from the fact that for both cases each symbol is affected by exactly  $\nu + 1$  fading coefficients. Therefore, for analytical studies, we assume  $\nu + 1 = L$  where  $\boldsymbol{\lambda}$  has independent components. Later we present experimental results that indicate our analytical findings are also valid for  $\nu + 1 \neq L$ .

As a result of the independence assumption, the multivariate exponential random vector  $\mathbf{X}$ , defined as  $X_i \triangleq |\lambda_i|^2$ , has PDF:

$$f(X_1, \dots, X_L) = \frac{\exp\left(-\sum_{k=1}^L \frac{X_k}{2\sigma_k^2}\right)}{\prod_{k=1}^L 2\sigma_k^2}. \quad (3.22)$$

In the following we provide the statistics of the decision-point signal-to-interference-and-noise ratio (SINR) of ZF-LE and MMSE-LE.

### **SINR of ZF-LE**

As seen in (3.16), ZF-LE cancels the interference fully. Hence, the SINR is equal to SNR.

The equivalent noise of ZF-LE output is correlated. Applying the symbol-by-symbol detection, the correlation between noise components is ignored, and only the diagonal elements of  $\mathbf{R}_{\bar{\mathbf{n}}}$  are involved in SNR calculation. Substituting  $\mathbf{Q}$  in (3.20), we have

$$\mathbf{R}_{\bar{\mathbf{n}}}(i, i) = \frac{\sigma_n^2}{L} \sum_{k=1}^L |\Lambda(k, k)|^{-2} = \frac{\sigma_n^2}{L} \sum_{k=1}^L |\lambda_k|^{-2} , \quad (3.23)$$

where  $\sigma_n^2$  is the AWGN variance. Since the diagonal elements of  $\mathbf{R}_{\bar{\mathbf{n}}}$  are equal, the decision-point SNR's of all symbols are also equal and determined by the random variable

$$\gamma = \frac{\rho}{\frac{1}{L} \sum_{k=1}^L |\lambda_k|^{-2}} , \quad (3.24)$$

where  $\rho = \frac{\mathcal{E}_s}{\sigma_n^2}$  is the signal to noise ratio. The decision-point SNR in (3.24) is the harmonic average of  $|\lambda_k|^2$ ,  $k = 1, \dots, L$ . We evaluate the statistics of  $\gamma$  as follows.

Let  $X$  be an exponential random variable with variance  $2\sigma^2$ , and PDF  $f_X(x) = \frac{1}{2\sigma^2} \exp\left(-\frac{x}{2\sigma^2}\right)$ . The MGF of  $Y = X^{-1}$  is

$$\begin{aligned} \Phi_Y(-s) &= \int_0^\infty e^{sy} f_Y(y) dy = \int_0^\infty e^{\frac{s}{x}} f_X(x) dx \\ &= \sqrt{\frac{2s}{\sigma^2}} K_1\left(\sqrt{\frac{2s}{\sigma^2}}\right) , \end{aligned} \quad (3.25)$$

where  $K_m(\cdot)$  is the  $m$ -th order modified Bessel function of the second kind [36, 37]. In evaluating (3.25), we have used Equation (3.471.9) in [37] which is reported here for convenience:

$$\int_0^\infty x^{m-1} \exp\left(-\frac{b}{x} - cx\right) dx = 2 \left(\frac{b}{c}\right)^{m/2} K_m\left(2\sqrt{bc}\right) . \quad (3.26)$$

Using (3.25), the MGF of  $Z = \frac{1}{L} \sum_{i=1}^L X_i^{-1}$  (arithmetic mean of inverse of  $L$  independent exponential random variables) is

$$\Phi_Z(-s) = \left(\frac{2s}{L\sigma^2}\right)^{\frac{L}{2}} K_1^L\left(\sqrt{\frac{2s}{L\sigma^2}}\right) . \quad (3.27)$$

Subsequently, using the Laplace transform differentiation property, we obtain the CDF of  $Z$

$$F_Z(z) = \mathcal{L}^{-1} \left( \frac{\Phi_Z(-s)}{s} \right).$$

Note that  $\Gamma = Z^{-1}$ . Thus

$$F_\Gamma(\gamma) = \Pr(\Gamma \leq \gamma) = \Pr \left( Z > \frac{1}{\gamma} \right) = 1 - F_Z \left( \frac{1}{\gamma} \right). \quad (3.28)$$

Using (3.27) and (3.28)

$$F_\Gamma(\gamma) = 1 - \mathcal{L}^{-1} \left( \left( \frac{2}{L\sigma^2} \right)^{\frac{L}{2}} s^{\frac{L}{2}-1} K_1^L \left( \sqrt{\frac{2s}{L\sigma^2}} \right) \right), \quad (3.29)$$

where the inverse Laplace transform is evaluated at  $\gamma^{-1}$ . The CDF of  $\Gamma$  in (3.29) does not have a closed form except for  $L = 2$ .

In the special case of  $L = 2$

$$\begin{aligned} F_\Gamma(\gamma) &= 1 - \mathcal{L}^{-1} \left( \frac{1}{\sigma^2} K_1^2 \left( \sqrt{\frac{s}{\sigma^2}} \right) \right) \\ &= 1 - \frac{\gamma}{2\sigma^2} \exp \left( -\frac{\gamma}{2\sigma^2} \right) K_1 \left( \frac{\gamma}{2\sigma^2} \right). \end{aligned} \quad (3.30)$$

Using the differentiation property of  $K_m(\cdot)$  functions [36, 37], the PDF of  $\Gamma$  is

$$f_\Gamma(\gamma) = \gamma e^{-\gamma} (K_0(\gamma) + K_1(\gamma)). \quad (3.31)$$

With the help of the Equation (6.621.3) of [37], the MGF is given by

$$\Phi_\Gamma(s) = \frac{2}{(2+s)^2} F \left( 2, 0.5; 2.5; \frac{s}{2+s} \right) + \frac{2}{(2+s)^3} F \left( 3, 1.5; 2.5; \frac{s}{2+s} \right), \quad (3.32)$$

where  $F(\cdot, \cdot; \cdot; \cdot)$  is the hypergeometric function [37].

In Figure 3.2(a), the MGF (3.32) along with the Monte-Carlo evaluation of  $\Phi_\Gamma(s)$  for  $\nu = 1, 3, 7$  are shown (in each case  $L = \nu + 1$ ). Asymptotic behavior of  $\Phi_\Gamma(s)$  does not depend on  $\nu$ .

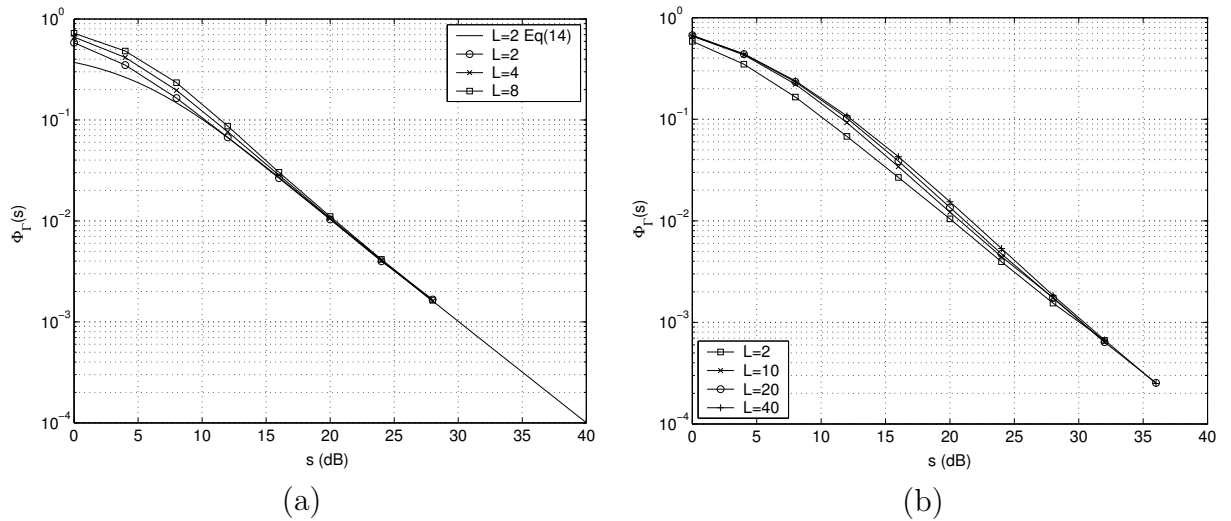


Figure 3.2. Moment generating function of  $\Gamma$  (a)  $L = \nu + 1 = 2, 4, 8$  (b)  $\nu = 1$  and  $L = 2, 10, 20, 40$ .

It is natural to ask: is this invariance to  $\nu$  (channel memory) specific to the case  $L = \nu + 1$ , or is it general? The Monte-Carlo evaluation of  $\Phi_\Gamma(s)$  for  $\nu = 1$  and  $L = 2, 10, 20, 40$  are shown in Figure 3.2(b). We observe that  $\Phi_\Gamma(s)$  for the various cases behave asymptotically the same, thus it seems that invariance to  $\nu$  is a general property. Figure 3.2 shows that the diversity order of the ZF-LE is one for arbitrary  $\nu$  and  $L$ . In the next subsection, we prove this observation for the case  $L = \nu + 1$ .

### SINR of MMSE-LE

The MMSE equalizer does not fully remove the interference. It can be shown that the output SINR is [38]

$$\gamma_k = \frac{1}{(\rho \mathbf{H}^H \mathbf{H} + \mathbf{I})_k^{-1}} - 1, \quad (3.33)$$

where  $(\mathbf{M})_k^{-1}$  denotes the  $k$ th diagonal element of the inverse of  $\mathbf{M}$ . Assuming the CP and the circulant channel matrix  $\mathbf{H}$  with eigenvalues  $\boldsymbol{\lambda}$ , we obtain the decision-point

SINR as

$$\gamma = \frac{L}{\sum_{k=1}^L \frac{1}{1+\rho|\lambda_k|^2}} - 1, \quad (3.34)$$

which is the same for all  $k$ 's. The harmonic average of the random variables  $1 + \rho|\lambda_k|^2$  is seen in (3.34).

Even the limited development that is provided for the statistics of the SINR in the case of ZF-LE is not possible for MMSE-LE, because the additive term in  $1 + \rho|\lambda_k|^2$  makes the respective integrals intractable. Thus we resort to outage probability analysis to show the performance of MMSE-LE.

### 3.3.1 Outage Probability of Linear Equalizers

The mutual information between the transmitted vector  $\mathbf{c}$  and the linearly processed received vector  $\hat{\mathbf{r}}$  in (3.16) and (3.18) is equal to the weighted sum of the mutual information of their components

$$\mathcal{I}(\mathbf{c}; \hat{\mathbf{r}}) = \frac{1}{L} \sum_{k=1}^L \mathcal{I}(c_k; \hat{r}_k) = \frac{1}{L} \sum_{k=1}^L \log(1 + \gamma_k). \quad (3.35)$$

In a circulant channel matrix  $\mathbf{H}$ , the SINR of all symbols are the same and we have  $\mathcal{I}(\mathbf{c}; \hat{\mathbf{r}}) = \log(1 + \gamma)$ . The outage occurs when the mutual information falls below a target rate  $R$ :

$$\Pr(\mathcal{O}) = \Pr(\mathcal{I}(\mathbf{c}; \hat{\mathbf{r}}) < R) = \Pr(\log(1 + \gamma) < R). \quad (3.36)$$

For ZF-LE, the SINR of each symbol is given by (3.24) which leads to

$$\Pr(\mathcal{O}) = \Pr\left(\sum_{k=1}^L \frac{1}{\rho\alpha_k} > \frac{L}{2^R - 1}\right), \quad (3.37)$$

where  $\alpha_k = |\lambda_k|^2$ , and  $R$  is in bits. For MMSE-LE, the SINR is given by (3.34) which gives

$$\Pr(\mathcal{O}) = \Pr\left(\sum_{k=1}^L \frac{1}{1 + \rho\alpha_k} > L2^{-R}\right). \quad (3.38)$$

We notice the apparent similarity between the outage region of ZF-LE and MMSE-LE in the multidimensional space of the eigenvalues  $\boldsymbol{\lambda}$ , however, the subtle difference in the expression of the above regions gives surprisingly different outage probability.

We consider the simple case of  $\nu = 1$ , i.e. a channel with two taps.

### Two-tap channel ( $\nu = 1$ )

With the simplifying assumption of independent  $\boldsymbol{\lambda}$ , the outage probability of ZF-LE, in a two-tap channel, is equal to

$$\Pr(\mathcal{O}) = \Pr\left(\frac{1}{\rho\alpha_1} + \frac{1}{\rho\alpha_2} > \frac{2}{2^R - 1}\right) \quad (3.39)$$

$$= \int_0^\infty e^{-\alpha_1} \int_0^{\frac{r\alpha_1}{\alpha_1\rho - r}} e^{-\alpha_2} d\alpha_2 d\alpha_1 \quad (3.40)$$

where  $r = \frac{2^R - 1}{2}$ . Notice that the outage region in this case is unbounded. For example, if the channel is singular, e.g. the eigenvalue  $\alpha_1 = 0$ , regardless of the value of  $\alpha_2$  the ZF-LE is in outage. To continue from (3.40):

$$\Pr(\mathcal{O}) = 1 - \int_0^\infty \exp\left(-\frac{\rho\alpha^2}{\rho\alpha - r}\right) d\alpha \quad (3.41)$$

$$= 1 - \frac{e^{-\frac{2r}{\rho}}}{\rho} \int_{-r}^\infty \exp\left(-\frac{z}{\rho} - \frac{r^2}{z\rho}\right) dz, \quad (3.42)$$

which is not tractable, however, we can write

$$\Pr(\mathcal{O}) = 1 - \frac{e^{-\frac{2r}{\rho}}}{\rho} \left( \int_{-r}^0 \exp\left(-\frac{z}{\rho} - \frac{r^2}{z\rho}\right) dz + 2rK_1\left(\frac{2r}{\rho}\right) \right) \quad (3.43)$$

where (3.26) is used in the evaluation. The integral in (3.43) can be upper and lower bounded as follows

$$0 \leq \int_{-r}^0 \exp\left(-\frac{z}{\rho} - \frac{r^2}{z\rho}\right) dz \leq r \exp\left(\frac{r}{\rho}\right).$$

The first order approximation yields  $\frac{2r}{\rho} < \Pr(\mathcal{O}) < \frac{3r}{\rho}$ , indicating that the diversity order is one.



Evaluating (3.38) for the two-tap channel, the outage probability of MMSE-LE is equal to

$$\Pr(\mathcal{O}) = \Pr\left(\frac{1}{1 + \rho\alpha_1} + \frac{1}{1 + \rho\alpha_2} > 2^{1-R}\right) \quad (3.44)$$

$$= 1 - \int_0^\infty \exp\left(-\alpha - \left(\frac{2r + \alpha\rho(r-1) - 1}{\rho(\alpha\rho - r + 1)}\right)^+\right) d\alpha, \quad (3.45)$$

where  $r = 2^{R-1}$ , and  $(x)^+ \triangleq \max(0, x)$ . Though (3.45) is not tractable, we evaluate it by approximating the outage regions in high and low spectral efficiencies.

Examples of the outage regions are shown in Figure 3.3 for target rates  $R = 0.5, 2$  bits. The outage region of MMSE-LE can be unbounded similar to that of ZF-LE (as in  $R = 2$ ), or bounded (e.g.  $R = 0.5$ ). When the channel is singular ZF-LE is in outage, hence its outage region includes both of the axes and is unbounded. However, depending on  $R$ , MMSE-LE may not be in outage even if the channel is singular. Seen from the outage event in (3.44), when  $R < 1$ , even if one of the eigenvalues is zero the MMSE-LE is not in outage unless the other eigenvalue is less than  $c_1 \triangleq \frac{2r-1}{\rho(r-1)}$ . This is seen for  $R = 0.5$  in Figure 3.3. On the other hand, one can see from the outage event in (3.44) that, when  $R > 1$ , having a singular channel takes MMSE-LE to outage (see the region of  $R = 2$  in Figure 3.3).

The smaller the rate, the closer the shape of the outage region to a isosceles right triangle with the side  $\alpha_1 + \alpha_2 = c_1$ . In this case, one can approximate (3.44) by integration over the simple right triangle region. For high spectral efficiency, the outage region has two unbounded strips, as in ZF-LE. Evaluation of (3.44) can be made simpler by approximating the outage region by the two unbounded strips.

In low spectral efficiency ( $R \ll 1$ ), considering the right triangle outage region

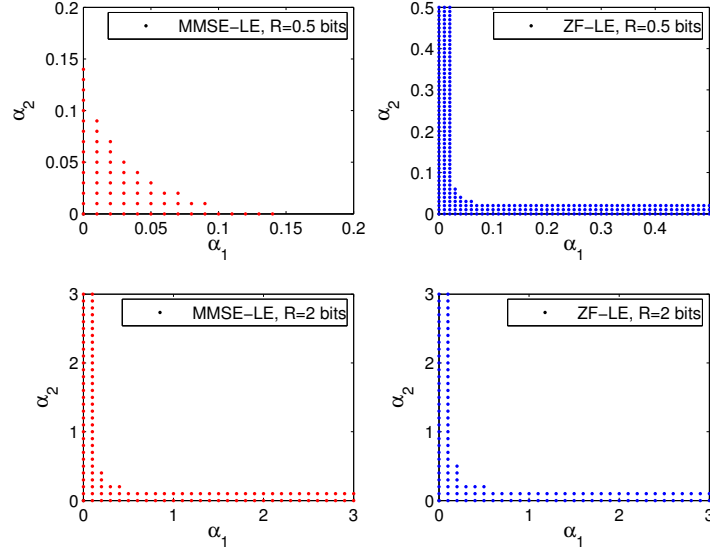


Figure 3.3. Outage regions of linear equalizers in a two-tap channel,  $\rho = 10$  dB

of MMSE-LE, the outage probability (3.44) is

$$\begin{aligned}
 \Pr(\mathcal{O}) &= \int_0^{c_1} e^{-\alpha_1} \int_0^{c_1 - \alpha_1} e^{-\alpha_2} d\alpha_2 d\alpha_1 \\
 &= 1 - e^{-c_1} - c_1 e^{-c_1} \doteq \frac{c_1^2}{2} = \frac{1}{2} \left( \frac{2r-1}{r-1} \right)^2 \rho^{-2}. \quad (3.46)
 \end{aligned}$$

In high spectral efficiency ( $R \gg 1$ ), the outage region becomes similar to that of ZF-LE, which is approximately two perpendicular strips (seen in Figure 3.3). Using this approximation:

$$\Pr(\mathcal{O}) = 2 \int_0^{\frac{r-1}{\rho}} e^{-\alpha_1} \int_0^{\infty} e^{-\alpha_2} d\alpha_2 d\alpha_1 = 2 - 2e^{-\frac{r-1}{\rho}} \doteq (2r-2)\rho^{-1}. \quad (3.47)$$

This counts the intersection of the two strips twice, but since the contribution of the intersection decays as fast as  $\rho^{-2}$ , the approximation does not change the asymptotic behavior.

The above results show that the outage probability of MMSE-LE has diversity two in low spectral efficiency and diversity one in high spectral efficiency. Equa-

tions (3.46) and (3.47) are only true for the extremes of high and low spectral efficiencies and do not give any information about the intermediate values of  $R$ . However, one expects for intermediate values of  $R$  the outage probability decays faster than  $\rho^{-1}$  but slower than  $\rho^{-2}$ .

The result of (3.47) also applies to ZF-LE in both low and high spectral efficiencies. The outage probability is

$$\Pr(\mathcal{O}) = 2 \int_0^{\frac{r}{\rho}} e^{-\alpha_1} \int_0^\infty e^{-\alpha_2} d\alpha_2 d\alpha_1 = 2 - 2e^{-\frac{r}{\rho}} \doteq (2r - 2)\rho^{-1}. \quad (3.48)$$

where  $r = \frac{2^R - 1}{2}$ , indicating the outage probability decays as fast as  $\rho^{-1}$ , regardless of  $R$ . Therefore the diversity order is one, which is in agreement with MGF analysis presented earlier.

Figure 3.4 presents simulation results for the outage probability of unconstrained receiver or ML equalizer<sup>3</sup> and linear equalizers in a two-tap channel ( $\nu = 1$ ) with frame size  $L = 10$  and target rates  $R = 1, 2, 3, 4$  bits. We see that the diversity of ZF-LE is always one regardless of  $R$ . For the low spectral efficiency  $R = 1$ , MMSE-LE and ML equalizers both have diversity order of two. As the target rate  $R$  increases the outage probability of MMSE-LE decays slower than  $\rho^{-2}$  and eventually shows diversity one.

The above experiment can be viewed from the perspective of capacity CDF, using the result of [39]. Figure 3.5 shows the capacity CDF of the frequency-selective channel and linear equalizers. The capacity CDF of the channel and MMSE-LE are almost the same in low spectral efficiency, indicating they would achieve the same diversity order.

Though the previous results are for independent fading coefficients, they hold

---

<sup>3</sup>Hereafter, we do not distinguish between the unconstrained receiver and the ML equalizer.

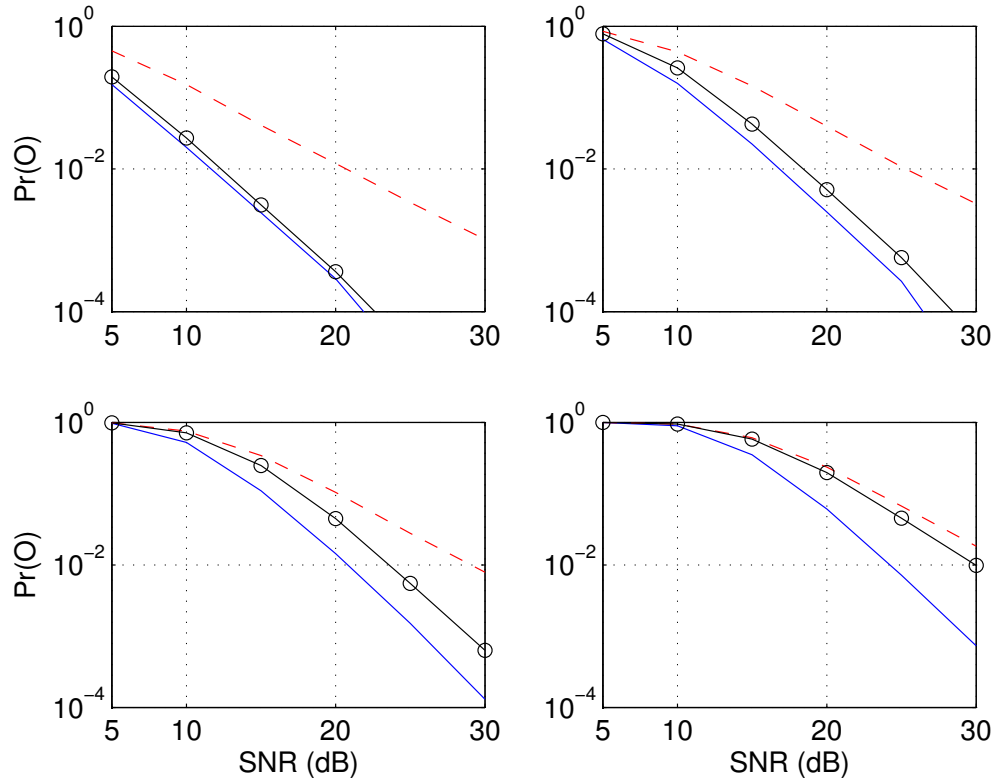


Figure 3.4. Outage probability of ML and linear equalizers,  $\nu = 1$ ,  $L = 10$ . ML (solid line), MMSE-LE (solid line marked with  $\circ$ ) and ZF-LE (dashed line). The curves correspond, from top left clockwise, to rates  $R=1,2,4,3$  bits.

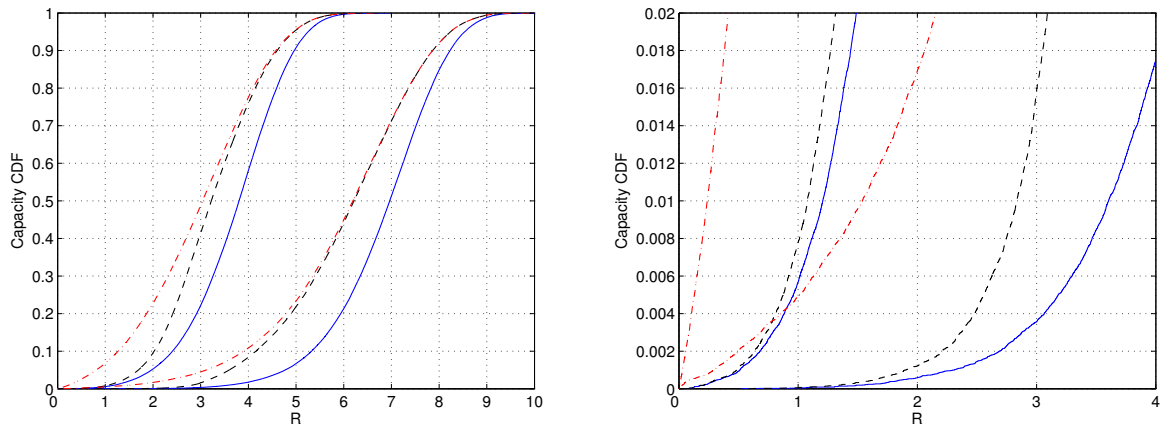


Figure 3.5. CDF of capacity of the frequency-selective channel (solid line), MMSE-LE (dashed line), and ZF-LE (dashed-dot line) in a two-tap channel,  $\nu = 1$ , and  $L = 8$ . In each plot, the SNR for the left set of curves is 13 dB, and 23 dB for the other set.

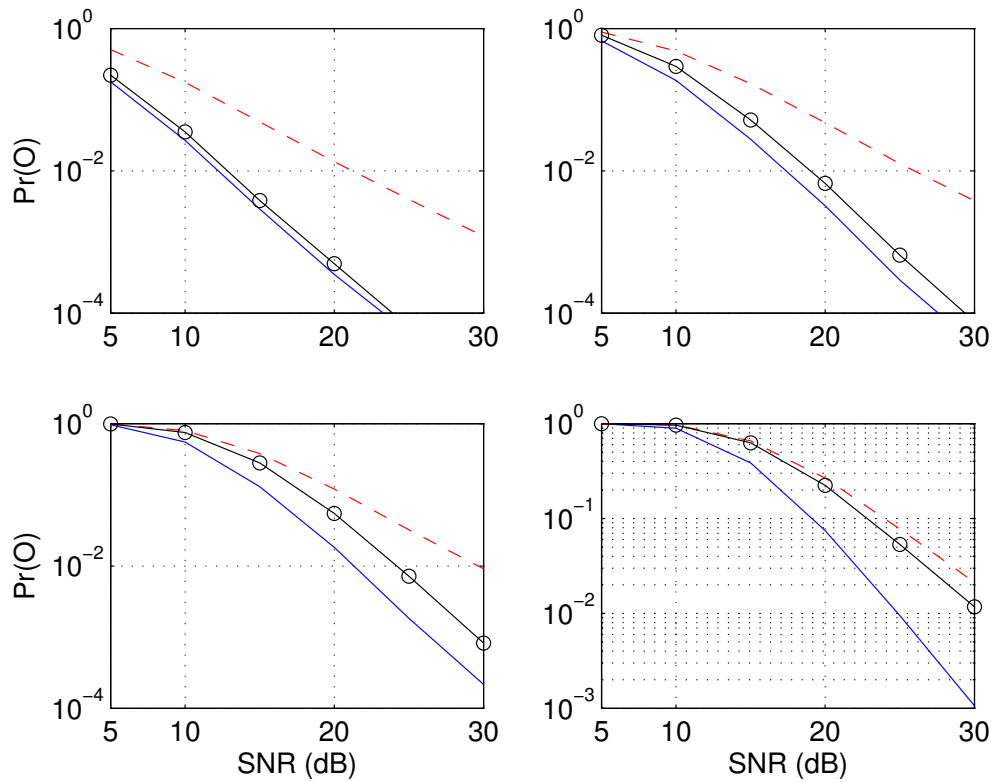


Figure 3.6. Outage probability of ML and linear equalizers in a two-tap channel with 0.5 correlation between the fading coefficients,  $\nu = 1$ ,  $L = 10$ . ML (solid line), MMSE-LE (solid line marked with  $\circ$ ) and ZF-LE (dashed line). The curves correspond, from top left clockwise, to rates  $R=1,2,4,3$  bits.

for correlated case as well. Figure 3.6 presents outage probability results for the two-tap channel where the taps are correlated by 0.5. The outage probabilities are slightly higher than the uncorrelated case, however, ZF-LE and MMSE-LE show similar trend as in Figure 3.4.

### $(\nu + 1)$ -tap channel

In the following, we extend the previous result to arbitrary  $\nu$ , using the assumption of independent  $\boldsymbol{\lambda}$  made earlier. In low spectral efficiency ( $R \ll \log(\frac{L}{L-1})$ ), the outage region is a polyhedron whose vertices are the points on the axes with value

$c_\nu$ , i.e. the bounded region in the positive cone separated by the plane  $\sum_{k=1}^{\nu+1} \alpha_k = c_\nu$  where

$$c_\nu \triangleq \frac{r(\nu+1)-1}{\rho(1-r\nu)},$$

and  $r \triangleq 2^R/L$ . The outage probability (3.38) is therefore

$$\Pr(\mathcal{O}) = \int_0^{c_\nu-d_1} e^{-\alpha_1} \int_0^{c_\nu-d_2} e^{-\alpha_2} \dots e^{-\alpha_\nu} \int_0^{c_\nu-d_{\nu+1}} e^{-\alpha_{\nu+1}} d\alpha_{\nu+1} \dots d\alpha_2 d\alpha_1, \quad (3.49)$$

where  $d_i = \sum_{j=1}^{i-1} \alpha_j$  and  $d_1 = 0$ .

$$\begin{aligned} \Pr(\mathcal{O}) &= 1 - e^{-c_\nu} \sum_{k=0}^{\nu} \frac{c_\nu^k}{k!} \\ &= 1 - e^{-c_\nu} \left( e^{c_\nu} - \sum_{k=\nu+1}^{\infty} \frac{c_\nu^k}{k!} \right) \\ &\doteq \frac{c_\nu^{\nu+1}}{(\nu+1)!} \\ &= \left( \frac{r(\nu+1)-1}{1-r\nu} \right)^{\nu+1} \cdot \frac{\rho^{-(\nu+1)}}{(\nu+1)!}, \end{aligned} \quad (3.50)$$

which shows that in low spectral efficiency, the diversity order is  $\nu+1$ , the same as that of the ML equalizer.

In high spectral efficiency ( $R \gg \log(\frac{L}{L-1})$ ), where the outage region of MMSE-LE and ZF-LE become similar, we approximate the outage region as follows. The outage event consists of  $\nu+1$  regions where the  $i$ th region,  $i = 1, \dots, \nu+1$ , is defined as  $0 \leq \alpha_i \leq \frac{r-1}{\rho}$ , and for  $k \neq i$ ,  $0 \leq \alpha_k$ . Extending the result of the two-tap channel, the outage probability (3.38) is equal to

$$\begin{aligned} \Pr(\mathcal{O}) &= (\nu+1) \int_0^{\frac{r-1}{\rho}} e^{-\alpha_1} d\alpha_1 \prod_{i=2}^{\nu+1} \int_0^{\infty} e^{-\alpha_i} d\alpha_i \\ &= (\nu+1) \left( 1 - e^{-\frac{r-1}{\rho}} \right) \\ &\doteq (\nu+1)(r-1)\rho^{-1}, \end{aligned} \quad (3.51)$$

where, again, the intersection of the above mentioned regions is counted  $\nu + 1$  times but this does not change the asymptotic behavior of the linearly-decaying outage probability.

The same approximation of the outage region of MMSE-LE, in high spectral efficiency, is applicable for ZF-LE for all values of  $R$ . With appropriate changes in (3.51) one can conclude that the outage probability of ZF-LE decays as fast as  $\rho^{-1}$  regardless of  $R$ .

Figure 3.7 shows the outage probability of the ML and linear receivers for a channel with three taps,  $\nu = 2$ , frame size  $L = 10$ , and outage rates  $R = 1, 2, 3, 5$  bits. Similar to the results of the two-tap channel in Figure 3.4, the outage probability of MMSE-LE has variable diversity order depending on  $R$ . In low spectral efficiency,  $R = 1$  in Figure 3.7, MMSE-LE has diversity order three, the same as that of ML receiver. In high spectral efficiency, e.g.  $R = 5$ , MMSE-LE and ZF-LE show the same diversity order one. In intermediate spectral efficiencies, the diversity order of MMSE-LE is less than three but larger than one.

### CDF of SINR

In addition to  $\Phi_{\Gamma}(s)$ , the behavior of the CDF of  $\Gamma$  around zero predicts the diversity order. The finding of [39] states if  $F_{\Gamma}(\gamma) = c\gamma^d + o(\gamma^d)$  as  $\gamma \rightarrow 0^+$ , then at high SNR the average error rate decays as fast as  $\gamma^{-d}$ .

The CDF of  $\gamma$  of ZF-LE, given by in (3.24), is calculated as follows:

$$F_{\Gamma}(\gamma) = \Pr(\Gamma \leq \gamma) = \Pr\left(\sum_{k=1}^L \frac{1}{\alpha_k} \geq \frac{\rho L}{\gamma}\right),$$

which is calculated in the same way as outage probability in (3.37). Similarly, for

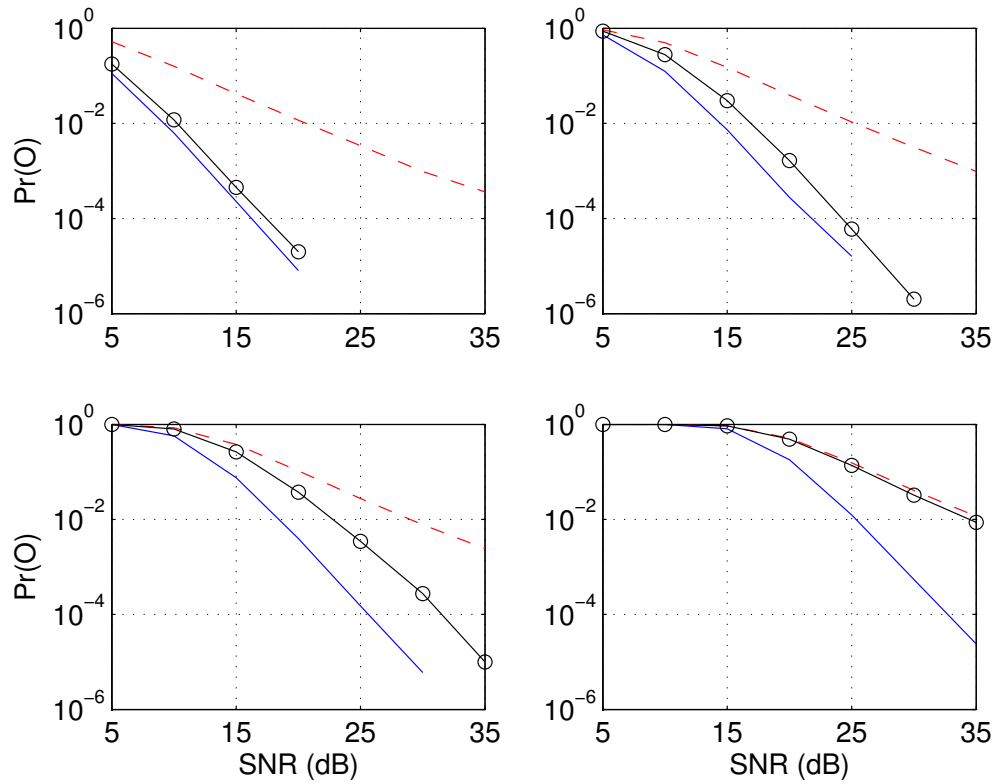


Figure 3.7. Outage probability of ML and linear equalizers,  $\nu = 2, L = 10$ . ML (solid line), MMSE-LE (solid line with  $\circ$ ) and ZF-LE (dashed line). The curves correspond, from top left clockwise, to rates  $R=1, 2, 5, 3$  bits/sec/Hz.



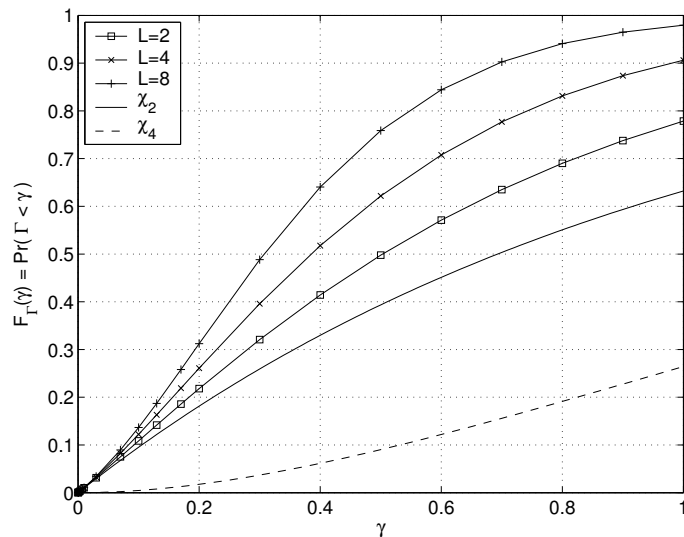


Figure 3.8. Numerical evaluation of CDF of  $\Gamma$  in (3.29)

MMSE-LE, the CDF of  $\gamma$  in (3.34) is given by

$$F_{\Gamma}(\gamma) = \Pr(\Gamma \leq \gamma) = \Pr\left(\sum_{k=1}^L \frac{1}{1 + \rho\alpha_k} \geq \frac{L}{\gamma + 1}\right).$$

The CDF of  $\Gamma$  for  $\nu = 1, 3, 7$ , depicted in Figure 3.8, is calculated through numerical evaluation of the Laplace inverse [40] in Equation (3.29). We notice that as  $\gamma \rightarrow 0^+$ ,  $F_{\Gamma}(\gamma)$  decays as slowly as the CDF of  $\chi_2$ . In the same plot, the CDF of  $\chi_4$  is given for comparison, indicating a diversity of two.

### 3.3.2 Simulation Results

We present simulation results for BPSK modulation transmission in a frequency-selective fading channel followed by linear equalizers.

Figure 3.9 shows the error rate performance of ZF-LE for a two tap channel,  $\nu = 1$ , and  $L = 4, 10, 20$ . The results confirm that ZF-LE achieves only the diversity order of one. It also shows that there is no significant dependence on the block size<sup>4</sup>.

<sup>4</sup>Of course, the CP overhead is smaller for larger  $L$ .

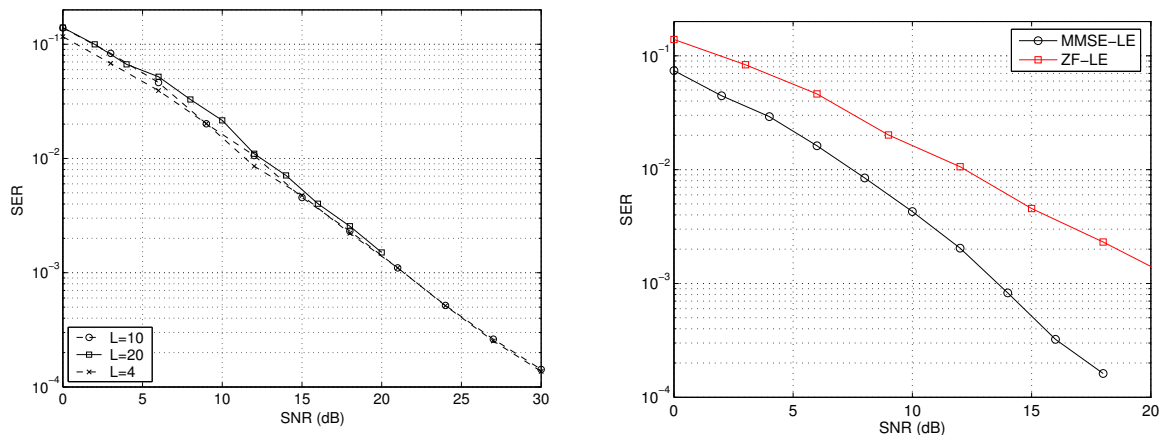


Figure 3.9. Symbol error rate of BPSK signaling and linear equalizers (left) ZF-LE  $\nu = 1$ , and  $L = 4, 10, 20$ , and (right) ZF-LE versus MMSE-LE  $\nu = 1$ , and  $L = 10$ .

Hence the reported results with the assumption  $L = \nu + 1$  are confirmed to be valid also for  $L \neq \nu + 1$ .

In Figure 3.9 the performance of MMSE-LE and ZF-LE are compared. The diversity order of MMSE-LE is two, showing the diversity that is predicted by the outage probability lower bound is achieved by a simple BPSK modulation at spectral efficiency of 1 bits/sec/Hz.

### 3.4 Decision-Feedback Equalizers

The performance of decision-feedback equalizers (DFE) in Gaussian channels have been investigated in [41, 42, 43]. With perfect feedback assumption, MMSE-DFE achieves the capacity of Gaussian channel either with infinite-length filters [41] or finite-length filters [38], hence achieving the maximum diversity of the channel. Similar results have not been established for ZF-DFE yet, except in some special cases. For two-tap channel, it is shown that ZF-DFE with infinite-length filters has the same performance as selection diversity, hence achieving the full diversity of two [44].

### 3.5 Chapter Summary

In this chapter, we analyze the performance of equalizers in frequency-selective single-antenna fading channels. We present new results on the performance of linear equalizers, and calculate their diversity order. We show that ZF-LE cannot achieve the frequency diversity of the channel. Our analytical and experimental results show that MMSE linear equalizers, depending on spectral efficiency, have outage probability that decays as fast as the outage probability of unconstrained receiver, and as slowly as that of ZF linear equalizers.

**CHAPTER 4**  
**PERFORMANCE OF EQUALIZERS IN FLAT FADING**  
**MULTIPLE-ANTENNA CHANNELS**

Multiple-input multiple output (MIMO) systems experience interference between signals transmitted simultaneously from transmit antennas. Various detection methods can be used to retain the transmitted data. In this chapter, we consider the performance of detection methods, also called equalizers, in flat fading MIMO channels.

We first review the performance of ML receiver in MIMO channel and develop performance bounds under spatially correlated fading. We then consider linear receivers and calculate their outage probability. We also present results for decision-feedback equalizers. In our derivation we consider two class of spatial encoders: separate and joint transmit-antenna encoding.

#### **4.1 Introduction**

Consider a multiple-antenna wireless system with  $M$  transmit antennas and  $N$  receive antennas, expressed by an  $N \times M$  random matrix  $\mathbf{H}_t$  whose elements are i.i.d. complex Gaussian random variables. The input-output system model for flat fading MIMO channel is

$$\mathbf{r}_t = \mathbf{H}_t \mathbf{c}_t + \mathbf{n}_t, \quad (4.1)$$

where  $\mathbf{c}_t$  is the  $M \times 1$  transmitted vector,  $\mathbf{n}_t \in \mathcal{C}^{N \times 1}$  is the noise vector, and  $\mathbf{r}_t$  is the  $N \times 1$  received vector at time instant  $t$ . In the following, the time index  $t$  is

sometimes suppressed for convenience. Equation (4.1) can be expanded to:

$$\begin{pmatrix} r_1 \\ r_2 \\ \vdots \\ r_N \end{pmatrix} = \begin{pmatrix} h_{1,1} & h_{1,2} & \cdots & h_{1,M} \\ h_{2,1} & h_{2,2} & \cdots & h_{2,M} \\ \vdots & \vdots & \ddots & \vdots \\ h_{N,1} & h_{N,2} & \cdots & h_{N,M} \end{pmatrix} \begin{pmatrix} c_1 \\ c_2 \\ \vdots \\ c_M \end{pmatrix} + \begin{pmatrix} n_1 \\ n_2 \\ \vdots \\ n_N \end{pmatrix}. \quad (4.2)$$

The vectors  $\mathbf{c}_t$  can be the output of two class of spatial encoders: separate and joint spatial encoder.

**Separate spatial encoding** The data sequence is first demultiplexed into  $M$  separate sub-streams. Each stream is independently channel encoded and mapped into an appropriate signal constellation, and then transmitted from the corresponding antenna. Since each data symbol is sent from only one transmit antenna, the diversity order of this scheme is at most  $N$ , the number of receive antennas. However, this architecture provides a simple receiver. An example of separate encoder is V-BLAST [45].

**Joint spatial encoding** The data stream goes under channel encoding and symbol mapping. The stream of coded symbols is then multiplexed into  $M$  sub-streams and each stream is transmitted from one antenna. Appropriate designs could give the maximum diversity order of  $MN$ , but it also has a complex receiver. Examples of joint encoding are D-BLAST [46] and space-time codes [47].

For both of the above encoding schemes, the receiver consists of an interference cancellation module followed by an appropriate decoder. In this section, the interference cancellation module is referred to as equalizer. The equalizer performs either linear or a non-linear process on the  $N$  received symbols. The results,  $M$  complex variables, are the estimates of the original  $M$  transmitted symbols.

In this chapter, we evaluate the performance of various equalizers in flat fading MIMO channels for both of the spatial encoders. Our evaluation excludes the channel coding, but it can be embedded into the analysis of channel codes of choice. Moreover, when the performance evaluation is in the form of outage probability, it gives a lower bound on the error rate of the corresponding equalizer, presenting the error rate of the best choice of channel codes.

## 4.2 Maximum Likelihood Equalizer

Consider the system model (4.1) and a block of  $L$  data vectors  $\mathbf{c}_t, t = 1, \dots, L$  transmitted over the MIMO channel. Assuming that the receiver has perfect knowledge of the channel matrix and performs coherent detection, the maximum likelihood (ML) metric is given by  $m(\mathbf{r}, \mathbf{c}) = \sum_{t=1}^L \|\mathbf{r}_t - \mathbf{H}_t \mathbf{c}_t\|^2$ , where  $\mathbf{r}$  is the received signal in the period of length  $L$ , and  $\mathbf{c}$  is the transmitted signal in the same period.

The probability that the decoder mistakenly detects a given transmitted vector  $\mathbf{c}$  as  $\hat{\mathbf{c}}$ , is given by:

$$\Pr(\mathbf{c}, \hat{\mathbf{c}}|\mathbf{H}) = Q \left( \sqrt{\frac{\rho}{2} \sum_{t=1}^L \|\mathbf{H}_t \mathbf{e}_t\|^2} \right) , \quad (4.3)$$

where  $\mathbf{e}_t$  is the difference, at time instance  $t$ , between the transmitted vector  $\mathbf{c}_t$  and the mistakenly detected vector  $\hat{\mathbf{c}}_t$ . Using a similar procedure as in Section 3.2, we average over  $\mathbf{H}$  and obtain

$$\Pr(\mathbf{c}, \hat{\mathbf{c}}) = \frac{1}{\pi} \int_0^{\frac{\pi}{2}} \Phi_{\Gamma} \left( -\frac{\rho}{2 \sin^2 \theta} \right) d\theta , \quad (4.4)$$

where  $\Gamma = \sum_{t=1}^L \|\mathbf{H}_t \mathbf{e}_t\|^2$ , and  $\Phi_{\Gamma}(\cdot)$  is the MGF of  $\Gamma$ . In a quasi-static channel,

where the channel  $\mathbf{H}_t$  remains fixed over the time span of the frame, we have

$$\begin{aligned} \Pr(\mathbf{c}, \hat{\mathbf{c}}) &= \frac{1}{\pi} \int_0^{\frac{\pi}{2}} \det^{-N} (\mathbf{I}_M - s \mathbf{\Delta} \mathbf{\Delta}^H) d\theta \\ &= \frac{1}{\pi} \int_0^{\frac{\pi}{2}} \prod_{i=1}^M \left( 1 + \frac{\rho}{2 \sin^2 \theta} \mu_i \right)^{-N} d\theta \end{aligned} \quad (4.5)$$

$$\leq \prod_{i=1}^M \left( 1 + \frac{\rho}{2} \mu_i \right)^{-N}, \quad (4.6)$$

where  $\mu_i$  are the eigenvalues of  $\mathbf{\Delta} \mathbf{\Delta}^H$ ,  $\mathbf{\Delta} = [\mathbf{e}_1, \dots, \mathbf{e}_L]$ , and  $s = -\frac{\rho}{4 \sin^2 \theta}$ . Equation (4.6) is the Chernoff bound for  $\Pr(\mathbf{c}, \hat{\mathbf{c}})$ , a result which was derived differently in [47].

In high SNR, Equation (4.6) decays like  $\rho^{-rN}$ , where  $r = \text{rank}(\mathbf{\Delta} \mathbf{\Delta}^H)$ . Therefore, if  $\mathbf{\Delta} \mathbf{\Delta}^H$  is full rank<sup>1</sup> the ML detector achieves the diversity order of  $MN$ . To obtain full diversity with the ML detector,  $\mathbf{\Delta} \mathbf{\Delta}^H$  must be full rank for all possible pairs of transmit vectors. This is the so-called *rank criterion* derived in [47].

The performance of ML equalizers in a spatially correlated flat fading channel has also been studied. A well-accepted model is to separate transmit- and receive-side correlation [48]:

$$\mathbf{H} = \mathbf{R}_{\text{Tx}}^{\frac{1}{2}} \tilde{\mathbf{H}} \mathbf{R}_{\text{Rx}}^{\frac{H}{2}} \quad (4.7)$$

where  $\mathbf{R}_{\text{Tx}}$  is the correlation between the transmit antennas, and  $\mathbf{R}_{\text{Rx}}$  is the correlation between the receive antennas. A similar procedure as in the uncorrelated case results in [49]:

$$\begin{aligned} \Pr(\mathbf{c}, \hat{\mathbf{c}}) &= \frac{1}{\pi} \int_0^{\frac{\pi}{2}} \det^{-1} (\mathbf{I}_{MN} - s (\mathbf{I}_N \otimes \mathbf{\Delta} \mathbf{\Delta}^H) (\mathbf{R}_{\text{Rx}} \otimes \mathbf{R}_{\text{Tx}})) d\theta \\ &= \frac{1}{\pi} \int_0^{\frac{\pi}{2}} \prod_{i=1}^M \prod_{j=1}^N \left( 1 + \frac{\rho \lambda_j \mu_i}{2 \sin^2 \theta} \right)^{-N} d\theta \leq \prod_{i=1}^M \prod_{j=1}^N \left( 1 + \frac{1}{2} \rho \lambda_j \mu_i \right)^{-1}, \end{aligned} \quad (4.8)$$

---

<sup>1</sup>Note that if  $L < M$  then  $\mathbf{\Delta} \mathbf{\Delta}^H$  cannot be full rank.

where  $\lambda_j$  are the eigenvalues of  $\mathbf{R}_{\text{Rx}}$  and  $\mu_i$  are the eigenvalues of  $\Delta\Delta^H\mathbf{R}_{\text{Tx}}$ .

High SNR approximation of (4.8) shows that the diversity order is not diminished as long as  $\mathbf{R}_{\text{Rx}}$  and  $\mathbf{R}_{\text{Tx}}$  are full rank.

### 4.3 Linear Equalizers

We consider linear equalizers and evaluate the outage probability of a flat fading MIMO channel, with  $N \geq M$ , followed by a ZF linear equalizer (ZF-LE) or MMSE linear equalizer (MMSE-LE). In our treatment, we consider both separate and joint spatial encoders.

Assume the system model (4.1):  $\mathbf{r} = \mathbf{H}\mathbf{c} + \mathbf{n}$ . The ZF equalizer is

$$\mathbf{F}_{\text{ZF}} = (\mathbf{H}^H\mathbf{H})^{-1}\mathbf{H}^H \quad (4.9)$$

which transforms the received signal to

$$\hat{\mathbf{r}} = \mathbf{F}_{\text{ZF}}\mathbf{r} = \mathbf{c} + (\mathbf{H}^H\mathbf{H})^{-1}\mathbf{H}^H\mathbf{n} . \quad (4.10)$$

The MMSE equalizer is

$$\mathbf{F}_{\text{MMSE}} = (\mathbf{H}^H\mathbf{H} + \rho^{-1}\mathbf{I})^{-1}\mathbf{H}^H \quad (4.11)$$

which transforms the received signal to

$$\hat{\mathbf{r}} = \mathbf{F}_{\text{MMSE}}\mathbf{r} = (\mathbf{H}^H\mathbf{H} + \rho^{-1}\mathbf{I})^{-1}\mathbf{H}^H\mathbf{H}\mathbf{c} + (\mathbf{H}^H\mathbf{H} + \rho^{-1}\mathbf{I})^{-1}\mathbf{H}^H\mathbf{n} . \quad (4.12)$$

Since the symbols are detected individually, the SINR of the individual symbols determine the performance.



### SINR of ZF-LE

The detection noise in (4.10),  $\tilde{\mathbf{n}} \triangleq (\mathbf{H}^H \mathbf{H})^{-1} \mathbf{H}^H \mathbf{n}$ , is a complex Gaussian vector with zero-mean and covariance matrix

$$\mathbf{R}_{\tilde{\mathbf{n}}} = \mathbb{E}((\mathbf{H}^H \mathbf{H})^{-1} \mathbf{H}^H \mathbf{n}) = \sigma_n^2 (\mathbf{H}^H \mathbf{H})^{-1} . \quad (4.13)$$

Since the interference from other transmit antennas is completely removed by zero-forcing, noise remains, which is characterized by the diagonal elements of  $\mathbf{R}_{\tilde{\mathbf{n}}}$ , given by:

$$\mathbf{R}_{\tilde{\mathbf{n}}}(k, k) = \sigma_n^2 (\mathbf{H}^H \mathbf{H})_k^{-1} = \sigma_n^2 \frac{\det(\hat{\mathbf{H}}^H \hat{\mathbf{H}})}{\det(\mathbf{H}^H \mathbf{H})} , \quad (4.14)$$

where  $(\mathbf{M})_k^{-1}$  represents the  $k$ th diagonal element of the inverse of  $\mathbf{M}$ , and  $\hat{\mathbf{H}}$  is obtained by removing the  $k$ th row of  $\mathbf{H}$ . In the following, without loss of generality, we assume  $k = 1$ , thus  $\mathbf{H} = [\mathbf{h}; \hat{\mathbf{H}}]$ , the following result is applicable when  $k \neq 1$ . A simple matrix algebra gives the following relation between the determinants involved in (4.14):

$$\det(\mathbf{H}^H \mathbf{H}) = \det(\hat{\mathbf{H}}^H \hat{\mathbf{H}}) \det(\mathbf{h}^H \mathbf{h} - \mathbf{h}^H \mathbf{P} \mathbf{h}) ,$$

where  $\mathbf{P} \triangleq \hat{\mathbf{H}} (\hat{\mathbf{H}}^H \hat{\mathbf{H}})^{-1} \hat{\mathbf{H}}^H$  is an  $N \times N$  matrix. Note that  $\det(\mathbf{h}^H \mathbf{h} - \mathbf{h}^H \mathbf{P} \mathbf{h}) = \mathbf{h}^H (\mathbf{I} - \mathbf{P}) \mathbf{h}$ . Substituting in (4.14) we obtain:

$$\mathbf{R}_{\tilde{\mathbf{n}}}(1, 1) = \frac{\sigma_n^2}{\mathbf{h}^H (\mathbf{I} - \mathbf{P}) \mathbf{h}} . \quad (4.15)$$

Considering the above noise variance and the eigen decomposition  $\mathbf{I} - \mathbf{P} = \mathbf{Q}^H \mathbf{\Lambda} \mathbf{Q}$ , we get the associated SNR

$$\gamma_1 = \rho \mathbf{h}^H (\mathbf{I} - \mathbf{P}) \mathbf{h} = \rho \mathbf{h}^H \mathbf{Q}^H \mathbf{\Lambda} \mathbf{Q} \mathbf{h} . \quad (4.16)$$

Since  $\mathbf{h} \in \mathcal{C}^{N \times 1}$  is an i.i.d. vector, its distribution is invariant under a unitary transformation. Therefore,  $\hat{\mathbf{h}} \triangleq \mathbf{Q} \mathbf{h}$  has the same distribution as  $\mathbf{h}$ , which results in

general non-central chi-square distribution for  $\gamma_1 = \rho \hat{\mathbf{h}}^H \mathbf{\Lambda} \hat{\mathbf{h}}$ . However, considering that  $\mathbf{P}$  and  $\mathbf{I} - \mathbf{P}$  are projection matrices<sup>2</sup>, we can provide the statistics of  $\gamma_1$  more specifically.

Since  $\mathbf{P}$  is a projection matrix  $\text{rank}(\mathbf{P}) = \text{tr}(\mathbf{P})$  [50], and we have

$$\text{rank}(\mathbf{P}) = \text{tr} \left( \hat{\mathbf{H}} \left( \hat{\mathbf{H}}^H \hat{\mathbf{H}} \right)^{-1} \hat{\mathbf{H}}^H \right) = M - 1 ,$$

which gives  $\text{rank}(\mathbf{I} - \mathbf{P}) = N - M + 1$ . Also, the eigenvalues of a projection matrix are either one or zero [50]. Hence,  $\mathbf{\Lambda}$ , the diagonal eigenvalue matrix of  $\mathbf{P}$ , has only  $N - M + 1$  non-zero diagonal elements which are all one. This results in central chi-square distribution with  $2(N - M + 1)$  degrees of freedom for  $\gamma_1$  in (4.16).

Above procedure can be applied to obtain the same result for the SNR of other symbols. Being the column of an i.i.d. channel matrix  $\mathbf{H}$ ,  $\mathbf{h}_k$ 's are independent which results in the independence of  $\gamma_k$ . Therefore, the independent  $\gamma_k$ 's are chi-square random variables with degrees  $2(N - M + 1)$ . The CDF of  $Y \sim \chi_{2(N-M+1)}$ , with variance 0.5 for the participating Gaussian random variables, is:

$$F_Y(y) = 1 - e^{-y} \sum_{i=1}^{N-M+1} \frac{y^{i-1}}{(i-1)!} . \quad (4.17)$$

Above result has appeared in literature previously. Perhaps, the first time it appeared in [51] in the context of multiple access interference, and recently in [52].

### SINR of MMSE-LE

In MMSE detection, unlike ZF detection, the channel is not fully inverted and there is residual interference left after linear processing. Hence, both noise and interference determine the performance. It has been shown [38] that the SINR of the

---

<sup>2</sup> $\mathbf{P}$  is a projection matrix if  $\mathbf{P}^m = \mathbf{P}$  for all positive integers  $m$ .

$k$ th symbol of MMSE detector is

$$\gamma_k = \mathbf{h}_k^H \left( \hat{\mathbf{H}}_k \hat{\mathbf{H}}_k^H + \rho^{-1} \mathbf{I} \right)^{-1} \mathbf{h}_k \quad (4.18)$$

$$= \frac{1}{(\mathbf{I} + \rho \mathbf{H}^H \mathbf{H})_k^{-1}} - 1, \quad (4.19)$$

where  $\mathbf{h}_k$  is the  $k$ th column of the channel matrix  $\mathbf{H}$  and removing this column from  $\mathbf{H}$  gives  $\hat{\mathbf{H}}_k \in \mathcal{C}^{N \times (M-1)}$ .

The statistics of  $\gamma_k$  in (4.18), although more complicated than the ZF case, has been investigated in the context of additive interference channels. Reference [53] is entirely devoted to the derivation of the CDF of the output SINR of an MMSE detector. Consider (4.18) and remove the subscript  $k$  for simplicity. The quadratic form  $Y = \mathbf{h}^H \mathbf{R}^{-1} \mathbf{h}$ , whose kernel depends on the random matrix  $\mathbf{R} \triangleq \hat{\mathbf{H}} \hat{\mathbf{H}}^H + \rho^{-1} \mathbf{I}$  and  $\hat{\mathbf{H}} \in \mathcal{C}^{N \times (M-1)}$ , has the CDF

$$F_Y(y) = 1 - \exp\left(-\frac{y}{\rho}\right) \sum_{n=1}^N \frac{A_n(y)}{(n-1)!} \left(\frac{y}{\rho}\right)^{n-1} \quad (4.20)$$

where the auxiliary functions  $A_n(y)$  are given by

$$A_n(y) = \begin{cases} 1 & N \geq M + n - 1 \\ \frac{1 + \sum_{i=1}^{N-n} C_i y^i}{(1+y)^{M-1}} & N < M + n - 1. \end{cases}, \quad (4.21)$$

and  $C_i$  is the coefficient of  $y^i$  in  $(1+y)^{M-1}$  [53].

Note that the SINR of the various symbols,  $\gamma_1, \dots, \gamma_M$ , are generally correlated, unlike the ZF-LE case. In fact, they are negatively correlated which leads to surprisingly different performance than ZF-LE in some rate regions.

### 4.3.1 Outage Probability in Separate Spatial Encoding

In separate spatial encoding, the data stream is demultiplexed to several substreams, each for one transmit antenna. A simple observation in the evaluation of the outage probability is that if any of the equivalent parallel channels is in outage, the

system is in outage. Hence, the outage event,  $\mathcal{O}$ , is the event when any of the sub-channels cannot support the rate that is assigned to it. In our analysis, we consider equal rate for the sub-channels, however, it is also possible to have a non-uniform rate assignment.

After linear transformation, the mutual information between the elements of  $\hat{\mathbf{r}}$ , in (4.10) and (4.12), and the transmitted data vector  $\mathbf{c}$  is :

$$\mathcal{I}(c_k; \hat{r}_k) = \log(1 + \gamma_k) . \quad (4.22)$$

Assume the target rate is  $R$ , and let  $L \triangleq N - M$ . The outage probability  $\Pr(\mathcal{O})$  is :

$$\begin{aligned} \Pr(\mathcal{O}) &= 1 - \Pr(\mathcal{O}^c) \\ &= 1 - \Pr\left(\mathcal{I}(c_1; \hat{r}_1) \geq \frac{R}{M}, \dots, \mathcal{I}(c_M; \hat{r}_M) \geq \frac{R}{M}\right) \\ &= 1 - \left(\Pr\left(\mathcal{I}(c_k; \hat{r}_k) \geq \frac{R}{M}\right)\right)^M \approx M \Pr\left(\mathcal{I}(c_k; \hat{r}_k) < \frac{R}{M}\right) . \end{aligned} \quad (4.23)$$

Notice that in the above derivation, we have used that fact that sub-channels outage events are independent. This is based on the independence between the SINR of various symbols. As we notice previously, this is a valid assumption for ZF-LE. While this assumption does not hold for MMSE-LE, it does give a useful approximation, providing the diversity order.

Substituting (4.17) and (4.22) in (4.23) gives the outage probability for ZF-LE which is

$$\Pr(\mathcal{O}) \approx MF_Y \left(\frac{2^{R/M} - 1}{\rho}\right) \quad (4.24)$$

$$\begin{aligned} &= M - Me^{-y} \left( e^y - \sum_{i=L}^{\infty} \frac{y^{i-1}}{(i-1)!} \right) \Bigg|_{y=\frac{2^{R/M}-1}{\rho}} \\ &\doteq \frac{M(2^{R/M} - 1)^{L+1}}{(L+1)!} \rho^{-(L+1)} , \end{aligned} \quad (4.25)$$

which shows the diversity order  $L + 1$  for the ZF-LE.

Substituting (4.20) and (4.22) in (4.23) results in the outage probability of MMSE-LE

$$\begin{aligned} \Pr(\mathcal{O}) &\approx MF_Y \left( 2^{\frac{R}{M}} - 1 \right) \\ &= M - Me^{-\frac{y}{\rho}} \left( e^{\frac{y}{\rho}} - \sum_{i=L+1}^{\infty} \frac{1}{i!} \left( \frac{y}{\rho} \right)^i + \sum_{i=L+2}^N \frac{A_i(y)}{(i-1)!} \left( \frac{y}{\rho} \right)^{i-1} \right) \Big|_{y=2^{\frac{R}{M}}-1} \end{aligned} \quad (4.26)$$

$$\doteq \frac{y^{L+1}}{(L+1)!} \cdot \frac{y^{M-1}}{(1+y)^{M-1}} \rho^{-(L+1)} \Big|_{y=2^{\frac{R}{M}}-1}, \quad (4.27)$$

which also shows the diversity order  $L + 1$  for the MMSE-LE, the same as that of ZF-LE. However, the two outage probabilities are not exactly the same. The ratio of the outage probability of (4.25) to (4.27) is the inverse of the middle term in (4.27):

$$\frac{\Pr(\mathcal{O})_{\text{ZF}}}{\Pr(\mathcal{O})_{\text{MMSE}}} = \frac{(1+y)^{M-1}}{y^{M-1}} \Big|_{y=2^{\frac{R}{M}}-1} = \left( \frac{2^{\frac{R}{M}}}{2^{\frac{R}{M}} - 1} \right)^{M-1}. \quad (4.28)$$

Note that the ratio of outage probabilities in (4.28) remains fixed throughout the range of SNR and it only depends on the relative target rate,  $\frac{R}{M}$ . When the relative target rate is small, the outage probability of ZF-LE becomes larger than that of MMSE-LE. When the target rate is large this difference between the outage probabilities becomes negligible. We demonstrate this fact in the experimental results in Section 4.3.3.

Generalization of the above results to non-uniform rate assignment is straightforward. Uniform and non-uniform rate assignment have the same diversity, though they have different performance.

It is also possible to obtain the diversity-multiplexing tradeoff, introduced in [54], for ZF-LE and MMSE-LE. In the framework of [54], the target rate is defined for a family of codes, whose members are designed to be employed each in a given

SNR. A family of codes achieves *the spatial multiplexing gain* of  $r$  if it supports the target rate  $R = r \log \rho$ .

For ZF-LE, a similar derivation as in (4.25) leads to

$$\begin{aligned}
\Pr(\mathcal{O}) &\approx MF_Y \left( \frac{\rho^{\frac{r}{M}} - 1}{\rho} \right) \\
&= M - Me^{-y} \left( e^y - \sum_{i=L}^{\infty} \frac{y^{i-1}}{(i-1)!} \right) \Bigg|_{y=\frac{\rho^{\frac{r}{M}} - 1}{\rho}} \\
&\doteq \frac{M}{(L+1)!} \rho^{-(L+1)(1-\frac{r}{M})^+}, \tag{4.29}
\end{aligned}$$

where  $(x)^+ = \max(0, x)$ . The above result indicates that ZF-LE achieves the *diversity gain* of  $d(r) = (L+1)(1 - \frac{r}{M})$ . We notice that for a multiplexing gain of  $r = 0$ , i.e. fixed target rate throughout the SNR region, the diversity is the same as what (4.25) indicates. However, when the multiplexing gain increases, the diversity gain decreases and in the limit of  $r = M$ , the maximum multiplexing gain, the diversity gain is zero.

Similarly for MMSE-LE, the derivation which led to (4.27) gives us:

$$\begin{aligned}
\Pr(\mathcal{O}) &\approx MF_Y (\rho^{\frac{r}{M}} - 1) \\
&\doteq \frac{y^{L+1}}{(L+1)!} \cdot \frac{y^{M-1}}{(1+y)^{M-1}} \rho^{-(L+1)} \Bigg|_{y=\frac{\rho^{\frac{r}{M}} - 1}{\rho}} \\
&\doteq \frac{M}{(L+1)!} \rho^{-(L+1)(1-\frac{r}{M})^+}, \tag{4.30}
\end{aligned}$$

which is the same diversity gain as that of ZF-LE.

### 4.3.2 Outage Probability in Joint Spatial Encoding

In joint spatial encoding, the data stream is encoded and then demultiplexed into sub-streams to be sent from the antennas. Effectively, each data symbol contribute to signals of all the transmit antennas. Considering the act of linear equalizers, outage occurs when the aggregate mutual information of all the sub-channels fails to support the target rate [38].

The mutual information between the elements of the linearly transformed receive signal,  $\hat{\mathbf{r}}$  in (4.10) and (4.12), and the transmitted data vector  $\mathbf{c}$  is  $\mathcal{I}(c_k; \hat{r}_k) = \log(1 + \gamma_k)$ . Assuming the target rate is  $R$ , the probability of the outage event  $\mathcal{O}$  is

$$\begin{aligned} \Pr(\mathcal{O}) &= \Pr\left(\sum_{k=1}^M \mathcal{I}(c_k; \hat{r}_k) < R\right) \\ &= \Pr\left(\sum_{k=1}^M \log(1 + \gamma_k) < R\right) \end{aligned} \quad (4.31)$$

$$= \Pr\left(\prod_{k=1}^M (1 + \gamma_k) < 2^R\right). \quad (4.32)$$

The SINR of the sub-channels of ZF-LE are independent chi-square random variables with degrees  $2(N - M + 1)$ . Let  $Y_k \sim \chi_{2(N-M+1)}$ ,  $k = 1, \dots, M$ . The outage probability of ZF-LE is given by the CDF of the random variable

$$\prod_{k=1}^M (1 + Y_k) = 1 + \sum_{k=1}^M Y_k + \dots + \prod_{k=1}^M Y_k. \quad (4.33)$$

Among the components of the above random variable, the last term, which is the product of  $Y_k$ 's, determines the diversity order. In the following, through recursion, we show that  $Y_1 \cdot Y_2 \cdots Y_M$  has diversity order  $L$ . Let us start by  $Z \triangleq Y_1 \cdot Y_2$ . The PDF of  $Z$  is given by

$$f_Z(z) = \frac{2}{((L-1)!)^2} z^L K_0(2\sqrt{z}), \quad (4.34)$$

where  $K_0(\cdot)$  is the zeroth order modified Bessel function of the second kind [36], which for small values of  $z$  is a constant<sup>3</sup>. Therefore, for small values of  $z$  the first order approximation of  $f_Z(z)$  is  $z^L$ . This shows that the CDF of  $Z$ ,  $F_Z(z)$ , has first order approximation equal to  $z^{L+1}$ , which indicates diversity order of  $L + 1$ . Now consider

---

<sup>3</sup>For small values of  $x$ :  $K_m(x) \sim \frac{\Gamma(m)}{2}(2/x)^m$  [37].

the CDF of  $W \triangleq Y_1 \cdot Y_2 \cdot Y_3 = Z \cdot Y$ , where  $Y \sim \chi_{2(N-M+1)}$ :

$$\begin{aligned}
F_W(w) &= \Pr(W \leq w) = \Pr(Z \cdot Y \leq w) = \int_0^\infty f_Z(z) F_Y\left(\frac{w}{z}\right) dz \\
&= \int_0^\infty \alpha z^L K_0(2\sqrt{z}) \left(1 - e^{-\frac{w}{z}} \sum_{k=1}^{L+1} \frac{w^{k-1}}{z^{k-1}(k-1)!}\right) dz \\
&= \alpha \int_0^\infty z^L K_0(2\sqrt{z}) e^{-\frac{w}{z}} \sum_{k=L+2}^\infty \frac{w^{k-1}}{z^{k-1}(k-1)!} dz, \tag{4.35}
\end{aligned}$$

where  $\alpha$  is the constant term in (4.34). The first order approximation of (4.35) around zero is

$$w^{L+1} \int_0^\infty \frac{\alpha}{z(L+1)!} K_0(2\sqrt{z}) dz.$$

Thus  $F_W(w)$  behaves like the  $L+1$ th power of  $w$ , indicating the diversity order  $L+1$ . This procedure can be applied recursively to find that the first order approximation of the CDF of  $Y_1 \cdot Y_2 \cdots Y_M$  behaves like  $w^{L+1}$ . As mentioned, the product term, among the ones in (4.33), dominates the diversity. We just showed that the product term  $Y_1 \cdot Y_2 \cdots Y_M$  has the diversity order  $L+1$ . Therefore, the diversity order of ZF-LE is  $L+1$ .

Recalling the results from Section 4.3.1, ZF-LE has the same diversity in joint and separate spatial encoding architecture.

To obtain the outage probability of MMSE-LE, we substitute the SINR of MMSE-LE from (4.19) in (4.32) which gives:

$$\Pr(\mathcal{O}) = \Pr\left(\prod_{k=1}^M (\mathbf{I} + \rho \mathbf{H}^H \mathbf{H})_k^{-1} > 2^{-R}\right). \tag{4.36}$$

The involvement of the diagonal elements of the random matrix  $(\mathbf{I} + \rho \mathbf{H}^H \mathbf{H})^{-1}$  makes further analysis intractable. We proceed to provide an upper bound to this probabil-



ity. Rewriting the sum mutual information as in (4.31), we have

$$\begin{aligned}
-\sum_{k=1}^M \mathcal{I}(c_k; \hat{r}_k) &= \sum_{k=1}^M \log \left( (\mathbf{I} + \rho \mathbf{H}^H \mathbf{H})_k^{-1} \right) \\
&\geq M \log \left( \sum_{k=1}^M \frac{1}{M} (\mathbf{I} + \rho \mathbf{H}^H \mathbf{H})_k^{-1} \right) \tag{4.37}
\end{aligned}$$

$$\begin{aligned}
&= M \log \left( \frac{1}{M} \text{tr} \left( (\mathbf{I} + \rho \mathbf{H}^H \mathbf{H})^{-1} \right) \right) \\
&= M \log \left( \frac{1}{M} \sum_{k=1}^M \frac{1}{1 + \rho \lambda_k} \right), \tag{4.38}
\end{aligned}$$

where (4.37) is due to Jensen's inequality, and  $\lambda_k$ 's are the eigenvalues of the Wishart matrix  $\mathbf{H}^H \mathbf{H}$ . Substituting (4.38) into (4.31) gives:

$$\Pr(\mathcal{O}) \leq \Pr \left( \sum_{k=1}^M \frac{1}{1 + \rho \lambda_k} \geq M 2^{-\frac{R}{M}} \right). \tag{4.39}$$

To evaluate the above probability, we need the joint PDF of the eigenvalues of  $\mathbf{H}^H \mathbf{H}$ . Assuming  $N \geq M$ , the joint PDF of the ordered eigenvalues  $\lambda_k$ 's,  $\lambda_1 \leq \lambda_2 \leq \dots \leq \lambda_M$ , is

$$f_{\mathbf{\Lambda}}(\boldsymbol{\lambda}) = K_{M,N} \prod_{i=1}^M \lambda_i^{N-M} \prod_{i < j} (\lambda_i - \lambda_j)^2 \exp \left( - \sum_i \lambda_i \right), \tag{4.40}$$

where  $K_{M,N}$  is a normalizing constant.

The evaluation of (4.39) for a specific outage rate  $R$  is rather difficult, due to the shape of the outage region. However, one can calculate the bound for small and large values of  $R$  where the the outage region can be approximated by regions with simpler shapes. In the following we evaluate (4.39) for a MIMO channel with  $M = 2$  and  $N \geq 2$ .

For a MIMO channel with  $M = 2$  and  $N \geq 2$ , the bound (4.39) on outage probability becomes

$$\Pr(\mathcal{O}) \leq \Pr \left( \frac{1}{1 + \rho \lambda_1} + \frac{1}{1 + \rho \lambda_2} \geq 2^{1 - \frac{R}{2}} \right). \tag{4.41}$$

For small values of  $R$ , the outage region is a isosceles right triangle with the side  $\lambda_1 + \lambda_2 = c_2$ , where  $c_2 \triangleq \frac{2-b}{\rho^{(b-1)}}$  and  $b \triangleq 2^{1-\frac{R}{2}}$ . When  $M = N = 2$ , above outage probability bound, up to the scaling factor  $K_{2,2}$ , is

$$\begin{aligned}
\Pr(\mathcal{O}) &\leq \int_0^{c_2} e^{-\lambda_1} \int_0^{c_2-\lambda_1} (\lambda_1 - \lambda_2)^2 e^{-\lambda_2} d\lambda_2 d\lambda_1 \\
&= 2 \left( 1 - e^{-c_2} \left( 1 + c_2 + \frac{c_2^2}{2} + \frac{c_2^3}{6} \right) \right) = 2e^{-c_2} \sum_{k=4}^{\infty} \frac{c_2^k}{k!} \\
&\doteq \frac{1}{12} c_2^4 = \frac{1}{12} \left( \frac{2-b}{b-1} \right)^4 \rho^{-4}, \tag{4.42}
\end{aligned}$$

which indicates diversity four. When  $N \geq 2$  the outage probability bound (4.39), up to the scaling factor  $K_{2,N}$ , is

$$\begin{aligned}
\Pr(\mathcal{O}) &\leq \int_0^{c_2} e^{-\lambda_1} \lambda_1^{N-2} \int_0^{c_2-\lambda_1} \lambda_2^{N-2} (\lambda_1 - \lambda_2)^2 e^{-\lambda_2} d\lambda_2 d\lambda_1 \\
&= 2(N-1)!(N-2)! \left( 1 - e^{-c_2} \sum_{k=1}^{2N-1} \frac{c_2^k}{k!} \right) \\
&\doteq \frac{2(N-1)!(N-2)!}{(2N)!} \left( \frac{2-b}{b-1} \right)^{2N} \rho^{-2N}, \tag{4.43}
\end{aligned}$$

where the achieved diversity is  $2N$ . In obtaining (4.42) and (4.43), the following identities are helpful:

$$\begin{aligned}
\int_0^u x^n e^{-x} dx &= n! - e^{-u} \sum_{k=0}^n \frac{n!}{(n-k)!} u^{n-k}, \\
\int_0^u x^n (u-x)^m dx &= u^{m+n+1} B(m+1, n+1),
\end{aligned}$$

where  $m$  and  $n$  are integers and  $B(\cdot, \cdot)$  is the Beta function which is  $B(b, c) = \frac{\Gamma(b)\Gamma(c)}{\Gamma(b+c)}$  [37], and  $\Gamma(\cdot)$  denotes the Gamma function.

For large values of  $R$ , the outage region is approximated by two orthogonal strips. The strips are defined as  $0 \leq \lambda_2$ ,  $0 \leq \lambda_1 \leq \hat{c}_2$  and  $0 \leq \lambda_1$ ,  $0 \leq \lambda_2 \leq \hat{c}_2$ , where

$\hat{c}_2 \triangleq \frac{1-b}{b\rho}$ . The outage probability bound, up to the scaling factor  $K_{2,N}$ , is

$$\begin{aligned}
\Pr(\mathcal{O}) &\leq 2 \int_0^{\hat{c}_2} e^{-\lambda_1} \lambda_1^{N-2} \int_0^\infty \lambda_2^{N-2} (\lambda_1 - \lambda_2)^2 e^{-\lambda_2} d\lambda_2 d\lambda_1 \\
&= 4(N-1)!(N-2)! e^{-\hat{c}_2} \sum_{k=N-1}^\infty \frac{x^k}{k!} \\
&\quad + 2(N-2)! e^{-\hat{c}_2} \left( (N-2)\hat{c}_2^{N-1} - \hat{c}_2^N \right) \\
&\doteq 2N(N-2)! \hat{c}_2^{N-1} \\
&= 2N(N-2)! \left( \frac{1-b}{b} \right)^{N-1} \rho^{-(N-1)}, \tag{4.44}
\end{aligned}$$

which indicates that the upper bound<sup>4</sup> has the diversity  $N-1 = L+1$ , where  $L = N-M$  as introduced previously. In the calculation of (4.44), the intersection of the two strips is calculated twice. This portion of integral, which decays as fast as  $\rho^{-2(N-1)}$ , does not affect the asymptotic behavior of (4.44).

The upper bounds in (4.42) and (4.43) show the surprising fact that MMSE-LE can achieve the same diversity as the ML receiver for small values of  $R$  in joint spatial encoding. However, for large values of  $R$  the performance of MMSE-LE and ZF-LE are the same. Hence, the diversity of MMSE-LE varies from the full diversity of an unconstrained detector to that of ZF-LE, depending of the target rate  $R$ .

Comparing to the results from Section 4.3.1 for separate spatial encoders, MMSE-LE has different diversity in joint spatial encoding architecture, except for large outage rate  $R$ .

The previous results of the case  $M=2, N \geq 2$  can be generalized to arbitrary values of  $M$  and  $N \geq M$ .

---

<sup>4</sup>In Section 4.3.3 is shown that the upper bound is tight in high spectral efficiency region.

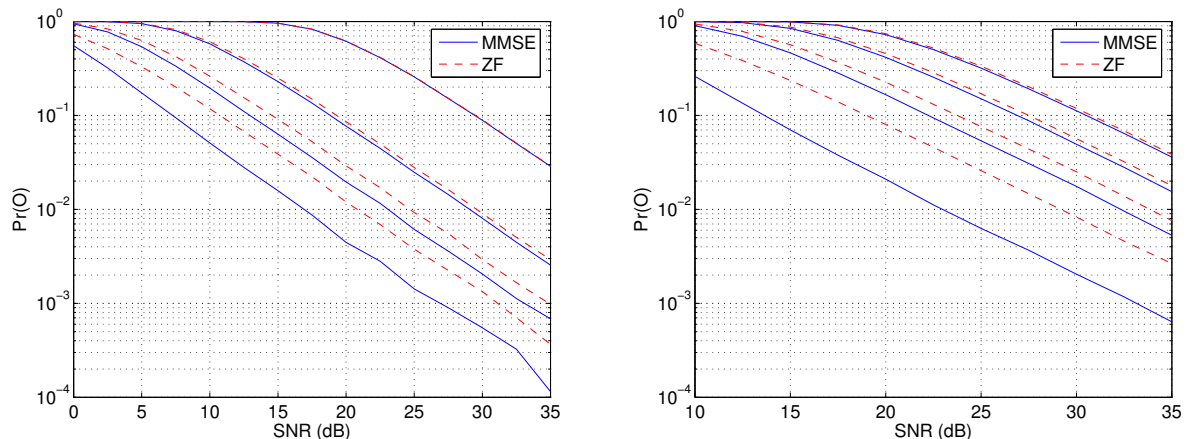


Figure 4.1. Outage probability of linear equalizers. Left:  $M = N = 2$ , the pairs solid and dashed lines, from left, correspond to MMSE-LE and ZF-LE for rates  $R=1,2,4,10$  bits/sec/Hz. Right:  $M = N = 4$ ,  $R=4,8,12,16$  bits/sec/Hz.

### 4.3.3 Simulation Results

First we consider a MIMO system with two antennas in transmit and receive sides:  $M = N = 2$ . The outage probability of the linear equalizers in the separate architecture are shown in Figure 4.1. The target rate is  $R = 1, 2, 4, 10$  bits/sec/Hz. As expected, both linear detectors show diversity order of one, regardless of the target rate. For higher values of  $R$  the difference in the performance of ZF-LE and MMSE-LE is negligible and they perform almost the same throughout the SNR region. This is expected traditionally from linear equalizers: similar performance specially at high SNR. But, for lower values of  $R$ , MMSE-LE performs better than ZF-LE in the whole SNR region. The dependency of the relative performance of these equalizers on the target rate  $R$  is in agreement with (4.28). In high SNR, the ratio of the outage probabilities remains fixed. Similar results are also shown in Figure 4.1 for a MIMO system with  $M = N = 4$ .

In Figure 4.2, the outage probability of the unconstrained receiver and linear equalizers in a joint spatial encoding architecture are shown. The unconstrained

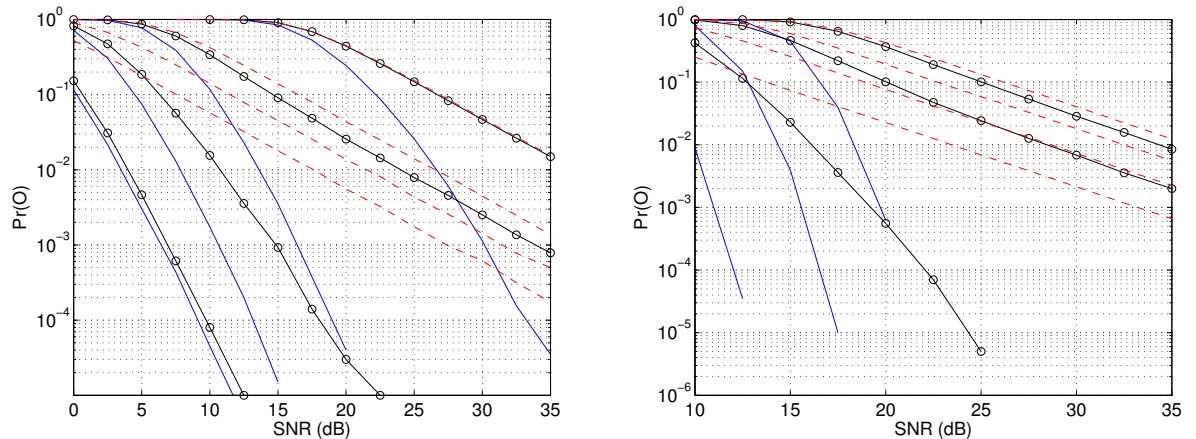


Figure 4.2. Outage probability of unconstrained receiver and linear equalizers, Left:  $M = N = 2$ , unconstrained receiver (solid line), MMSE-LE (solid line with  $\circ$ ) and ZF-LE (dashed line),  $R=1,2,4,10$  bits/sec/Hz. Right:  $M = N = 4$ ,  $R=4,8,12,16$  bits/sec/Hz.

receiver achieves the full diversity of the channel. The ZF-LE equalizer has diversity one as expected from the analysis in Section 4.3.2. The diversity order of ZF-LE remains fixed regardless of the target rate  $R$ . Surprisingly, MMSE-LE shows diversity rate that depends on  $R$ : in lower values of  $R$  the diversity order is very close to that of the unconstrained receiver, and in higher values of  $R$  its diversity becomes the same as the diversity of ZF-LE. These results are in agreement with the analysis in Section 4.3.2. Figure 4.2 also presents similar results for a MIMO system with  $M = N = 4$ .

In Figure 4.2, the outage probability of MMSE-LE and the upper bound (4.39) are also shown. The bound is tight is either low or high values of  $R$ . Though the bound is loose in the intermediate values of  $R$ , it does predict diversity order varying with  $R$ .

Figure 4.4 presents similar results for a flat fading MIMO channel with  $M = N = 2$  and correlated transmit antennas with correlation factor  $\rho_t = 0.5$ . Outage probabilities are slightly higher than the results in Figure 4.2 and Figure 4.3, however,

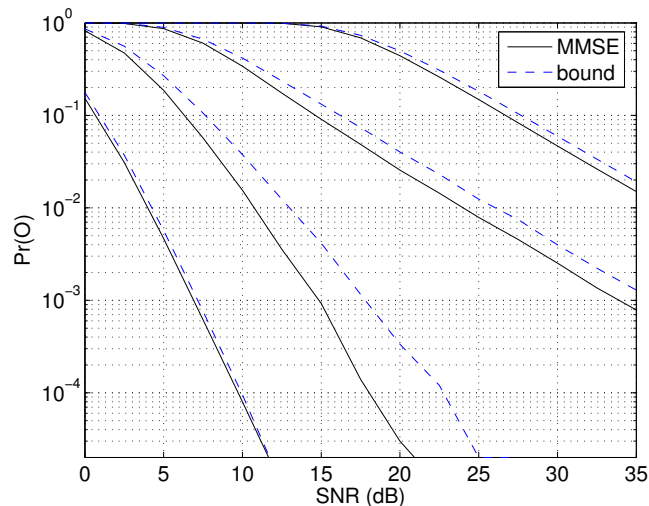


Figure 4.3. Outage probability of MMSE-LE and the upper bound (4.39).  $M = N = 2$ , the curves correspond, from left to right, to rates  $R=1, 2, 4, 10$  bits/sec/Hz.

the behavior of outage probabilities are the same as uncorrelated cases.

To see the surprising outage probability of MMSE-LE from a different perspective, the CDF of the capacity of the unconstrained receiver and linear equalizers at  $\text{SNR} = 5, 10, 15, 20, 25$  are shown in Figure 4.5. To see the slope of the CDF at low values of  $R$ , the right plot in Figure 4.5 zooms on a small region from the left plot. We notice the significant difference in outage probability of ZF-LE and MMSE-LE in low target rates.

The CDF capacity of two other MIMO systems with  $M = 2, N = 4$  and  $M = N = 4$  are shown in Figure 4.6. We notice that in a higher diversity environment, case  $M = 2, N = 4$ , the performance of ZF-LE becomes the same as MMSE-LE in lower target rates, compared to the cases where no diversity is available ( $M = N$ ).

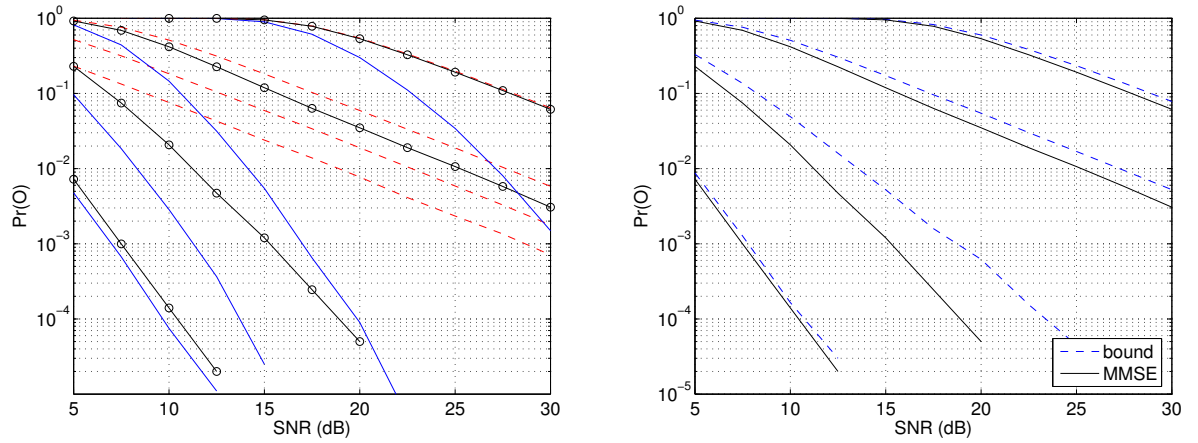


Figure 4.4. Outage probability of unconstrained receiver and linear equalizers,  $M = N = 2$  and correlated transmit antennas,  $\rho_t = 0.5$ . Left: unconstrained receiver (solid line), MMSE-LE (solid line with  $\circ$ ) and ZF-LE (dashed line). Right: MMSE outage probability and the upper bound.  $R=1,2,4,10$  bits/sec/Hz.

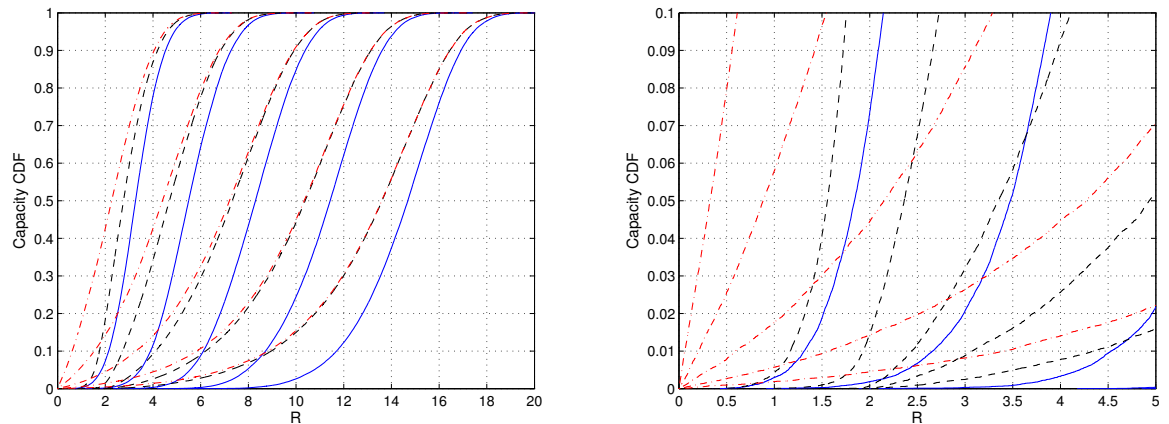


Figure 4.5. CDF of capacity of the unconstrained receiver (solid line), MMSE-LE (dashed line), and ZF-LE (dashed-dot line) in a MIMO channel with  $M = N = 2$ . The SNR is, from left to right, 5,10,15,20,25 dB.

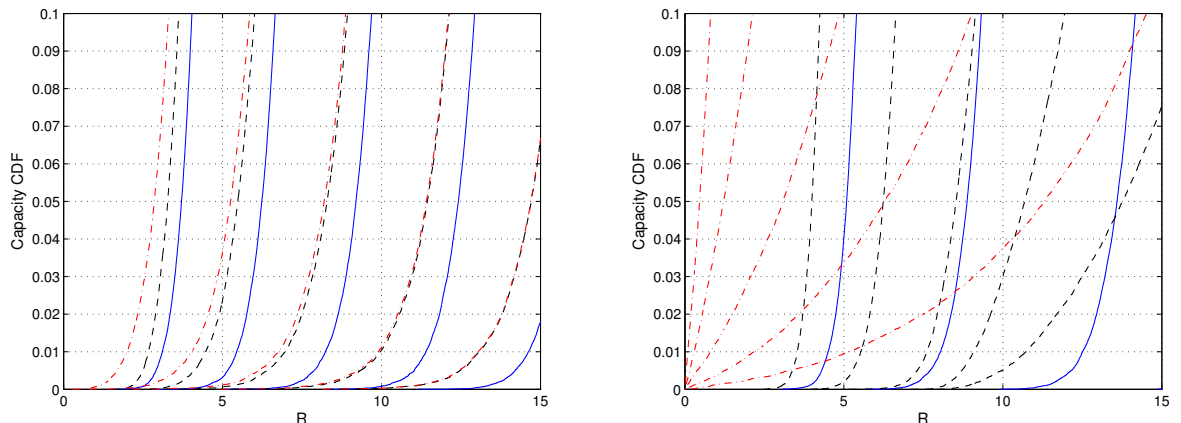


Figure 4.6. CDF of capacity of the unconstrained receiver (solid line), MMSE-LE (dashed line), and ZF-LE (dashed-dot line) in a MIMO channel with (left)  $M = 2, N = 4$ , and (right)  $M = N = 4$ . The SNR is, from left to right, 5,10,15,20,25 dB.

#### 4.4 Decision-Feedback Equalizers

Decision-feedback equalizers (DFE) are combination of linear equalizers and a cancelling process which is performed iteratively. In terms of complexity they are less complex than ML equalizers but obviously more complex than linear equalizers. Their performance is better than the linear equalizers but inferior to ML equalizers.

The basic process in DFE is as follows. Consider the system model (4.1):  $\mathbf{r} = \mathbf{H}\mathbf{c} + \mathbf{n}$ . Let the QR decomposition of random matrix  $\mathbf{H}$  be  $\mathbf{H} = \mathbf{Q}\mathbf{R}$ , where  $\mathbf{Q}$  is a unitary matrix,  $\mathbf{Q}^H\mathbf{Q} = \mathbf{I}$ , and  $\mathbf{R}$  is an  $M \times M$  lower triangular matrix with positive diagonal elements. Consider

$$\hat{\mathbf{r}} = \mathbf{Q}^H \mathbf{r} = \mathbf{R}\mathbf{c} + \mathbf{Q}^H \mathbf{n} = \mathbf{R}\mathbf{c} + \tilde{\mathbf{n}} .$$

Note that  $\tilde{\mathbf{n}} \in \mathcal{C}^{M \times 1}$  since the distribution of the Gaussian vector  $\mathbf{n}$  is invariant to unitary operation. Since  $\mathbf{R}$  is a lower triangular matrix, the first element of  $\hat{\mathbf{r}}$  has no interference from other antennas i.e.,  $\hat{r}_1 = R_{1,1}c_1 + \tilde{n}_1$ , and can be detected by either ZF or MMSE criterion. Having  $c_1$  detected, its contribution can be cancelled from other received symbols. Eliminating the first column of  $\mathbf{H}$  and the first components



of  $\hat{\mathbf{r}}$  and  $\tilde{\mathbf{n}}$ , we obtain a system with fewer of unknowns, to which we apply the same process iteratively. The performance can be further improved if one starts detecting the symbol with highest SNR in each iteration [45].

In a separate spatial encoder, above detecting and cancelling procedure can be combined with the outer decoding. This is done by carrying out each iteration for all the time indices in  $\mathbf{r}_t = \mathbf{H}_t \mathbf{c}_t + \mathbf{n}_t$ , and then decode the detected  $\hat{r}_k$ 's,  $1 \leq k \leq M$ , by the associated outer decoder of the  $k$ th antenna [45, 55].

The analysis of DFE structures usually relies on the assumption that the decision that is fed back for next cancelling process is perfect, i.e., error propagation is ignored.

#### 4.4.1 Outage Probability in Separate Spatial Encoding

The performance of DFE equalizers with separate spatial encoders has been evaluated in the literature, mainly for the V-BLAST architecture [56, 55, 54].

The following celebrated result facilitates the analysis of detecting and cancelling process: In the QR factorization of  $\mathbf{H} = \mathbf{Q}\mathbf{R}$ , the diagonal elements of the lower triangular matrix  $\mathbf{R}$  are i.i.d. with chi-square distribution with degree  $2(N - M + k)$ , where  $k$  is the index of the diagonal element [57].

Based on the above result, the outage probability for the separate spatial encoder, such as V-BLAST, is obtained from a similar analysis that led to (4.23):

$$\Pr(\mathcal{O}) = 1 - \prod_{k=1}^M \Pr\left(\mathcal{I}(c_k; \hat{r}_k) \geq \frac{R}{M}\right), \quad (4.45)$$

where, in the context of detecting and cancelling process,  $\hat{r}_k$  is the resulting received signal after the  $(k - 1)$ th cancelling process.

For the DFE equalizer with ZF detection (ZF-DFE), the above results lead to

$$\Pr(\mathcal{O}) = 1 - \prod_{k=1}^M \left( 1 - \Pr \left( Y_k < \frac{2^{R/M} - 1}{\rho} \right) \right), \quad (4.46)$$

where  $Y_k \sim \chi_{2(N-M+k)}$ . The diversity of (4.46) is simply obtained by observing that the cumulative term  $\sum_k F_{Y_k}(\frac{2^{R/M}-1}{\rho})$  dominates the diversity of (4.46). Among the  $M$  components of this term, the first term has the smallest diversity of  $N - M + 1$ , which is the diversity of ZF-DFE. Thus we have the same diversity as of ZF-LE. This is not surprising since in the separate spatial encoder, the performance and diversity is determined by the sub-channel which has the smallest diversity, the first sub-channel [54].

For the DFE equalizer with MMSE detection (MMSE-DFE), Equation (4.45) leads to

$$\Pr(\mathcal{O}) = 1 - \prod_{k=1}^M \left( 1 - \Pr \left( \mathbf{h}_k^H \mathbf{A}_k \mathbf{h}_k < \frac{2^{R/M} - 1}{\rho} \right) \right), \quad (4.47)$$

where  $\mathbf{h}_k$  is the  $k$ th column of  $\mathbf{H}$  and  $\mathbf{A}_k = \left( \hat{\mathbf{H}}_k \hat{\mathbf{H}}_k^H + \rho^{-1} \mathbf{I} \right)$ , and  $\hat{\mathbf{H}}_k$  is a submatrix of  $\mathbf{H}$  which excludes its first  $k$  columns. Carrying out a similar argument as in ZF-DFE case, and considering the statistics of the Gaussian quadratic form in Section 4.3, we see that the diversity of MMSE-DFE is also  $N - M + 1$ . Note that the starting equation (4.45) assumes that the SINR of the subchannels are independent, which may not hold. Therefore, (4.47) is only an approximation of the outage probability of MMSE-DFE.

Considering the terms which determine diversity in (4.46) and (4.47), we get the same ratio of the outage probability of ZF-DFE and MMSE-DFE as (4.28).

The diversity gain of V-BLAST, in the framework of diversity multiplexing tradeoff, is shown in [54] to be  $d(r) = (1 - \frac{r}{M})^+$  when  $M = N$ . Similar to the

procedure in Section 4.3.1, above result can be extended to the case where  $N \geq M$  which gives  $d(r) = (L + 1)(1 - \frac{r}{M})^+$ .

#### 4.4.2 Outage Probability in Joint Spatial Encoding

The outage probability for the joint encoding structure has been investigated in the literature. Particularly, the D-BLAST architecture has been analyzed in the early work of [46] and recently in [54].

In the joint spatial encoding architecture, outage occurs when the sum of mutual information of the sub-channels is less than the target rate. The sum mutual information is given by (4.31), except that  $\hat{r}_k$  is the result of the  $(k - 1)$ th cancelling process.

When the ZF-DFE equalizer is applied to D-BLAST, [54] has shown that the diversity is  $N(N + 1)/2$ , assuming  $M = N$ .

With perfect decision-feedback, the MMSE-DFE equalizer is actually capacity-achieving (see e.g. [38]), hence it achieves the full diversity of the unconstrained decoder. In the general context of joint spatial encoding, [38] shows that the sum mutual information in (4.31) is the capacity of the MIMO system. In the context of diversity multiplexing tradeoff, [54] shows that MMSE-DFE receiver for D-BLAST structure achieves the tradeoff of the underlying MIMO channel.

### 4.5 Simulation Results

We consider a MIMO system with  $M = N = 2$ . The outage probability of DFE equalizers in separate spatial encoding is shown in Figure 4.7. Both ZF-DFE and MMSE-DFE equalizers show the diversity  $M - N + 1 = 1$ , the same as their linear counterparts, but they have better performance compared to linear equalizers. We

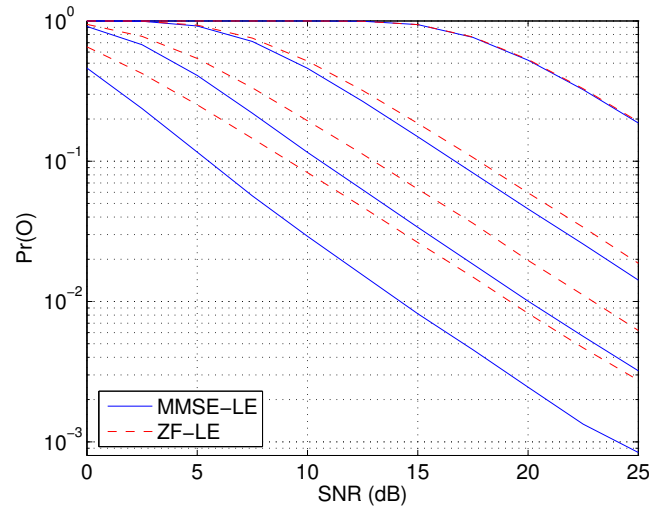


Figure 4.7. Outage probability of DFE equalizers in separate spatial encoding,  $M = N = 2$ . The pairs of solid and dashed lines, from left, correspond to MMSE-DFE and ZF-DFE for rates  $R = 1, 2, 4, 10$  bits/sec/Hz.

notice that for higher values of  $R$  the difference in the performance of ZF-DFE and MMSE-DFE is negligible. In low spectral efficiencies, MMSE-DFE performs better than ZF-DFE.

In Figure 4.8, the outage probability of the DFE equalizers with joint spatial encoders is shown. The outage probability of the unconstrained receiver is the same as that of MMSE-DFE and is not shown. Both achieve full diversity order of four. The ZF-DFE equalizer has diversity order three, which is in agreement with the finding of [54], as reported in Section 4.4.2.

## 4.6 Chapter Summary

In this chapter, we focus on the performance of equalizers in flat fading channels. We present new results on the performance of linear equalizers, and calculate their diversity order. Our analytical and experimental results show that MMSE linear

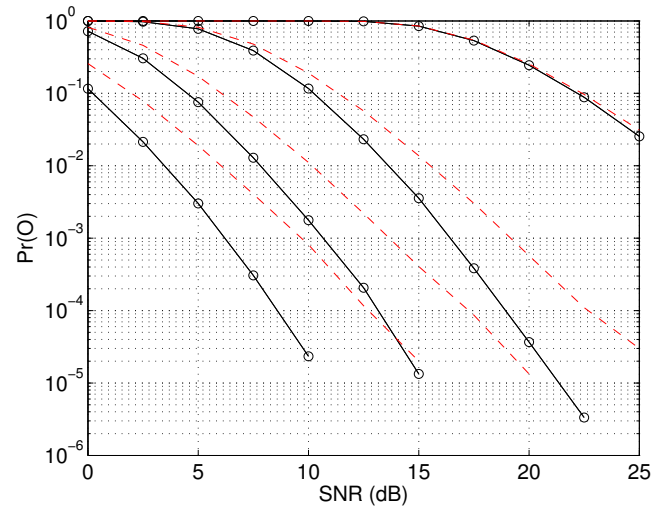


Figure 4.8. Outage probability of DFE equalizers in joint spatial encoding,  $M = N = 2$ . The pairs of solid and dashed lines, from left, correspond to MMSE-DFE and ZF-DFE for rates  $R = 1, 2, 4, 10$  bits/sec/Hz. Unconstrained equalizer has the same outage probability as MMSE-DFE.

equalizers, depending on spectral efficiency, have outage probability that decays as fast as the outage probability of unconstrained receiver, and as slowly as that of ZF linear equalizers. We also briefly present some results on the performance of DFE equalizers and presented some new results as well.

## CHAPTER 5

### PERFORMANCE OF EQUALIZERS IN FREQUENCY-SELECTIVE MULTIPLE-ANTENNA FADING CHANNELS

In frequency-selective MIMO channels interference occurs across both time and space. In this section, we analyze the performance of various equalizers in frequency-selective MIMO channels. Prior work in this area were focused mainly on diversity combining [44, 58, 59]. The performance of ML receiver is evaluated first in spatially uncorrelated and correlated channels. We also provide results for channels whose multipath fading components are correlated. Next, we analyze the performance of linear equalizers and calculate their achievable diversity order.

#### 5.1 Introduction

Assume a MIMO channel with  $M$  transmit antennas,  $N$  receive antennas, and memory  $\nu$ . Such a channel is represented by matrix channels  $\mathbf{H}_0, \mathbf{H}_1, \dots, \mathbf{H}_\nu \in \mathcal{C}^{N \times M}$ , with the system model  $\mathbf{r} = \mathcal{H}\mathbf{c} + \mathbf{n}$ , i.e.

$$\begin{pmatrix} \mathbf{r}_L \\ \mathbf{r}_{L-1} \\ \vdots \\ \mathbf{r}_1 \end{pmatrix} = \begin{pmatrix} \mathbf{H}_0 & \mathbf{H}_1 & \cdots & \mathbf{H}_\nu & \mathbf{0} & \cdots & \mathbf{0} \\ \mathbf{0} & \mathbf{H}_0 & \mathbf{H}_1 & \cdots & \mathbf{H}_\nu & \cdots & \mathbf{0} \\ \vdots & \ddots & \ddots & \ddots & \ddots & \ddots & \vdots \\ \mathbf{0} & \cdots & \mathbf{0} & \mathbf{H}_0 & \mathbf{H}_1 & \cdots & \mathbf{H}_\nu \end{pmatrix} \begin{pmatrix} \mathbf{c}_L \\ \mathbf{c}_{L-1} \\ \vdots \\ \mathbf{c}_1 \end{pmatrix} + \begin{pmatrix} \mathbf{n}_L \\ \mathbf{n}_{L-1} \\ \vdots \\ \mathbf{n}_1 \end{pmatrix}, \quad (5.1)$$

where  $L$  is the block length,  $\mathbf{c}_t$  is the  $M \times 1$  transmit vector at time index  $t$ ,  $\mathbf{r}_t$  is the  $N \times 1$  received vector at the same time index,  $\mathbf{n}_t \in \mathcal{C}^{N \times 1}$  is AWGN, and  $\mathcal{H} \in \mathcal{C}^{LN \times LM}$  is the equivalent channel.

## 5.2 Maximum Likelihood Equalizer

In this section, we use methodology and notation similar to Section 3.2. Let  $\mathbf{H} = (\mathbf{H}_\nu, \mathbf{H}_{\nu-1}, \dots, \mathbf{H}_0)$ , where  $\mathbf{H} \in \mathcal{C}^{N \times (\nu+1)M}$ , and denote the  $j$ th row of  $\mathbf{H}$  with  $\mathbf{h}_j$ . The ML metric in this case is

$$\|\mathcal{H}\Delta\|^2 = \Delta^H \mathcal{H}^H \mathcal{H} \Delta$$

where  $\Delta = (\Delta_1^H, \Delta_2^H, \dots, \Delta_L^H)^H$ , and  $\Delta_t = \mathbf{c}_t - \hat{\mathbf{c}}_t$ , where  $\mathbf{c}_t$  and  $\hat{\mathbf{c}}_t$  are the  $t$ th subvector of the codewords  $\mathbf{c}$  and  $\hat{\mathbf{c}}$ . The structure of the matrix  $\mathcal{H}$  simplifies the ML metric to

$$\|\mathcal{H}\Delta\|^2 = \sum_{i=0}^{L-\nu} \mathbf{A}_i^H \mathbf{H}^H \mathbf{H} \mathbf{A}_i \quad (5.2)$$

$$= \sum_{i=0}^{L-\nu} \sum_{j=1}^N \mathbf{A}_i^H \mathbf{h}_j^H \mathbf{h}_j \mathbf{A}_i = \sum_{j=1}^N \mathbf{h}_j \mathbf{\Omega} \mathbf{h}_j^H, \quad (5.3)$$

where  $\mathbf{A}_i \triangleq (\Delta_i^H, \dots, \Delta_{\nu+i}^H)^H$  and  $\mathbf{\Omega} = \sum_{i=0}^{L-\nu} \mathbf{A}_i \mathbf{A}_i^H$ . The ML metric is a sum of quadratic forms. Using the result of [32], appeared as a Lemma in Section 3.2, we obtain the following MGF for  $\Gamma = \|\mathcal{H}\Delta\|^2$ , assuming the channel components  $\mathbf{H}_i$  are independent:

$$\Phi_\Gamma(s) = \prod_{i=0}^{\nu M} (1 - s\lambda_i)^{-N}, \quad (5.4)$$

where  $s \triangleq -\frac{\rho}{4\sin^2\theta}$ ,  $\rho = \frac{\xi_x}{N_0}$ , and  $\lambda_i$  is an eigenvalue of  $\mathbf{\Omega}$ . Asymptotically,  $\Phi_\Gamma(s)$  behaves like

$$\Phi_\Gamma(-s) \doteq \prod_{\lambda_i \neq 0} (s\lambda_i)^{-N} = \frac{s^{-NM(\nu+1)}}{\det(\mathbf{\Omega})^N},$$

where for the second equality it is assumed that all the eigenvalues  $\lambda_i$  are nonzero. If  $\mathbf{\Omega}$  is full rank,  $\Phi_\Gamma(s)$  decays with the  $(\nu+1)MN$  power of SNR, indicating the maximum obtainable diversity. However, to achieve this diversity, coding is necessary, as demonstrated below.

If the vector  $\mathbf{c}$  does not have any redundancy, then  $\mathbf{c}$  and  $\hat{\mathbf{c}}$  are different in at most one position, hence only one  $\mathbf{\Delta}_t$  is non-zero. Assume that the position of the nonzero  $\mathbf{\Delta}_t$  is far enough from the edges of  $\mathbf{\Delta}$  such that exactly  $\nu+1$  of  $\mathbf{A}_i$  vectors are nonzero. Therefore,  $\mathbf{\Omega} = \mathbf{I} \otimes \mathbf{D}$ , where  $\mathbf{D}$  is an  $M \times M$  matrix which has exactly one nonzero diagonal element. Hence  $\mathbf{\Omega}$  has rank  $\nu+1$ , i.e., diversity order  $(\nu+1)N$ . It follows that frequency and receive diversity are possible without coding, but transmit diversity requires coding, or otherwise a carefully designed signaling that guarantees a full rank  $\mathbf{\Omega}$ .

We now calculate the MGF of  $\Gamma$  when the channel matrices  $\mathbf{H}_i$  are not independent. Assume  $\mathbf{H}_\nu(i, j), \dots, \mathbf{H}_0(i, j)$  are correlated with correlation matrix  $\mathbf{R}_t$ , which is fixed for all pairs of  $i$  and  $j$ . This model assumes that all antenna pairs in the MIMO system have the same temporal dynamics. The covariance of  $\mathbf{h}_j$ , the  $j$ th row of  $\mathbf{H}$ , is  $\mathbf{R}_t \otimes \mathbf{I}_M$ . The vector  $\mathbf{h}_j$  can be decorrelated by the transform  $\mathbf{h}_j = \tilde{\mathbf{h}}_j (\mathbf{R}_t \otimes \mathbf{I}_M)^{\frac{1}{2}}$  where  $\tilde{\mathbf{h}}_j$  is a white vector. Hence

$$\|\mathcal{H}\mathbf{\Delta}\|^2 = \sum_{j=1}^N \mathbf{h}_j (\mathbf{R}_t \otimes \mathbf{I}_M)^{\frac{1}{2}} \mathbf{\Omega} (\mathbf{R}_t \otimes \mathbf{I}_M)^{\frac{H}{2}} \mathbf{h}_j^H ,$$

which results in the following MGF

$$\Phi_\Gamma(s) = \prod_{i=0}^{\nu M} (\mathbf{I} - s\mu_i)^{-N} , \quad (5.5)$$

where  $\mu_i$  are eigenvalues of  $(\mathbf{R}_t \otimes \mathbf{I}_M)\mathbf{\Omega}$ . We notice that as long as the covariance matrix  $\mathbf{R}_t$  is full-rank, the diversity obtained by ML equalizer is not affected by channel correlation, but it incurs performance loss characterized by  $(\det(\mathbf{R}_t))^M$ .

We now consider the spatial correlation between the elements of  $\mathbf{H}_i$ . We again use the channel model (4.7). In case of transmit-side correlation only ( $\mathbf{R}_{\text{Rx}} = \mathbf{I}_N$  and  $\mathbf{R}_{\text{Rx}} \neq \mathbf{I}_M$ ), we obtain the following MGF:

$$\Phi_\Gamma(s) = \prod_{i=0}^{\nu M} (\mathbf{I} - s\mu_i)^{-N} ,$$



where  $\mu_i$  are eigenvalues of  $(\mathbf{R}_t \otimes \mathbf{R}_{R_x})\boldsymbol{\Omega}$ . If  $\mathbf{R}_{R_x} \neq \mathbf{I}_N$  and  $\mathbf{R}_{R_x} \neq \mathbf{I}_M$ , the procedure we have the following expression for MGF:

$$\Phi_{\Gamma}(s) = \det(\mathbf{I} - s(\mathbf{R}_t \otimes \mathbf{R}_{R_x})(\mathbf{R}_{R_x} \otimes \boldsymbol{\Omega}))^{-1} .$$

We notice that in the correlated channel cases, asymptotic behavior of MGF is independent of correlation as long as the correlation matrices are full-rank, and the loss in performance is quantified with the determinant of the correlation matrices, similar to (3.14).

### 5.3 Linear Equalizers

We consider block transmission and apply linear equalization in matrix-form. A linear transformation is applied to the received signal in a single step to remove both temporal and spatial interference (see [38], among others).

Assume the system model (5.1). The block ZF-LE has the matrix form:

$$\mathbf{F}_{ZF} = (\boldsymbol{\mathcal{H}}^H \boldsymbol{\mathcal{H}})^{-1} \boldsymbol{\mathcal{H}}^H , \quad (5.6)$$

which transforms the received signal to

$$\hat{\mathbf{r}} = \mathbf{F}_{ZF} \mathbf{r} = \mathbf{c} + (\boldsymbol{\mathcal{H}}^H \boldsymbol{\mathcal{H}})^{-1} \boldsymbol{\mathcal{H}}^H \mathbf{n} . \quad (5.7)$$

The MMSE-LE is

$$\mathbf{F}_{MMSE} = (\boldsymbol{\mathcal{H}}^H \boldsymbol{\mathcal{H}} + \rho^{-1} \mathbf{I})^{-1} \boldsymbol{\mathcal{H}}^H , \quad (5.8)$$

which transforms the received signal to

$$\hat{\mathbf{r}} = \mathbf{F}_{MMSE} \mathbf{r} = (\boldsymbol{\mathcal{H}}^H \boldsymbol{\mathcal{H}} + \rho^{-1} \mathbf{I})^{-1} \boldsymbol{\mathcal{H}}^H \boldsymbol{\mathcal{H}} \mathbf{c} + (\boldsymbol{\mathcal{H}}^H \boldsymbol{\mathcal{H}} + \rho^{-1} \mathbf{I})^{-1} \boldsymbol{\mathcal{H}}^H \mathbf{n} . \quad (5.9)$$

For mathematical tractability, we assume that the data sent from each transmit antenna is appended by a cyclic prefix (CP). The CP converts the channel matrix

$\mathcal{H}$  to a block circulant matrix. A block circulant matrix with size  $LN \times LM$  is a matrix whose sub-matrices, each with size  $N \times M$ , appear in a circulant fashion. Block diagonalization of block circulant matrices is possible using the following fact.

**Fact:** Let  $\mathcal{H}$  be a block circulant matrix of size  $LN \times LM$ . Then  $\mathcal{H} = (\mathbf{Q} \otimes \mathbf{I}_N)\mathbf{\Lambda}(\mathbf{Q}^H \otimes \mathbf{I}_M)$ , where  $\mathbf{Q}$  is the Discrete Fourier Transform (DFT) matrix as defined in Section 3.3, and  $\mathbf{\Lambda}$  is a block diagonal matrix whose diagonal matrices are

$$\mathbf{\Lambda}_\ell = \frac{1}{\sqrt{L}} \sum_{k=1}^{\nu+1} \mathbf{H}_k e^{-(k-1)(\ell-1)/L} ,$$

for  $\ell = 1, \dots, L$ , and  $\nu + 1 \leq L$ . □

Assuming  $\mathbf{H}_i \in \mathcal{C}^{N \times M}$ ,  $i = 1, \dots, \nu + 1$  are independent, then  $\mathbf{\Lambda}_\ell \in \mathcal{C}^{N \times M}$  for  $\ell = 1, \dots, L$ , since  $\mathbf{\Lambda}_\ell(i, j)$  is a weighted sum of  $\mathbf{H}_k(i, j)$ . However,  $\mathbf{\Lambda}_\ell$ 's are not necessarily independent. If  $L = \nu + 1$ , which the circulant channel matrix  $\mathcal{H}$  becomes fully populated,  $\mathbf{\Lambda}_\ell$ 's are independent. Our analysis is limited to this case, but our experimental results confirm that the findings of the uncorrelated case is also valid for  $L \neq \nu + 1$ .

### 5.3.1 ZF-LE

In the case of ZF-LE, the equivalent noise is  $\tilde{\mathbf{n}} \triangleq (\mathcal{H}^H \mathcal{H})^{-1} \mathcal{H}^H \mathbf{n}$ , with covariance matrix  $\mathbf{R}_{\tilde{\mathbf{n}}} = \sigma_n^2 (\mathcal{H}^H \mathcal{H})^{-1}$ . Using the block circulant channel model, the noise covariance is

$$\mathbf{R}_{\tilde{\mathbf{n}}} = \sigma_n^2 (\mathbf{Q} \otimes \mathbf{I}_M) (\mathbf{\Lambda}^H \mathbf{\Lambda})^{-1} (\mathbf{Q}^H \otimes \mathbf{I}_M) . \quad (5.10)$$

The properties of the orthogonal matrix  $\mathbf{Q}$  result in a block diagonal structure for  $\mathbf{R}_{\tilde{\mathbf{n}}}$  whose blocks, denoted by  $\mathbf{B}$ , are all the same

$$\mathbf{B} = \frac{1}{L} \sum_{\ell=1}^L (\mathbf{\Lambda}_\ell^H \mathbf{\Lambda}_\ell)^{-1} . \quad (5.11)$$

Each  $\mathbf{\Lambda}_\ell^H \mathbf{\Lambda}_\ell$  is a Wishart matrix, hence  $\mathbf{B}$  is a sum of independent inverse Wishart matrices whose diagonal elements determine the decision-point SINR. In Section 4.3, we show that the diagonal elements of an inverse Wishart matrix are independent. The decision-point SINR of each symbol, denoted by  $\gamma_i$  for  $i = 1, \dots, M$ , is

$$\gamma_i = \frac{\rho}{\frac{1}{L} \sum_{\ell=1}^L Y_{\ell,i}}, \quad (5.12)$$

where  $Y_{\ell,i}$ ,  $\ell = 1, \dots, L$ , is the  $i$ th diagonal elements of  $(\mathbf{\Lambda}_\ell^H \mathbf{\Lambda}_\ell)^{-1}$  and  $X_{\ell,i} \triangleq \frac{1}{Y_{\ell,i}} \sim \chi_{2(N-M+1)}$ . Since the diagonal blocks of  $\mathbf{R}_{\mathbf{n}}$  are equal, we have  $\gamma_{(jM+i)} = \gamma_i$  for  $j = 0, \dots, L-1$ . Equation (5.12) is a generalization of the decision-point SINR in frequency-selective SISO channel given by (3.24). Since the CDF of  $\gamma_i$ 's are the same, the subscript  $i$  is dropped in the following unless needed for clarity.

$$\begin{aligned} F_\Gamma(\gamma) &= \Pr(\Gamma < \gamma) \\ &= \Pr\left(\sum_{\ell=1}^L \frac{1}{X_\ell} > \frac{\rho L}{\gamma}\right). \end{aligned} \quad (5.13)$$

We evaluate (5.13) for  $\gamma \rightarrow 0^+$  based on the similarity between the integration region of (5.13) and what we carry out in Section 3.3.

When  $\gamma \rightarrow 0^+$  the integration region of (5.13) is approximated by  $L$  regions where the  $\ell$ th region is defined as  $0 \leq X_\ell \leq \frac{\gamma}{\rho L}$ , and for  $k \neq \ell$ ,  $0 \leq X_k$ . Recalling that  $X_\ell \sim \chi_{2(N-M+1)}$ , and denoting  $\alpha \triangleq \frac{\gamma}{\rho L}$ , (5.13) gives

$$\begin{aligned} F_\Gamma(\gamma) &= L \int_0^\alpha f_{X_1}(x_1) dx_1 \prod_{\ell=2}^L \int_0^\infty f_{X_\ell}(x_\ell) dx_\ell \\ &= L F_{X_1}(\alpha) = L \left(1 - e^{-\alpha} \sum_{i=1}^{N-M+1} \frac{\alpha^{i-1}}{(i-1)!}\right) \\ &\doteq \frac{1}{(N-M+1)! L^{N-M}} \left(\frac{\gamma}{\rho}\right)^{N-M+1}, \end{aligned} \quad (5.14)$$

where the multiple count of the intersection of the regions is ignored because it decreases as fast as  $\gamma^{L(N-M+1)}$  when  $\gamma \rightarrow 0^+$ , hence does not change the result of (5.14).

The achievable diversity is  $N - M + 1$ , which is the same diversity order as what ZF-LE achieves in flat fading channel (see Section 4.3). Therefore, ZF-LE is incapable of achieving the frequency diversity.

### Outage Probability

We analyze the outage probability of ZF-LE in frequency-selective channel for separate and joint spatial encoders. In separate spatial coding, the CDF of the SNR of the individual symbols determine the outage probability, seen from (4.23) and (4.24). From (5.14), we conclude that the outage probability of ZF-LE decreases as  $\rho^{-(N-M+1)}$ .

In the joint spatial encoding architecture, Equation (4.31) can be rewritten as follows

$$\begin{aligned} \Pr(\mathcal{O}) &= \Pr\left(\frac{1}{L} \sum_{k=1}^{LM} \log(1 + \gamma_k) < R\right) \\ &= \Pr\left(\sum_{k=1}^M \log(1 + \gamma_k) < R\right) \end{aligned} \quad (5.15)$$

$$\approx \Pr\left(\sum_{k=1}^M \log(\gamma_k) < R\right) \quad (5.16)$$

where  $\gamma_k$  is given by (5.12), Equation (5.15) is due to  $\gamma_{(jM+i)} = \gamma_i$ ,  $j = 0, \dots, L - 1$ , and the approximation in (5.16) is made for tractability. Applying Jensen's inequality, and substituting (5.12) in, we obtain the following upper bound

$$\Pr(\mathcal{O}) \leq \Pr\left(\sum_{k=1}^M \sum_{\ell=1}^L \frac{1}{X_{\ell,k}} > \rho L 2^{-R}\right). \quad (5.17)$$

The earlier result of independence of  $X_{jM}, \dots, X_{jM+i}$ , for a given  $j$  where  $j = 0, \dots, L - 1$ , and the assumption of  $L = \nu + 1$  make all  $X_k$ 's independent with chi-square distribution with  $2(N - M + 1)$  degrees of freedom. Calculated in the

same manner as (5.13), in high-SNR region (5.17) is

$$\Pr(\mathcal{O}) \leq \frac{M2^{R(N-M+1)}}{(N-M+1)!L^{N-M}}\rho^{-(N-M+1)}. \quad (5.18)$$

### 5.3.2 MMSE-LE

The decision-point SINR of the received symbols after MMSE linear equalization are equal to [38]

$$\gamma_i = \frac{1}{(\rho\mathcal{H}^H\mathcal{H} + \mathbf{I})_i^{-1}} - 1, \quad (5.19)$$

for  $i = 1, \dots, LM$ , where  $\mathbf{M}_i^{-1}$  is the  $i$ th diagonal element of the inverse of the matrix  $\mathbf{M}$ . Using  $\mathbf{I}_{LM} = (\mathbf{Q} \otimes \mathbf{I}_M)(\mathbf{Q}^H \otimes \mathbf{I}_M)$  and

$$\rho\mathcal{H}^H\mathcal{H} + \mathbf{I}_{LM} = (\mathbf{Q} \otimes \mathbf{I}_M) (\rho\mathbf{\Lambda}^H\mathbf{\Lambda} + \mathbf{I}_{LM}) (\mathbf{Q}^H \otimes \mathbf{I}_M),$$

the SINR in (5.19), for  $i = 1, \dots, M$ , can be simplified to

$$\gamma_i = \frac{1}{\frac{1}{L} \sum_{\ell=1}^L (\mathbf{I}_M + \rho\mathbf{\Lambda}_\ell^H\mathbf{\Lambda}_\ell)_i^{-1}} - 1. \quad (5.20)$$

Statistical evaluation of (5.20) appears to be difficult. To obtain the performance and diversity order of MMSE-LE, we resort to outage analysis.

### Outage Probability

In joint spatial encoding architecture, starting from (5.15), the outage probability is:

$$\begin{aligned} \Pr(\mathcal{O}) &= \Pr\left(\sum_{k=1}^M \log(1 + \gamma_k) < R\right) \\ &= \Pr\left(\sum_{k=1}^M \log\left(\frac{1}{L} \sum_{\ell=1}^L (\mathbf{I}_M + \rho\mathbf{\Lambda}_\ell^H\mathbf{\Lambda}_\ell)_k^{-1}\right) > -R\right), \end{aligned} \quad (5.21)$$

where the involvement of the diagonal elements makes the evaluation of the outage probability intractable. However, an upper bound to above outage probability can be calculated as follows. Denote  $\mathbf{A}_\ell \triangleq \frac{1}{L}(\mathbf{I}_M + \rho\mathbf{\Lambda}_\ell^H \mathbf{\Lambda}_\ell)^{-1}$ . Applying Jensen's inequality to the argument of (5.21) gives

$$\begin{aligned} \sum_{k=1}^M \log \left( \sum_{\ell=1}^L (\mathbf{A}_\ell)_k \right) &\leq M \log \left( \frac{1}{M} \sum_{\ell=1}^L \text{tr}(\mathbf{A}_\ell) \right) \\ &= M \log \left( \frac{1}{LM} \sum_{\ell=1}^L \sum_{k=1}^M \frac{1}{1 + \rho\lambda_{\ell,k}} \right), \end{aligned} \quad (5.22)$$

where  $\lambda_{\ell,i}$  are eigenvalues of  $\mathbf{\Lambda}_\ell^H \mathbf{\Lambda}_\ell$ . Application of (5.22) in (5.21) gives the following upper bound :

$$\Pr(\mathcal{O}) \leq \Pr \left( \sum_{\ell=1}^L \sum_{k=1}^M \frac{1}{1 + \rho\lambda_{\ell,k}} \geq LM2^{-\frac{R}{LM}} \right). \quad (5.23)$$

For SISO channel, above bound becomes exact and the same as (3.38). In flat fading channel ( $L = 1$ ), the above upper bound becomes the same (4.39). We evaluate (5.23) for high and low spectral efficiencies.

For small values of  $R$ , the outage region of (5.23) is a polyhedron in the space of eigenvalues  $\lambda_{\ell,k}$  whose vertices are the points on the axes with value

$$c_{\nu,M} \triangleq \frac{1 + M - Lb}{\rho M(Lb - 1)}$$

where  $b = 2^{-\frac{R}{M}}$ . This region is the bounded region in the positive cone separated by the plane  $\sum_{\ell=1}^L \sum_{k=1}^M \lambda_{\ell,k} = c_{\nu,M}$ . The upper bound (5.23) can be evaluated by plugging in the distribution of the eigenvalues  $\lambda_{\ell,k}$  and integrating over the polyhedron outage region. For  $M = N = 2$  and a two-tap channel, the upper bound for small values of

$R$  is

$$\begin{aligned}
\Pr(\mathcal{O}) &\leq \Pr\left(\frac{1}{1+\rho\lambda_{1,1}} + \frac{1}{1+\rho\lambda_{1,2}} + \frac{1}{1+\rho\lambda_{2,1}} + \frac{1}{1+\rho\lambda_{2,2}} \geq 2^{2-\frac{R}{2}}\right) \\
&= \int \int_{\mathcal{A}_1} (\lambda_{1,1} - \lambda_{1,2})^2 e^{-\lambda_{1,1}-\lambda_{1,2}} \\
&\quad \times \int \int_{\mathcal{A}_2} (\lambda_{2,1} - \lambda_{2,2})^2 e^{-\lambda_{2,1}-\lambda_{2,2}} d\lambda_{1,1} d\lambda_{1,2} d\lambda_{2,1} d\lambda_{2,2} \\
&\doteq \frac{4}{45} c_{1,2}^8 = \frac{4\tilde{c}_{1,2}^8}{45} \rho^{-8}, \tag{5.24}
\end{aligned}$$

where  $\mathcal{A}_1 \equiv \{\lambda_{1,1} + \lambda_{1,2} \leq c_{1,2}\}$  and  $\mathcal{A}_2 \equiv \{\lambda_{2,1} + \lambda_{2,2} \leq c_{1,2} - \lambda_{1,1} - \lambda_{1,2}\}$ , and  $\tilde{c}_{1,2} = \frac{3-2^{1-R/2}}{2^{1-R/2}-1}$ . The above upper bound decays as fast as  $\rho^{-8}$ , indicating the diversity order of eight. For other values of  $M$ ,  $N$ , and  $\nu$ , the upper bound (5.23) can be calculated to obtain the diversity order of  $MN(\nu + 1)$  in low spectral efficiency.

For large values of  $R$ , the outage region of (5.23) is approximated by  $LM$  regions. The  $(\ell, k)$ th region,  $\ell = 1, \dots, L$  and  $k = 1, \dots, M$ , is defined as  $0 \leq \lambda_{\ell,k} \leq \hat{b}_{\nu,M}$ , and for  $(\hat{\ell}, \hat{k}) \neq (\ell, k)$ ,  $\lambda_{\hat{\ell},\hat{k}} \geq 0$ , where  $\hat{b}_{\nu,M} = \frac{1}{\rho} \left( \frac{2^{\frac{R}{LM}}}{LM} - 1 \right)$ . The evaluation of (5.23) is similar to (4.44) and results in an expression which decays as fast as  $\rho^{N-M+1}$ . Therefore, the diversity order in high spectral efficiencies is  $N - M + 1$ .

### 5.3.3 Simulation Results

Consider a MIMO system with two antennas in the transmit and receive sides ( $M = N = 2$ ) in a two-tap Rayleigh frequency-selective channel ( $\nu = 1$ ) and block length  $L = 10$ . The outage probability of the linear equalizers in joint spatial architecture are shown in Figure 5.1. The target rate is  $R = 2, 4, 6, 8$  bits/sec/Hz. As expected, ZF-LE shows diversity order of  $N - M + 1 = 1$ , regardless of the target rate. This confirms that ZF-LE cannot harvest the frequency diversity of the channel.

However, MMSE-LE behaves differently in various spectral efficiencies. For small values of  $R$ , the diversity order is very close to that of the unconstrained receiver.

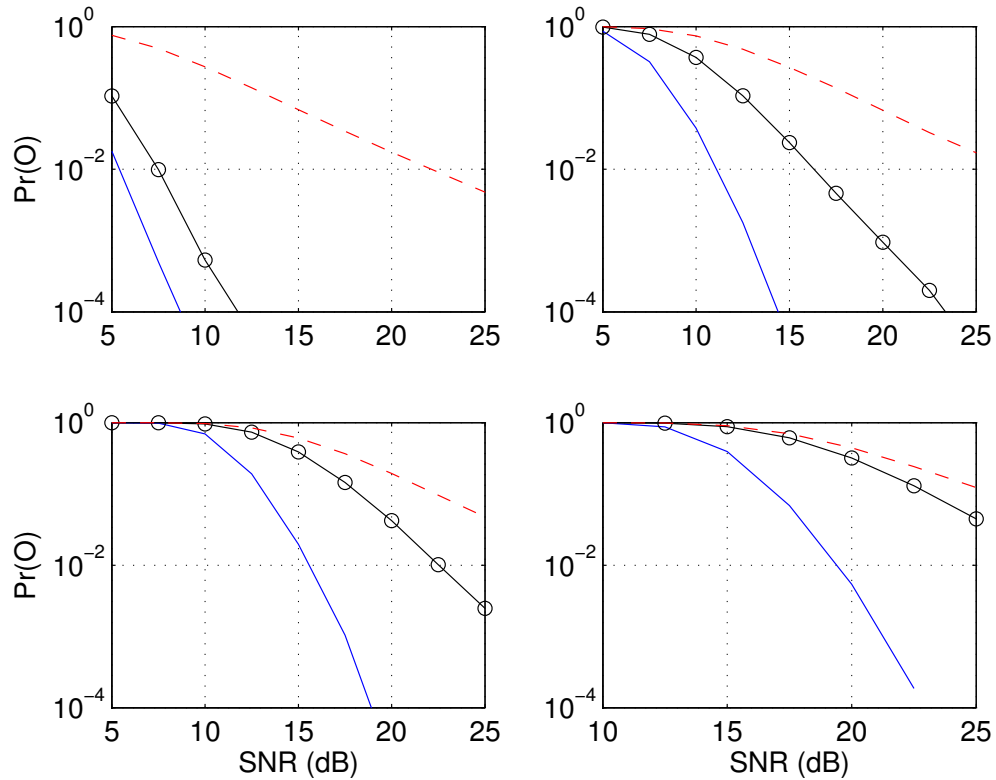


Figure 5.1. Outage probability of unconstrained and linear equalizers,  $M = N = 2$ ,  $\nu = 1$ ,  $L = 10$ . Unconstrained (solid line), MMSE-LE (solid line with  $\circ$ ) and ZF-LE (dashed line). The curves correspond, from top left clockwise, to rates  $R=2,4,8,6$  bits/sec/Hz.

As the spectral efficiency increases the diversity order of MMSE-LE decreases, and eventually achieves diversity order of  $N - M + 1$ . This indicates that MMSE-LE can achieve varying portions of the frequency diversity of the channel, depending of the spectral efficiency. The upper bound (5.23) and the outage probability of MMSE-LE are shown in Figure 5.2.



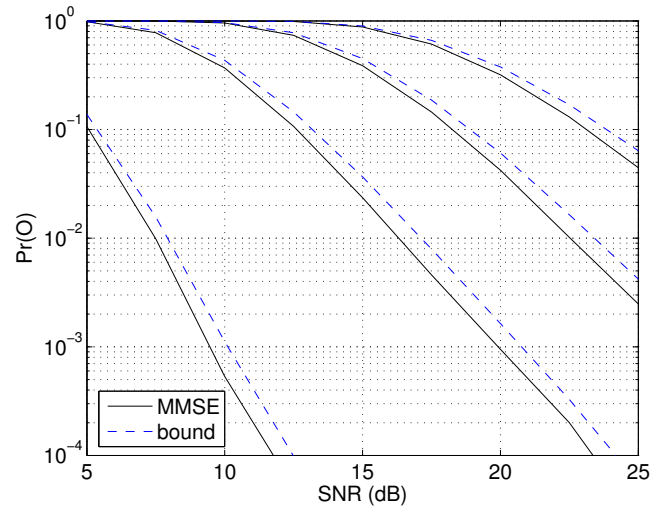


Figure 5.2. Outage probability of MMSE-LE and the upper bound (5.23).  $M = N = 2, \nu = 1, L = 10$ , the curves correspond, from left to right, to rates  $R=2, 4, 6, 8$  bits/sec/Hz.

#### 5.4 Chapter Summary

In this chapter, we evaluate the performance of ML and linear equalizers in frequency-selective fading channels. We present new results on the performance of linear equalizers, and calculate their diversity order. Our analytical and experimental results show that MMSE linear equalizers, depending on spectral efficiency, have outage probability that decays as fast as  $MNL$ , the same as that of unconstrained receiver, and as slowly as  $L - M + 1$ .

## CHAPTER 6

### CONCLUSIONS AND FUTURE WORK

#### 6.1 Contributions

In Chapter 2, we analyze the role of redundancy in a concatenated entropy and channel code. The significance of such concatenated codes is indisputable because entropy coding is part of any compression system, and channel codes are always used for reliable transmission.

Previous work in the area of joint entropy and channel coding were limited in either decoding or the amount of redundancy in the entropy code. In some of the early works, the redundancy of the entropy codes was exploited by simple but sub-optimal decoding, such as bi-directional decoding in RVLC, which has the limitation of separate source channel decoding. In some recent works [1, 9], joint source channel decoding was used via iterative decoding methods. However, no attention was given to the amount of redundancy in entropy codes.

We extend the prior work in joint entropy and channel coding as follows. We generalize the role of entropy codes by using variable-length error correcting codes of [4, 5]. Subject to a total rate, we allow the outer entropy code and inner channel code freely share the available rate. We analyze the error rate of the concatenated code to obtain design rules for the constituent codes. We consider iterative decoding and improve upon it by using list iterative decoding. Our results indicate that allowing more redundancy in entropy codes improves the overall code significantly compared to the concatenated RVLC and channel code.

We also compare the proposed concatenated code with a code that consists of Huffman entropy code and a serial concatenated channel code. We conclude that there is no clear and universal advantage of any of the two codes.

In Chapters 3, 4, and 5 we analyze the performance of equalizers in fading channels which experience interference in time or space or both. Our analysis relies on either the statistical evaluation of the decision-point SNR, or outage probability.

In Chapter 3, we consider a frequency selective single-antenna fading channel and analyze the performance of various linear and decision-feedback equalizers. We determine the diversity order of linear equalizers and show that ZF-LE does not achieve any of the available frequency diversity. However, MMSE-LE may achieve the full diversity if the spectral efficiency is low, or none if the spectral efficiency is high. In intermediate spectral efficiencies, MMSE-LE achieves some diversity which is less than the full diversity order.

We consider a flat fading multiple-antenna in Chapter 4, and analyze the performance of various equalizers for two spatial encoding architectures. The diversity order of ZF-LE has been shown by [51] to be  $N - M + 1$ . Traditionally, it is expected that MMSE-LE performs the same as ZF-LE in high SNR regime. However, our findings show that it can perform quite differently than ZF-LE. In separate spatial encoding, both linear equalizers have the diversity order  $N - M + 1$ , however, MMSE-LE performs better in low spectral efficiencies regardless on SNR. In joint spectral efficiency, ZF-LE achieves the same diversity order  $N - M + 1$ . In low spectral efficiency, MMSE-LE achieves the full spatial diversity of the system. As the spectral efficiency grows, the diversity order of MMSE-LE decreases and eventually becomes the same as ZF-LE. In Chapter 4, we also present some new results on the performance of decision-feedback equalizers. In separate spatial encoding, ZF-DFE and MMSE-

DFE do not achieve any higher diversity order than the linear equalizers, although they have better performance.

In Chapter 5, frequency-selective multiple-antenna fading channels are considered where the interference occurs in both space and time. We analyze the performance of ML equalizers in uncorrelated and correlated channels. Though the performance of ML equalizers degrade in correlated channels, the diversity order remains unchanged. We also analyzed the performance of linear equalizers. Our findings show that ZF-LE achieve the diversity order of  $N - M + 1$  which is the same as what it achieves in flat fading channel. Therefore, similar to the results of Chapter 3, ZF-LE is incapable of harvesting the available frequency diversity. However, MMSE-LE achieves the full spatial and frequency diversity of  $MN(\nu + 1)$  if it operates in low spectral efficiency. As the spectral efficiency grows, the diversity order of MMSE-LE decreases and finally becomes the same as that of ZF-LE.

## 6.2 Future Work

Related to the material in Chapter 2, the issue of rate allocation in concatenated codes is an open problem. Given a fixed total rate, there is a tradeoff in what share of the rate the outer and inner codes of a serially concatenated code should have. The higher amount of redundancy given to the outer code, the larger interleaving gain. However, less amount of redundancy becomes available to the inner code and the overall performance may not be optimum especially in low to moderate SNR.

The issue of rate allocation to constituent codes of a concatenated code is of value in many scenarios. In the framework of Chapter 2, it is of interest to know how much the outer VLC code should be redundant to have the best performance. For example, in Section 2.7, we notice that the concatenated code with higher  $d_f^o$  does

not perform better than a code with a more balanced rate allocation. Similarly, serially concatenated convolutional codes that allocate the overall rate efficiently have better performance. The optimal rate allocation is of importance in other concatenated codes [60], such as hybrid concatenated codes and double serially concatenated codes [61].

In Chapters 3, 4, and 5, we evaluate the performance of various equalizers in a single-user environment where the interference occurs between the components of each user's signal in time or space or both. In multiuser environments, the interference may also occur between the users' signals if they do not communicate in orthogonal channels. While the performance of equalizers has been investigated in multiuser environments [51, 62, 63], a comprehensive analysis of linear and decision-feedback equalizers has not been presented yet. The performance of ZF-LE in a multiple-access flat fading channel with receive diversity is investigated in [51]. In [62], it is shown that MMSE-DFE achieves the capacity of a multiple-access Gaussian channel. The focus of [51, 62] is limited to frequency-nonselctive channels. Tse, Viswanath and Zheng [63] presented the most comprehensive analysis recently by considering a multiple-access channel where the users and the receiver have multiple antennas.

However, there are many open problems when the channel is frequency-selective. The performance of equalizers in a frequency-selective multi-user environment has not been yet investigated analytically. In such a scenario, when the receiver has multiple antennas, multiuser interference can be removed more easily. When users are also equipped with multiple antennas, although the available diversity of the channel increases, the spatial interference of each user's data must be dealt with along with temporal and multiuser interference.

Performance of frequency-selective channels can also be investigated in the framework of diversity-multiplexing tradeoff [54, 63]. Recently, the diversity-multiplexing

tradeoff of frequency-selective channels in a single-antenna single-user environment has been investigated [64]. The optimal tradeoff of frequency-selective multiple-access channels has not been reported yet and is considered an open problem. It is also of interest to see how linear and decision-feedback equalizers perform, compared to the optimal tradeoff of the channel, and what portion of the maximum diversity they can achieve.

## BIBLIOGRAPHY

- [1] R. Bauer and J. Hagenauer, “On variable length codes for iterative source/channel decoding,” in *Proc. Data Compression Conference*, April 2001, pp. 273–282.
- [2] S. Benedetto, D. Divsalar, G. Montorsi, and F. Pollara, “Serial concatenation of interleaved codes: performance analysis, design, and iterative decoding,” *IEEE Transactions on Information Theory*, vol. 44, no. 3, pp. 909–926, May 1998.
- [3] Y. Takishima, M. Wada, and H. Murakami, “Reversible variable length codes,” *IEEE Transactions on Communications*, vol. 43, pp. 158–162, February/March/April 1995.
- [4] V. Buttigieg, “Variable-Length Error-Correcting Codes,” *Ph.D. Thesis, Department of Electrical Engineering, University of Manchester*, 1995.
- [5] V. Buttigieg and P. G. Farrell, “Variable-length error-correcting codes,” *IEE Proceedings-Communications*, vol. 147, no. 4, pp. 211–215, August 2000.
- [6] K. P. Subbalakshmi and J. Vaisey, “On the joint source-channel decoding of variable-length encoded sources: The BSC case,” *IEEE Transactions on Communications*, vol. 49, pp. 2052–2055, December 2001.
- [7] K. P. Subbalakshmi and J. Vaisey, “Joint source-channel decoding of entropy coded markov sources over binary symmetric channels,” in *Proc. IEEE ICC*, 1999, pp. 446–450.

- [8] C. Berrou and A. Glavieux, “Near optimum error correcting coding and decoding: Turbo codes,” *IEEE Transactions on Communications*, vol. 44, pp. 1261–1271, October 1996.
- [9] R. Bauer and J. Hagenauer, “Iterative source/channel decoding using reversible variable-length codes,” in *Proc. Data Compression Conference*, April 2000, pp. 93–102.
- [10] N. Goertz, “On the iterative approximation of optimal joint source-channel decoding,” *Journal on Selected Areas in Communications*, September 2001.
- [11] A. Guyader, E. Fabre, C. Guillemot, and M. Robert, “Joint source-channel turbo decoding of entropy-coded sources,” *Journal on Selected Areas in Communications*, vol. 9, pp. 1680–1696, September 2001.
- [12] K. Lakovic and J. Villasenor, “Combining variable-length codes and turbo codes,” in *Proc. IEEE Vehicular Technology Conference*, Spring 2002, pp. 1719–1723.
- [13] A. Hedayat and A. Nosratinia, “List-decoding of variable-length codes with application in joint source-channel coding,” in *Proc. Asilomar Conference on Signals, Systems and Computers*, 2002.
- [14] A. Hedayat and A. Nosratinia, “On joint iterative decoding of variable-length source codes and channel codes,” in *Proc. of 40th Annual Allerton Conference on Communication, Control, and Computing*, 2002.
- [15] A. Hedayat and A. Nosratinia, “Concatenated error-correcting entropy codes and channel codes,” in *Proc. IEEE ICC*, May 2003, vol. 5, pp. 3090–3094.



- [16] A. Hedayat and A. Nosratinia, "Performance analysis and design criteria for finite-alphabet source/channel codes," *IEEE Transaction on Communications*, to appear, November 2004.
- [17] A. Hedayat and A. Nosratinia, "Iterative and list decoding of concatenated source/channel codes," *Eurasip Journal of Applied Signal Processing, Special issue on Turbo Processing*, to appear, November 2004.
- [18] T. Okuda, E. Tanaka, and T. Kasai, "A method for correction of grabbed words based on the Levenshtein metric," *IEEE Transactions on Computers*, vol. C-25, pp. 172–176, February 1976.
- [19] V. B. Balakirsky, "Joint source-channel coding with variable length codes," in *Proc. IEEE ISIT*, June 1997, p. 419.
- [20] A. Murad and T. Fuja, "Robust transmission of variable-length encoded sources," in *Proc. IEEE Wireless Communications and Networking Conference*, September 1999.
- [21] D. Divsalar and R. J. McEliece, "On the design of generalized coding systems with interleavers," *JPL Progress Report*, August 1998.
- [22] J. Hagenauer, E. Offer, and L. Papke, "Iterative decoding of binary block and convolutional codes," *IEEE Transactions on Information Theory*, vol. 42, pp. 429–445, March 1996.
- [23] S. Benedetto, D. Divsalar, G. Montorsi, and F. Pollara, "A soft-input soft-output APP module for iterative decoding of concatenated codes," *IEEE Communications Letters*, vol. 1, no. 1, pp. 22–24, January 1997.

- [24] L. R. Bahl, J. Cocke, F. Jelinek, and J. Raviv, “Optimal decoding of linear codes for minimizing symbol error rate,” *IEEE Transactions on Information Theory*, vol. 20, pp. 284–287, March 1974.
- [25] D. Divsalar, S. Dolinar, and F. Pollara, “Iterative turbo decoder analysis based on density evolution,” *Journal on Selected Areas in Communications*, vol. 19, pp. 891–907, May 2001.
- [26] S. ten Brink, “Convergence behavior of iteratively decoded parallel concatenated codes,” *IEEE Transactions on Communications*, vol. 49, pp. 1727–1737, October 2001.
- [27] N. Seshadri and C.-E. W. Sundberg, “List Viterbi decoding algorithms with applications,” *IEEE Transactions on Communications*, vol. 43, pp. 313–323, February/March/April 1994.
- [28] K. R. Narayanan and G. L. Stüber, “List decoding of turbo codes,” *IEEE Transactions on Communications*, vol. 46, pp. 754–762, June 1998.
- [29] S. B. Wicker, *Error Control Systems for Digital Communication and Storage*, Englewood Cliffs, NJ: Prentice Hall, 1995.
- [30] A. Hedayat, A. Nosratinia, and N. Al-Dhahir, “On the diversity order of linear equalizers in fading channels,” in *Proc. Asilomar Conference on Signals, Systems and Computers*, 2004.
- [31] M. K. Simon and M.-S. Alouini, *Digital Communication over Fading Channels: A Unified Approach to Performance Analysis*, John Wiley and Sons, New York, 2000.

- [32] G. L. Turin, “The characteristic function of Hermetian quadratic forms in complex normal random variables,” *Biometrika*, pp. 199–201, June 1960.
- [33] H. Sari, G. Karam, and I. Jeanclaude, “Frequency-domain equalization of mobile radio and terrestrial broadcast channels,” in *Proc. IEEE GLOBECOM*, 1994, pp. 1–5.
- [34] D. Falconer, S. L. Ariyavisitakul, A. Benyamin-Seeyar, and B. Eidson, “Frequency domain equalization for single-carrier broadband wireless systems,” *IEEE Communications Magazine*, vol. 40, no. 4, pp. 58–66, April 2002.
- [35] R. K. Mallik, “On multivariate rayleigh and exponential distributions,” vol. 49, no. 6, pp. 1499–1515, June 2003.
- [36] M. Abramowitz and I. A. Stegun, *Handbook of Mathematical Functions with Formulas, Graphs, and Mathematical Tables*, New York, NY: Dover, 9th edition, 1970.
- [37] I. S. Gradshteyn and I. M. Ryzhik, *Table of Integrals, Series, and Products*, San Diego, CA: Academic Press, 5th edition, 1994.
- [38] E. K. Onggosanusi, A. G. Dabak, T. Schmidl, and T. Muharemovic, “Capacity analysis of frequency-selective MIMO channels with sub-optimal detectors,” in *Proc. IEEE ICASSP*, 2002, pp. 2369–2372.
- [39] Z. Wang and G. B. Giannakis, “A simple and general parameterization quantifying performance in fading channels,” *IEEE Transactions on Communications*, vol. 51, pp. 1389–1398, August 2003.
- [40] P. P. Valko and J. Abate, “Comparison of sequence accelerators for the gaver method of numerical laplace transform inversion,” *To appear in Computers and Mathematics with Application*, 2004.

- [41] J. M. Cioffi, G. P. Dudevoir, M. V. Eyuboglu, and Jr. G. D. Forney, “MMSE decision-feedback equalizers and coding I: Equalization results,” *IEEE Transactions on Communications*, vol. 44, pp. 2582 – 2594, October 1995.
- [42] J. M. Cioffi, G. P. Dudevoir, M. V. Eyuboglu, and Jr. G. D. Forney, “MMSE decision-feedback equalizers and coding II: Coding results,” *IEEE Transactions on Communications*, vol. 44, pp. 2595–2604, October 1995.
- [43] N. Al-Dhahir and J. M. Cioffi, “MMSE decision-feedback equalizers: Finite-length results,” *IEEE Transactions on Information Theory*, vol. 41, no. 4, pp. 961–975, July 1995.
- [44] K. E. Baddour and P. J. McLane, “Analysis of optimum diversity combining and decision feedback in dispersive Rayleigh fading,” in *Proc. IEEE ICC, 1999*, pp. 21–26.
- [45] G. Foschini, G. Golden, R. Valenzuela, and P. Wolniansky, “Simplified processing for high spectral efficiency wireless communication employing multi-element arrays,” *Journal on Selected Areas in Communications*, vol. 17, pp. 1841–1852, Nov. 1999.
- [46] G. J. Foschini, “Layered space-time architecture for wireless communication in a fading environment when using multi-element antennas,” *Bell Labs Technical Journal*, vol. 1, no. 2, pp. 41–59, 1996.
- [47] V. Tarokh, N. Seshardi, and A.R. Calderbank, “Space-time codes for high data rate wireless communication: Performance criteria and code construction,” *IEEE Transactions on Information Theory*, vol. 44, no. 2, pp. 744–765, March 1998.

- [48] C. Chuah, D. Tse, J. Kahn, and R. Valenzuela, “Capacity scaling in MIMO wireless systems under correlated fading,” *IEEE Transactions on Information Theory*, vol. 48, no. 3, pp. 637–650, March 2002.
- [49] A. Hedayat, H. Shah, and A. Nosratinia, “Analysis of space-time coding in correlated fading channels,” *IEEE Transactions on Wireless Communications*, *accepted*, Oct. 2004.
- [50] R. Horn and C. R. Johnson, *Matrix Analysis*, Cambridge University Press, 1st edition, 1985.
- [51] J. H. Winters, J. Salz, and R. D. Gitlin, “The impact of antenna diversity on the capacity of wireless communication systems,” *IEEE Transactions on Communications*, vol. 43, pp. 1740–1750, February/March/April 1994.
- [52] M. Rupp, C. Mecklenbrauker, and G. Gritsch, “High diversity with simple space time block-codes and linear receivers,” in *Proc. IEEE GLOBECOM*, San Francisco, CA, November 2003, pp. 302–306.
- [53] H. Gao, P. J. Smith, and M. V. Clark, “Theoretical reliability of MMSE linear diversity combining in Rayleigh-fading additive interference channels,” *IEEE Transactions on Communications*, vol. 46, pp. 666–672, May 1998.
- [54] L. Zheng and D. Tse, “Diversity and multiplexing: A fundamental tradeoff in multiple-antenna channels,” *IEEE Transactions on Information Theory*, vol. 49, no. 5, pp. 1073–1096, May 2003.
- [55] N. Prasad and M. K. Varanasi, “Outage analysis and optimization for multiaccess and V-BLAST architecture over MIMO Rayleigh fading channels,” in *Proc. of 41th Annual Allerton Conference on Communication, Control, and Computing*, 2003.

- [56] T. Guess, H. Zhang, and T. V. Kotschiev, “The outage capacity of BLAST for MIMO channels,” in *Proc. IEEE ICC*, May 2003, pp. 2628–2632.
- [57] R. J. Muirhead, *Aspects of Multivariate Statistical Theory*, John Wiley & Sons, 1982.
- [58] P. Balaban and J. Salz, “Optimum diversity combining and equalization in digital data transmission with applications to cellular mobile radio—Part I: Theoretical considerations,” *IEEE Transactions on Communications*, vol. 40, no. 5, pp. 885–894, May 1992.
- [59] P. Balaban and J. Salz, “Optimum diversity combining and equalization in digital data transmission with applications to cellular mobile radio—Part II: Numerical results,” *IEEE Transactions on Communications*, vol. 40, no. 5, pp. 895–907, May 1992.
- [60] D. Divsalar and F. Pollara, “Hybrid concatenated codes and iterative decoding,” in *Proc. IEEE ISIT*, July 1997, p. 10.
- [61] S. Benedetto, D. Divsalar, G. Montorsi, and F. Pollara, “Analysis, design, and iterative decoding of double serially concatenated codes with interleavers,” *Journal on Selected Areas in Communications*, vol. 2, pp. 231–244, February 1998.
- [62] M. V. Varanasi and T. Guess, “Optimum decision feedback multiuser equalization with successive decoding achieves the total capacity of the gaussian multiple-access channel,” in *Proc. Asilomar Conference on Signals, Systems and Computers*, November 1997, pp. 1405 – 1409.
- [63] D. Tse, P. Viswanath, and L. Zheng, “Diversity-multiplexing tradeoff in multiple-access channels,” *IEEE Transactions on Information Theory*, vol. 50, no. 9, pp. 1859–1874, September 2004.

- [64] L. Gökop and D. Tse, “Diversity multiplexing tradeoff in ISI channels,” in *Proc. IEEE ISIT*, June-July 2004.

## VITA

Ahmadreza Hedayat was born in Behbahan, Khozestan, Iran, in 1972, the son of Morteza Hedayat and Kheyri Ebrahimian. He received the degree of Bachelor of Science in Electrical Engineering from The University of Tehran, Tehran, Iran, in 1994 and the degree of Master of Science in Electrical Engineering from The University of Tehran in 1997. In January 2000 he began working toward the Ph.D. degree in Electrical Engineering in The University of Texas at Dallas.

Permanent address: No 3, Omid Alley, Edalat Ave.,  
Postal code 63617, Behbahan, Khozestan, Iran

This dissertation was typeset with  $\text{\LaTeX}^\dagger$  by the author.

---

<sup>†</sup> $\text{\LaTeX}$  is a document preparation system developed by Leslie Lamport as a special version of Donald Knuth's  $\text{\TeX}$  Program.